INVESTIGATIONS INTO NON-DESTRUCTIVE METHODS OF STRUCTURAL TESTING USING FINITE ELEMENT MODELS

BY

FUK-LUN ALEXANDER WONG

B.Sc.

A thesis submitted for the Degree of

Doctor of Philosophy

UNIVERSITY OF EDINBURGH

1987

To My Parents

Acknowledgements

The author wishes to thank Professor A.W. Hendry, Head of the Department of Civil Engineering and Building Science, University of Edinburgh, for his support of this research.

The author is particularly grateful to Dr. B.H.V. Topping for his supervision, assistance and valuable suggestions throughout this research.

The author is also greatly indebted to The Croucher Foundation for their continuing support and funding of this work in the form of a scholarship.

Many thanks to the advisory staff of ERCC (Edinburgh Regional Computing Centre) for their help in writing the computer programs and using the graphics facilities available.

The author wishes to thank the Librarian, Mrs. V. Thomson for traking down some obscure references.

Thanks are also due to Dr. R.G. Hipkin, Lecturer of the Geophysics Department, for providing a software to prepare data for plotting equipotential contours using the General Purpose Contouring Package (GPCP).

The research students of this department who contributed in the preparation of this thesis in a number of ways, particularly, Mr. H.F.C. Chan and Dr. A.M. Abu Kassim, are gratefully acknowledged.

Many thanks to Mr. C.H. Lau for proof reading.

Stephen Lam and Bernard Cheng are to be thanked for their friendship and support.

Last and not the least, to the author's parents for their patience, constant encouragement and extra financial support at all times.

Abstract

The research described in this thesis is concerned with the investigation of Non-destructive Methods of Structural Testing using Finite Element Models. Non-Destructive methods of structural testing have growing popularity in their application to the quality control of buildings and structures. Reports on successful applications of the methods are widespread. In this research, the finite element models are used as a tool to investigate the theories behind the non-destructive testing methods. The non-destructive testing methods considered are the earth resistance method, the sonic echo method and the vibration methods of pile testing. Finite element simulations are used to investigate the sensitivity of the testing methods in detecting a defect in a structural member under an ideal situation. Finite element models are used to represent a pile, a beam or a column. The application of the finite element simulations to the interpretation of the field test data from non-destructive tests is shown. The prediction of the behaviour of a structure or a structural member using the finite element models is also discussed.

Revealing the shortcomings in the application of the testing methods, some suggestions to modify the operation of the testing methods have been made. Studies on the application of the sonic echo method of testing structural members have lead to an investigation into its application for the assessment of the integrity of brickwork columns and an idealised masonry bridge. The study has shown that the propagation of a sonic pulse in a brickwork structural member may be considered to be the same as the propagation of the sonic pulse in an homogeneous, anisotropic structural member. The velocity of propagation of a sonic pulse in media such as brickwork may be found from the elastic properties of the constituent materials.

Due to the similarity in the operations between the sonic echo test and the shock test, the vibration methods of non-destructive testing have also been investigated. Thus, test data from a site may be interpreted in both time and frequency domain to assess the integrity of a structural member. The sensitivity of the vibration methods of non-destructive testing in locating defects in foundation piles has been studied using simple examples.

Contents

This thesis consists of two volumes. The text is to be found in Volume 1 and the figures and graphs are to be found in Volume 2 of this thesis.

Volume 1

Chapter 1

Introduction

1.1 Background

Over recent years the increase in design loadings for new structures has resulted in renewed efforts to ensure the quality in construction. One approach suitable for quality control of building structures is the assessment of the integrity or the quality of structural members using the Non-Destructive Testing Methods. The increased use and the increased loading on existing structures has also made it necessary to assess the integrity as well as the strength of many existing structures. A typical case of this is the masonry bridge of which many were built hundreds of years ago and have to cope with the heavy loading from the modern traffic.

In civil engineering structures, a defective pile undetected at an early stage may affect the safety and the stability of the finished structure. The cost for the remedial work may be substantial, therefore, non-destructive methods of testing have been developed to help the engineers to assess the integrity or quality of foundation piles. In Great Britain, two of the most common non-destructive testing methods for testing foundation piles are the sonic echo method and the vibration methods. Research has also been undertaken to apply the earth resistance method of integrity test for foundation piles (Ref. 1.1).

Successful applications of these methods to locate defects in piled foundations has been frequently reported. The interpretation of the tests has usually relied on expert advice. Due to marketing and other commercial reasons, companies concerned with the development of non-destructive testing methods usually favour one method rather than any other methods. A more enlightened approach is to select the most appropriate method for each situation. Further development of the method, which may become similar to another testing method promoted by another proprietor, is also avoided. In fact, some methods may be combined so that more information about the integrity of a structural member or a structure may be obtained from the test.

In the development of these non-destructive testing methods, the earth resistance method, the sonic echo method and the vibration methods, model studies were used to verify the applied theory for the testing method. The model studies were also found useful in providing some basis for the interpretation of field test results. Electric analogue models were used by McCarter (Ref. 1.1) and Davis et. al. (Ref. 1.2) to study the earth resistance method and the steady state vibration tests respectively. Steinbach (Ref. 1.3) employed the scaled physical model for his studies on the stress wave propagation method (sonic echo method).

1.2 The Non-Destructive Methods of Testing to be Studied

The non-destructive testing methods which will be investigated in this research are the Earth Resistance Method and the Sonic Echo Method of testing for foundation piles. Practical research on both of these non-destructive testing methods have been undertaken in the Edinburgh University, hence, field test results may be used for the verification of the finite element simulations.

The earth resistance method of pile testing consists of forming an electric circuit between the pile and the return current electrode (Figure 1.1). The integrity of a pile-soil system may be interpreted by examining the potential field established around the pile or by the measurement of the surface potentials at intermediate distances between the pile head and the return current electrode.

A hammer blow is applied to the pile head in the sonic echo test (Figure 1.2). The input pulse and the pulses reflected from the anomalies along the pile shaft or from the base are recorded by a transducer mounted on the pile head. The integrity of the pile may be interpreted from the traces showing the pile head responses in the time domain.

1.3 The Approach Adopted

With the advances in the computing equipment, more and more problems are being solved by analysing a computer-generated model using computer software. One of the most popular analysis technique for engineering studies is the finite element technique. The finite element analysis method has been used by the civil and structural engineers to analyse the stress and strain within a structure. In this research it is shown that the analysis may be applied to the development of a non-destructive method of testing for structures or structural members. The analysis may also help the engineer in interpreting the test results.

The application of computer-generated models to the study of a non-destructive method of testing a structure or a structural member may provide a quick, convenient and inexpensive means of assessing and improving the test at the stage of development of the testing method. The finite element technique is used in this research to investigate the application of the non-destructive testing methods, which have been mentioned in section 1.2, to test civil engineering structural members and structures, and in particular piled foundations. This modelling technique enables a rigorous study of the testing method where the effects of changes to each constituent of the test may be identified by the model (finite element model). The responses of a structure or a structural member being tested by a non-destructive testing method may be predicted by the finite element models. This may be useful in the interpretation of the field test results. In addition the testing procedure may be improved by studying the simulation which leads to an improved design or the selection of the more suitable testing equipment. The modelling technique enables a 'real' environment to be analysed which is particularly suitable for the study of the pile soil interaction in a non-destructive test on foundation piles.

1.4 Objectives

This research concerns with the development of a comprehensive computer-generated modelling tool which enables the investigations into the non-destructive testing methods. The finite element technique has been chosen for the simulation of the non-destructive methods of testing. Despite the popularity of the non-destructive testing methods, little detail concerning the interpretation and the limitations on the application of the non-destructive testing methods has been disclosed. It is hope that more understanding of the application of the non-destructive testing method may be gained through a series of computer simulated model studies. Subsequent modifications and improvements to the testing method may be proposed using the results of the numerical modelling as a guide. The interpretation of the test results based on the finite element simulations may be easier understandable by the engineers. Some test results may have found to be difficult to interpret due to difficult ground conditions. The finite element simulation may provide the engineers with ideas in interpreting such results. In addition, the behaviour of the pile-soil system under working load may be predicted. The simulations may also help the engineer in inferring the test results with more confidence. The required signal processing on the test results will also be simulated and the interpretation of test results using processed data will be discussed. Further development of the method to the testing of other types of civil engineering structures may also be investigated using the finite element simulations. This type of preliminary studies may avoid the expense of building physical models.

The research also studied the feasibility of applying the sonic echo method to test the integrity of a brickwork column and a masonry structure, a masonry bridge, using the finite element approach. This included the study of the propagation of a sonic echo pulse within a multi-layered column such as a brickwork column and how the pulse propagation velocity in such column may be determined.

Due to the similarity in the operations between the sonic echo test and the transient vibration (shock) method of testing, the application of the vibration methods of testing for foundation piles has been studied. The similarity of the steady state vibration test by the shock test has been investigated. The interpretation of the test results in the frequency domain will also be discussed.

References 1.

1. McCarter, W.J., Whittington, H.W., Forde, M.C., "An Experimental Investigation of the Earth-Resistance Response of a Reinforced Concrete Pile", Proceedings of the Institution of Civil Engineers, Vol. 70, Part 2, 1101-1129, December, 1981.

2. Davis, A.G., Dunn, C.S., "From Theory to Field Experience with the Non-Destructive Vibration Testing of Piles", Proceedings of The institution of Civil Engineers, Part 2, 571-593, December, 1974.

3. Steinbach, J., Vey, E., "Caisson Evaluation by the Stress Wave Propagation Method", Journal of the Geotechnical Engineering Division, Proceedings of the American Society of Civil Engineers, Vol. 101, No. GT4, 361-378, April, 1975.

Chapter 2

In-Situ Test Methods

2.1 Introduction

It is often necessary to test concrete for structural use in order to assist the engineer in determining the soundness and suitability of a structure. Concrete cube tests may be used to give an indication of the variation of the concrete mixes between batches. Since cube tests take no account of the different compaction or curing conditions of the corresponding concrete in a structure, it may become important to test the actual structure in particular when the tested cube strengths are lower than the specified cube strength, additional tests may be required to ensure the quality of the structure. Furthermore, the suitability of a structure for a change in use or the possibility of structural alterations may be confirmed by tests. In-situ methods of testing concrete have been developed to satisfy these needs. These in-situ testing methods may be classified as load tests; destructive tests; partially destructive tests; and non-destructive tests. All these testing methods may be used to obtain an estimate of the concrete strength that should be used as an aid for the engineering assessment of the structure.

A structural member may be load tested to 1.5 - 2 times its designed working load to determine its suitability for the design. Alternatively, the structural member may be loaded to failure to assess its ultimate strength. Loading the structural member to failure is obviously a destructive test. Other destructive methods of testing involve the removal of parts of the concrete by coring or sawing, and the testing of these specimens in a laboratory in a standard manner. In partially destructive tests, the concrete is tested to failure while the destruction resulting is very localised and the member under test is not weakened to any significant extent. The non-destructive tests involve the measurement of some properties of the concrete, which may be obtained without the need for destructive forces. These methods could be used to estimate the concrete's strength by the use of a suitable calibration relationship.

Piled foundations especially cast-in-situ piles are frequently installed under difficult sub-surface conditions and are susceptible to constructional defects. Poor quality workmanship frequently contributes towards the construction of faulty piles. Common defects of piles are complete voids, overbreaks, neckings and poor quality concrete. When such defects are found in piles the effects may be more dramatic and costly than the development of many structural faults above ground. The inaccessible nature of these defects, which occur below ground, makes remedial work difficult and expensive. It may be even worse when the defects are undetected until after the super structure has been built. Therefore, the assessment of the load bearing capacity or the structural integrity of a foundation pile may assist the engineer in appraising some aspects of the quality of the pile. Although load testing of piles is still widely used in the construction industry, the selection of a pile for load testing is frequently made at random. Alternatively a pile may be selected for testing when there are doubts as to its integrity because of bad working conditions or poor workmanship. Weltman (Ref. 2.1) has proposed that integrity tests of all piles in a population on a site may aid in the selection of suspicious piles for load tests. The selection may be based on the anomalous response of a pile to an integrity test. In addition, Savage (Ref. 2.2) has suggested that the continual monitoring of important structures, such as bridges, by non-destructive tests may provide the engineer with information about the structure's gradual deterioration over a period of time.

Although only the pile head is normally accessible for testing, most in-situ methods of structural testing may be applied to test piles or bridges. However, some testing methods may have to be modified for a particular application. Some of the frequently used testing methods will be reviewed in this chapter. The testing methods has been focused on pile testing methods. The principles of the operation of the non-destructive methods of testing which will be studied in the latter chapters will also be given in this chapter.

2.2 In-Situ Test Methods

2.2.1 Load Tests

Load tests are generally performed by simply loading the pile head or jacking against a reaction system sunk on either side of the pile. As part of the design sequence several test piles are typically constructed on a site. These piles are usually constructed in areas of minimum bearing capacity or difficult conditions. The preliminary test by the constant rate of penetration (CRP) test may be carried out to determine the ultimate load on a pile (Ref. 2.3). In the CRP test, the compressive force applied to the pile head is progressively increased to cause the pile to penetrate the soil at a constant rate until failure occurs. Alternatively, the preliminary test piles may be loaded to 1.5 - 2 times the working load to determine the suitability of the design from the load-settlement relationship of the pile during the test.

Before the construction of the superstructures, foundation piles may be selected for load testing at random or where there is doubt as to the integrity. The maintained load (ML) test may be used for proof loading tests on these piles (Ref. 2.3). In this test, the load is increased in stages to some multiples, say 1.5 times or twice the design load with the time-settlement curve recorded at each stage of loading and unloading.

Load tests may also be applied to test tension piles. The constant rate of uplift (CRU) test or an incremental loading (ML) test may be used in this application.

Lateral loading tests may be made by pulling a pair of piles together, or jacking them apart.

The integral compression test involves the application of a compressive force over the length of the pile by the stressing of internally cast and recoverable rods or cables. A fault which has significantly weakened a pile may be identified by a downward movement of the pile head when the defect is nearer to the pile head. A fault near to the base may be indicated by an upward movement of a lower pile section which results in a greater elongation of the stressing element than that due to stressing alone.

2.2.2 Destructive Tests

The load tests used to determine the ultimate load bearing capacity of a structural member may be considered as one form of destructive test. Other destructive tests such as the cutting of cores or cubes from a concrete member may enable the strength of the concrete to be measured.

Drilling can be used to assess the integrity of a concrete pile. Drilling may be undertaken using a percussion drill, rotary rock roller bit or by rotary coring (Ref. 2.3). Heavy losses when the drill hole is filled with water may indicate a defective pile. The cores obtained from a cored hole may be compression tested to identify the strength of the concrete. The drilled hole may be flushed clear so that close circuit TV may be lowered down the hole to look for any cavity or honeycombed concrete. The hole produced by coring or drilling may also be used for caliper logging in which a three armed probe is lowered down the hole giving a surface read-out of the borehole diameter (Ref. 2.3, 2.4). Sonic pulse equipment may also be lowered down the drilled hole, where anomalies along the pile shaft may be identified from the irregularities shown in the sonic log.

2.2.3 Partially Destructive Tests

For slender beams or relatively thin structural members where coring is not possible, partially destructive tests are preferred (Ref. 2.5). Whereas, very slender members should be avoided (Ref. 2.6). Although these tests involve destructive forces, the damage only takes place on a small scale. Therefore, the structural member is not significantly weakened and the repair work is superficial. The compressive strength may be estimated using calibration graphs. These tests may not be used for pile testing where the tests can only provide estimates of concrete strength near the pile head.

Keiller (Ref. 2.6) has investigated the partially destructive test methods for the assessment of concrete strength in structures. The methods investigated are the Building Research Establishment (BRE) Internal Fracture Test; the Direct Pull Internal Fracture Test; the Winsor Probe Test; and the Pull-Off Test. The accuracy of the strength estimation from these tests depends on the correlation data available for the type of concrete under investigation. Most of the test methods require a specific calibration. One possible exception of this is the direct pull internal fracture test, for which the results obtained by independent authors have shown good agreement (Ref. 2.6)

A description of these test methods are given in sections 2.2.3.1 to 2.2.3.4 respectively.

2.2.3.1 BRE Internal Fracture Test

This method was developed at the Building Research Establishment (Ref. 2.7, 2.8). The test involves drilling a 6 mm diameter hole in which a wedge anchor is placed. This is then pulled out by tightening a nut (80 mm in diameter) against a reaction frame using a torque meter. The maximum torque on the nut gives an indication of strength from a calibration chart.

2.2.3.2 Pull Internal Fracture Test

Keiller (Ref. 2.9) modified the BRE internal fracture test by pulling out the bolts directly using a hydraulic jack. The geometry of the pull-out core remained unaltered and the load was measured using the hydraulic oil pressure.

2.2.3.3 Winsor Probe Test

This method was developed in the USA in the 1960's (Ref. 2.6). The test involves firing a probe 6.3 mm in diameter and 79.5 mm long into the surface of the concrete using a special gun and powder charge. The length of probe exposed is measured and may be correlated with compressive strength.

2.2.3.4 Pull-Off Test

Pull-off tests have been proposed by Stehno et. al. (Ref. 2.10) and Long et. al. (Ref. 2.11). The tests involve the bonding of a circular metal probe to the surface of the concrete using a high strength epoxy resin adhesive. A tensile force is then applied to the probe to cause concrete failure. The maximum load may be used to estimate the compressive strength using a calibration graph. The tests may be applied to either a plain surface or after drilling an annulus round the position of the disc.

2.2.4 Non-Destructive Tests

Savage (Ref. 2.2, 2.12) has reviewed the non-destructive testing methods which are used by the civil engineering discipline to locate faults and assess structural integrity. Some of these methods will be described in sections 2.2.4.1 to 2.2.4.10. Particular interest has been placed on testing methods which are suitable for in-situ testing of piles. The methods are frequently given different names by different authors or proprietors, the methods which will be discussed in the following sections are generally known in the civil engineering field.

2.2.4.1 Photoelastic Tests

Models of the entire structure or parts of the structure can be made using photoelastic resin based material. Polarised light may be passed through the model under load and a polariscope may be used to obtain a three-dimensional picture of the stresses from the fringe patterns. Locations of concentrated stress or strain may be identified from the model.

2.2.4.2 Hardness Methods

The Schmidt rebound hammer is the most widely accepted instrument for measuring the surface hardness of concrete members (Ref. 2.13, 2.14). A plunger is held in contact with the surface of the concrete and a spring-loaded mass strikes the free end and rebounds. The magnitude of the rebound is a measure of the hardness of the surface and the result is known as the rebound number. Empirical relationships between rebound number and strength have been established (Ref. 2.14). Usually a higher rebound number implies a stronger concrete.

2.2.4.3 Infra-red Thermography

Infra-red Thermograph may be used to assess integrity of a building by observing the thermal flow in the structure when an artificial heat or cool source is applied to the structure. A crack in a structure under continuous oscillation due to disturbance may become a heat source in the structure when heat is generated through the friction in the crack. Provided the temperature contrast in the structure is sufficient the infra-red thermograph may be applied to assess the integrity of a structure.

2.2.4.4 Acoustic Emission

When a structure is stressed, local macroscopic failure in the structure causes a rapid release of locally stored elastic energy. The released energy travels in a wavelike manner to all parts of the structure until the energy has dissipated by heat and friction. A high degree of technical knowledge and experience is required to choose the suitable location on a structure where the piezoelastic sensors should be placed. Good experience and interpretive skill are required to interpret the results recorded by the piezometric sensors. The location of a fault may be found by triangulation.

2.2.4.5 Sonic Coring

Instead of forming a hole in a pile by drilling or coring as mentioned in section 2.2.2, several vertical tubes may be cast into a pile during construction. The tubes are usually made of metal or plastic. Sonic pulse equipment is lowered down two of the tubes and a sonic signal is transmitted from one to the other. The tubes are filled with water to provide good contact between the transducer and the wall of the tube. The two probes are raised or lowered together while signals are sent out at regular intervals and the full length of the pile is scanned.

The use of the ultrasonic pulse technique for locating flaws, voids or other defects in concrete is based on the differential transmission of ultrasonic energy across a concrete-anomaly interface (Ref. 2.13). Thus any anomaly lying immediately between two probes will obstruct the direct ultrasonic beam. When this happens the first pulse to arrive at the receiving transducer will be deflected or diffracted around the periphery of the defect and the transmission time will be longer than in homogeneous concrete. In addition to the apparent lower pulse velocity, the amplitude of the received pulse is usually smaller than in homogeneous concrete.

A single hole technique may also be employed using a combined transmitter/receiver unit. An transmitter at the top is separated by an acoustic insulator from a receiver at the base. Transmission time for the signals to pass through the pile concrete and received by the receiver indicates the integrity and quality of concrete adjacent to the probe.

2.2.4.6 Radiometric Methods

The method is similar to the sonic coring method. Either the single tube method (Backscattering Method) or the twin tube method may be used. Two popular radiations used for pile testing are the gamma radiation and the neutron radiation. The gamma ray transmission responds to changes in the density of the concrete while the neutron transmission varies with the moisture content of the concrete.

For the backscattering method, the radiation leaves the source and collides with particles in the pile material before it arrives at the detector. The detector is situated in the same pile tube, but separated from the source by a lead shield. A stronger source may be required in the twin tube method which may cause a radiation hazard.

2.2.4.7 Excavation

This method requires clearing the soil from around the pile to expose the doubtful pile. In the case of large piles, a pit or heading may be required. The method is not suitable for friction piles. It is only used in exceptional circumstances such as a dispute over a foundation failure.

2.2.4.8 Electrical Methods

These methods are operated by forming a circuit between the pile reinforcement and a non-polarising electrode sunk in the soil some distance from the pile. The integrity of the pile-soil system may be assessed by measuring the response of a pile and/or the pile-soil system to an electrical input. Or, the integrity of the pile-soil system may be indicated by the electrical currents inherent in the pile-soil system. Four electrical methods of testing are generally recognized (Ref. 2.1). They are the self potential technique; the resistivity technique; the resistance to earth technique; and the induced polarisation technique. Among these methods, the resistance to earth technique has been shown to be most promising.

Some successful applications of the resistance to earth technique have been reported by Bobrowski (Ref. 2.15). Further investigations into the method has been undertaken by McCarter (Ref. 2.16). The method involves the application of a known current between the pile reinforcement and a non-polarising return electrode placed at about one pile length away from the pile. The surface potentials at intermediate points between the pile and the return electrode can be measured. The quotient of the measured potential drop from the reinforcement to that point divided by the applied current is the earthing resistance of the pile for that particular point. The integrity of the pile may be inferred from the earth resistance curve which is a plot of the earthing resistances between the pile head and the return current electrode.

2.2.4.9 The Sonic Echo Method

The base of a foundation pile is generally inaccessible once in position. Therefore, this testing method which based on the transmission of sound waves involves the echo technique. The sonic echo method of testing foundation piles has been studied in France (Ref. 2.17), the U.S.A. (Ref. 2.18), Holland (Ref. 2.19) and the U.K. (Ref. 2.4). The method involves the introduction of an impulse at the pile head. Stress waves developed in the pile propagate down the length of the pile. A reflection from the pile base or some discontinuities may be recorded by a transducer mounted on the pile head. The distance of the pile base or the discontinuities from the pile head may be found using the recorded reflection time and the velocity of sound in the concrete. The velocity of sound in the concrete may be estimated from the velocity of surface Rayleigh wave or from the concrete cubes for the pile concrete. The reflection characteristics of the reflection surface along the pile will determine the nature of the reflected signal. However, multiple defects along the pile length may produce a confused echo signal.

2.2.4.10 Vibration Tests

The most widely used vibration tests are the continuous vibration method (Refs. 2.20, 2.21, 2.22) and the transient vibration method (the shock method) (Ref. 2.23, 2.24). In the vibration tests, a vibration or a shock is applied to the pile and the frequency response of the pile is monitored over a selected frequency spectrum. A continuous vibration is applied to the prepared and levelled pile head using an electrodynamical vibrator. The vibrator excites the pile head at a broad frequency band, usually 20-1000 Hz. The steady state response of the pile is recorded by velocity transducer mounted on the pile head. The recorded resonance peaks from the transducer may be used to deduce the effective length of the pile and to reveal apparent defects. The response of the pile-soil system may also be expressed graphically as a plot of the mechanical admittance of the pile against the applied frequencies. The mechanical admittance is defined as the quotient of the maximum vertical velocity of the pile head, V_0, in ms^{-1} divided by the maximum vertical force applied to the pile, F_0, in N. Thus the mechanical admittance of the pile may be expressed as V_0/F_0 in $ms^{-1}N^{-1}$.

In the transient vibration method, the mechanical vibrator is replaced by a single hammer blow on the pile head. The pile is forced into transient vibration by the hammer blow. The applied force signal and the pile head velocity vibration are measured in time domain. The response of the pile may be obtained by transforming the time domain signal into the frequency domain signal using Fourier transformation. The results may be displayed as a plot of the mechanical admittance of the pile head against the frequency. The interpretation of the test results is similar to the continuous vibration tests (Ref. 2.23).

2.3 Close Form Solutions to Describe the Non-Destructive Testing Methods

Closed form solutions may be employed to study the interrelationship between the system variables in a non-destructive method of pile testing using approximate theories. The approach may also be used to assess quantitatively the effects of an anomaly in a pile-soil system on the measured response from a non-destructive testing method. The non-destructive methods of pile testing to be studied are the earth-resistance method, the sonic echo method and the vibration method. The earth-resistance method and the sonic echo method are studied because some practical experience on the application of these methods has been gained at Edinburgh University (Ref. 2.4, 2.16). The vibration methods of pile testing are investigated due to its similarity to the sonic echo method. Therefore, a combination of the two testing methods may provide the engineer with more confident information about the integrity of a pile under test. The finite element approach may be applied to predict problems which may be encountered in the field; to improve the methodology before practising the method in a site; and to interpret field data.

2.3.1 The Earth Resistance Method

A continuous current flow or a low frequency a.c. current is applied between the pile reinforcement and a return current electrode. The potential drop between the pile reinforcement and the return current electrode is measured. (Figure 1.1) The earth resistance of the pile for that particular position of electrode is obtained by dividing the measured voltage drop (V) from the reinforcement by the total applied current (I) (Figure 1.1). The integrity of a pile-soil system may be interpreted from the earth resistance curve for the system. The Earth Resistance Curve is a plot of the earth resistance (V/I) at a point against its distance from the centre of the pile head, d, between the pile reinforcement and the return current electrode (Figure 1.1).

The behaviour of the current flow in the pile-soil system may be understood by considering the pile-soil system as regions having constant resistivities. The potential distribution about a point current source in an infinite medium may be found using Ohm's Law:

$$\underline{J} = \sigma \underline{E} \tag{2.1}$$

where $\underline{J}$ is the current density in amperes per square metre flowing through a surface dA (Figure 2.1); σ is the conductivity of the medium in mhos per metre; and $\underline{E}$ is the electric field (potential gradient) in volts per metre. The electric field is the gradient of a scalar potential:

$$\underline{E} = -\nabla V \tag{2.2}$$

where V is the scalar potential in volts; and ∇ is the differential operator:

$$\nabla = \frac{\partial}{\partial x}\,\underline{i} + \frac{\partial}{\partial y}\,\underline{j} + \frac{\partial}{\partial z}\,\underline{k} \tag{2.3}$$

∇V is called the gradient of the scalar potential V. Thus, equation (2.1) may be expressed as:

$$\underline{J} = -\sigma \nabla V \tag{2.4}$$

The electric charge is conserved within the volume enclosed by the surface A (Figure 2.1), then:

$$\int \underline{J} dA = 0 \tag{2.5}$$

Applying the Divergence Theorem of Gauss (Ref. 2.25) to this problem such that the volume integral of the divergence of current throughout a given region is equal to the total charge enclosed:

$$\int \nabla \cdot \underline{J} d(vol) = 0 \tag{2.6}$$

where $\nabla \cdot \underline{J}$ is called the divergence of $\underline{J}$.

$$\nabla \cdot \underline{J} = \frac{\partial J_x}{\partial x} + \frac{\partial J_y}{\partial y} + \frac{\partial J_z}{\partial z} \tag{2.7}$$

where J_x, J_y and J_z are the components of $\underline{J}$. For a point enclosed in an infinitesimal volume:

$$\nabla \cdot \underline{J} = -\nabla \cdot \nabla(\sigma V) = 0 \tag{2.8}$$

and hence,

$$\nabla\sigma \cdot \nabla V + \sigma\nabla^2 V = 0 \tag{2.9}$$

Since σ is constant throughout, the first term in equation (2.9) is zero. Therefore, in a homogeneous electric conduction field, the potential, V, at any point in the medium may be solved using the second term of equation (2.9) and appropriate boundary conditions. That is:

$$\sigma\nabla^2 V = 0 \tag{2.10}$$

which may be expressed as:

$$\nabla^2 V = \frac{\partial^2 V}{\partial x^2} + \frac{\partial^2 V}{\partial y^2} + \frac{\partial^2 V}{\partial z^2} = 0 \tag{2.11}$$

which is Laplace's equation.

2.3.1.1 Earthing Resistance of a Buried Reinforcement Cage

The reinforcement cage is idealised as a line source in the ground (Figure 2.2). Assuming that the applied current is uniformly distributed along the reinforcement, McCarter (Ref. 2.16) applied two boundary conditions to solve the Laplace's equation. The boundary conditions are:

1. as z (Figure 2.2) tends to infinity, potential V must approach zero; and
2. the potential gradient at the surface of the earth is zero.

It was found (Ref. 2.16) that the mean potential on the surface of the reinforcement cage is:

$$V = \frac{I\rho_1}{2\pi} \ln\frac{2h}{a} \qquad (2.12)$$

where I is the applied current per unit length; ρ_1 is the resistivity of the medium; h is the length of the reinforcement and a is the radius of the reinforcement cage. The earthing resistance of the reinforcement may be obtained by dividing the mean potential by the total applied current, Ih, thus:

$$R = \frac{\rho_1}{2\pi h} \ln\frac{2h}{a} \qquad (2.13)$$

2.3.1.2 The Disturbing Effect of the Soil

A current flowing from a medium of one resistivity into another resulted in a distortion of the current flow as well as the potential distribution in the medium. The potential field in the media may be determined by solving Laplace's equation (Refs. 2.26, 2.27) to obtain a closed form solution or by using the analogue approach which has been adopted by the geophysicists (Refs. 2.28, 2.29, 2.30). Geometrical optics are usually employed as the analogue approach. The analogy between the electrical situation and the optics is based on the fact that the current density, like light ray intensity, decreases with the inverse square of distance from a point source.

Using this analogue approach to calculate the additional resistance representing the disturbing effect of medium resistivity ρ_2, McCarter (Ref. 2.16) approximated a circular pile by a square pile having its sides equal to the diameter of the circular pile. It was shown that (Ref. 2.16) the additional resistance, Ra, due to the soil is:

$$R_a = \frac{\rho_1}{\pi h} \sum_{n=0}^{\infty} \sum_{m=1}^{\infty} k^{(m+n)} \left[\ln\left(\frac{1+\sqrt{(1+C^2)}}{C}\right) - \sqrt{(1+C^2)} + C \right] \qquad (2.14)$$

where:

$$C = \sqrt{[(mp/h)^2 + (np/h)^2]} \qquad (2.15)$$

and

$$k = (\rho_2 - \rho_1)/(\rho_2 + \rho_1) \qquad (2.16)$$

k is known as the reflection coefficient and m and n are the number of optical images in the x and y directions respectively.

The total earthing resistance of the pile-soil system is the sum of the earthing resistance of the reinforcement if it were buried in semi-infinite medium of resistivity ρ_1, R, and the additional resistance representing the disturbing effect of the medium resistivity ρ_2, R_a:

$$R_\infty = R + R_a \qquad (2.17)$$

where R and R_a are given in equations (2.13) and (2.14) respectively. From the analysis it may be seen that the resistance measured at infinity on the ground surface is related to the physical dimensions of the pile in the ground, the electrical resistivity of the pile concrete and the reflection coefficient.

R_a is calculated using a computer program and a graph of R_a against p/h is shown in Figures 2.3a and 2.3b similar to McCarter's (Ref. 2.16) approach.

2.3.1.3 Location of the Return Current Electrode

The return current electrode has been considered to be placed at an infinite distance from the pile head in section 2.3.1.3. Here, placing the return current electrode at an infinite distance from the pile is impossible. In practice, the return current electrode should be placed at a more practical distance from the pile. The return current electrode which is struck into the soil may act as a point sink to the electric current. This may affect the earth resistance curve for the pile-soil system. The rapid voltage drop near to the return current electrode, a point sink, may result in an extraordinarily higher measured earth resistance which may be bigger than the earth resistance with the return current electrode placed at infinity, R_∞. Figure 2.4 shows the effect on the E-R curve by placing the return current electrode at a finite distance (5.0 m) from the pile head using the finite element simulation. The graph illustrates that the total earthing resistance of the pile-soil system R_∞ may not be suitable for interpreting the earth resistance testing results. Although the potential between the pile and the return current electrode may be found approximately using the closed form solution, it was suggested that modelling methods is appropriate for the interpretation of the field test results (Ref. 2.16).

2.3.1.4 The Effect of a Defect in a Pile

Similar to the disturbing effects caused by the soil surrounding a pile, defective concrete or a soil inclusion over part of a pile shaft distorts the current flow and potential distribution in the pile-soil system. The extent of this distortion (Figure 2.5) affects the earth resistance measurements on the ground surface. The amount of distortion depends on the size and the reflection coefficient between the pile concrete and the material in the defective section.

2.3.2 The Sonic Echo Method

When a force is applied to an elastic solid, waves of stress and deformation radiate from the loaded region with finite velocity of propagation. In a semi-infinite elastic solid, there are compression, shear, and Rayleigh waves each propagates with a different characteristic wave velocity.

In the application of the acoustic method for testing slender members such as beams and piles, the study of the wave propagation in a bar type structure is appropriate. The most important types of waves involved in this method of pile testing are the longitudinal wave (compression wave) and the surface wave (Rayleigh wave). Since only the pile head is accessible in the case of pile testing, the testing entails the measurement of the echo signals. The reflections of the longitudinal wave from the discontinuities along a pile shaft may reveal the integrity of the pile shaft. Knowing the wave propagation velocity in a pile, the location of a reflecting interface may be inferred from the traces showing the displacement, or the velocity, or the acceleration responses recorded at the pile head using a transducer or an accelerometer. These traces, in fact, give the particle displacement, or the particle velocity, or the particle acceleration at the point where the transducer or the accelerometer is placed. The total distance travelled by the longitudinal wave before it arrives at the pile head, which is equal to twice the distance between the pile head and the reflecting interface, may be found by multiplying the longitudinal wave velocity in the pile by the reflection time, which may be measured from the displacement, velocity, or acceleration response traces.

2.3.2.1 The Longitudinal Wave

It was noted by Fegen (Ref. 2.4) that the equations derived from the elementary theory for the wave propagation in a uniform bar is sufficient for the sonic echo testing of concrete piles. The elementary theory has been given in many standard physics books on Vibrations and Waves (for example Refs. 2.31, 2.32). The derivations of the equations for wave propagation in this section are mainly due to Richart et. al. (Ref. 2.33).

In the elementary theory, it is assumed that stress over any cross section of the bar is uniform and purely axial, and that plane cross sections remain undistorted by the motion. That is, the inertia forces caused by the lateral motions of particles are neglected. Considering an element originally between cross sections at x and x+dx in a bar (Figure 2.6) which has cross-sectional area A, Young's modulus E, and bulk density ρ, the sum of forces, F, in the x-direction is:

$$F = -\sigma_x A + (\sigma_x + \frac{\partial \sigma_x}{\partial x} dx)A$$

$$= \frac{\partial \sigma_x}{\partial x} dxA \qquad (2.18)$$

If the displacement of the element in the x-direction is u, then Newton's second law may be written as:

$$\frac{\partial \sigma_x}{\partial x} dxA = \rho A dx \frac{\partial^2 u}{\partial t^2} \tag{2.19}$$

that is,

$$\frac{\partial \sigma_x}{\partial x} = \rho \frac{\partial^2 u}{\partial t^2} \tag{2.20}$$

Relating the stress and strain in the element, thus:

$$\sigma_x = E \frac{\partial u}{\partial x} \tag{2.21}$$

and

$$\frac{\partial \sigma_x}{\partial x} = E \frac{\partial^2 u}{\partial x^2} \tag{2.22}$$

Substituting equation (2.22) into equation (2.20), equation (2.20) may be written as :

$$\frac{\partial^2 u}{\partial t^2} = \frac{E}{\rho} \frac{\partial^2 u}{\partial x^2} \tag{2.23}$$

or

$$\frac{\partial^2 u}{\partial t^2} = c \frac{\partial^2 u}{\partial x^2} \tag{2.24}$$

where $c = E/\rho$ is defined as the phase velocity or the longitudinal wave propagation velocity in the bar. Equation (2.24) is a linear differential equation, therefore, if there are two solutions of the equation, their sum is also a solution of the equation (Ref. 2.34). It follows that in the investigation of pulse propagation along a bar, the method of superposition may be applied. The solution for equation (2.24) may be written in the form:

$$u = f(x-ct) + g(x+ct) \tag{2.25}$$

where f and g are arbitrary functions which depend on the shape of the pulse. The function f may be regarded as a pulse propagation in the x-direction. It can be seen that after time dt, the pulse is repeated as x is displaced by cdt. That is, $f(x-ct)$ is equal to $f[(x+cdt)-c(t+dt)]$. Hence, the pulse is moving with velocity c without a change in shape. Similarly, it can be seen that function g represents a pulse propagating in the negative x-direction with velocity c.

It is important to distinguish between the wave propagation velocity, c, and the velocity of particles in the stressed zone for the sonic echo testing. This is because the sonic pulse propagates along the pile shaft at bar velocity, c, while the amplitudes of the measured signals depend on the velocity of the particles. The velocity of the particle, v, may be found by considering the compressed zone at the end of the rod in Figure 2.7. Due to the compressive stress σ_x applied to the end of the bar for a period of time t_n (Figure 2.8), the stressed zone shortens by an amount u_n equal to $\sigma_x c t_n / E$. That is:

$$u_n = \sigma_x c t_n / E \tag{2.26}$$

Since the velocity of the end of the bar is the same as the particle velocity at that point, the particle velocity v is equal to the end displacement divided by the contact time of the applied pulse. That is:

$$v = u_n / t_n \tag{2.27}$$

$$= \sigma_x c / E \tag{2.28}$$

In this case, a compressive stress is applied, the particle velocity and the wave propagation velocity are in the same direction. If instead of a compressive stress, a tensile stress is applied at the end of the bar, the displacement at the end of the bar will be negative, $-u_n$. Thus:

$$v = -u_n/t_n \tag{2.29}$$

$$= -\sigma_x c/E \tag{2.30}$$

Therefore, the directions of the two particle velocities are opposite to each other.

It should also be noted from equations (2.23), (2.24), (2.29) and (2.30) that the wave propagation velocity, c, depends on the material properties only when the particle velocity, v, is a function of the intensity of the stress. These indicate that the wave propagation velocity may relate to the properties of the pile concrete.

The solution for the wave propagation velocity in the bar is accurate as long as the wave length of the longitudinal pulse is long in comparison with the cross-sectional dimension of the bar (Ref. 2.33). For a hammer applied pulse, initially a spherical wave will radiate from the source and travel into the bar at the longitudinal velocity in an unbounded medium $c_l = [[E(1-\nu)]/[\rho(1+\rho)(1-2\nu)]]^{0.5}$. This wave front may propagate for some distance down the bar axis depending on the frequency and the rate of absorption in the medium. When the spherical wave strikes the side of the wave guide reflections will take place and the propagation down the wave guide will be a combination of longitudinal, transverse and surface waves. The bulk of the energy will travel in the form of a longitudinal pulse at the bar velocity, c. In a long bar this pulse will be the first arrival at the far end. The pulse will be a grouping of the dominant waves excited by the source. The extent to which this pulse is dispersed will depend on the frequencies composing the pulse, the pulse width and the lateral dimensions of the wave guide. The pulse width is the contact time between the hammer and the structural member when the pulse is applied. Where the pulse width is long compared to the width of the bar, the pulse will travel with little distortion for a considerable distance. Fegen (Ref. 2.4) noted that for a bar of square cross section, the wave propagation velocity is within a few percent of the theoretical values for a cylindrical bar of equal cross-sectional area.

2.3.2.2 Reflection of Pulses in Bars

The amplitude and form of a pulse reflected from the end of a bar are dependent on the nature of the reflecting end and on the medium with which the end is in contact. This may provide information on the type of support at the base of a pile.

It was mentioned in section 2.3.2.1 that the method of superposition can be applied to the study of pulse propagation in a bar. If two pulses travelling in opposite directions come together, the resulting stress and the resulting velocity of particles may be obtained by superposition (Ref. 2.34). Particular interest has been placed on two pulses having same wavelength and with same magnitude of stress approaching each other from opposite directions. In the crossover zone of the bar in which the pulses are superposed as shown in Figure 2.9, the stress there is doubled and the particle velocity is zero. After the pulses pass by each other, they return to their original shape and magnitude. The cross-section at $x = 0$ remains stationary during the whole process, and, if one half of the bar is removed, the axis at $x = 0$ can be considered as a fixed end of the bar. It may be concluded that a compression pulse is reflected from a fixed end of a bar as a compression pulse of the same magnitude and shape. The stress at the fixed end of the bar is twice as much as it was applied.

Consider a compression pulse is moving along the bar in the positive x-direction and a tension pulse of the same wavelength and with the same magnitude of stress is moving in the negative x-direction. Again, by superposing the stress and particle velocities of the two pulses at the crossover zone when the two pulses pass by each other, it may be demonstrated that the particle velocities are doubled while the stress is zero in that zone. It is shown in equations (2.28) and (2.30) that the particle velocity associated with a compression pulse is in the same direction as the pulse propagation while that for a tension pulse is in the opposite direction to the pulse propagation. Therefore, the particle velocities of both pulses are in the same direction and at the crossover zone, the particle velocities become doubled. After the two waves have passed, the particle velocities return to zero at the crossover point. The compressive and tensile pulses then return to their initial shape and magnitude. In this case, the stress along the x = 0 axis is zero all the time which is similar to a free end of a bar. By taking one half of the bar away, the axis at x = 0 may be considered as a free end of a bar. It may be concluded that a compression pulse is reflected from a free end of a bar as a tension pulse as the case in the left hand side of Figure 2.10. Similarly, a tension pulse is reflected as a compression pulse from the same end as shown in the right hand side of Figure 2.10. This study has shown that the interpretation of the sonic echo method may be based on the characteristics of the reflected pulses.

2.3.2.3 Partial Reflection

When a pulse of plane wave strikes a boundary separating two sections of different material characteristics, some of the energy is transmitted and the remainder reflected. The transmitted and reflected intensities may be expressed by the reflection and transmission coefficients, the value of which will depend on the acoustic impedance of each section. The characteristic impedance defined by Main (Ref. 2.31) for a travelling wave in a string is equal to the stress force per unit velocity at any point along the string. The same definition is also applicable to the sonic echo test of foundation piles. The characteristic acoustic impedance Z is defined as:

$$Z = A\rho c \qquad (2.31)$$

$$= A(E\rho)^{0.5} \qquad (2.32)$$

where A is the cross-sectional area of the bar section; ρ is the density of the bar; c is the longitudinal wave velocity in the bar; and E is the Young's modulus of the material.

To find the reflection and transmission amplitude coefficients, that is, the relative amplitude of the reflected and transmitted pulse compared to the incident pulse, a section of discontinuity in acoustic impedance as shown in Figure 2.11 is considered. Two conditions must be satisfied at the impedance discontinuity boundary, at section x = 0 in Figure 2.11. The boundary conditions are:

1. A geometrical condition that the particle displacement is the same immediately to the left and right of x = 0 for all time, so that there is no discontinuity of displacement across the section.
2. A dynamical condition that there is a continuity of the transverse force at x = 0

Considering the incident pulse as $u_i(x,t)$, the reflected pulse as $u_r(x,t)$; and the transmitted pulse as $u_t(x,t)$, and condition 1 becomes:

$$u_i(0,t) + u_r(0,t) = u_t(0,t) \tag{2.33}$$

and using condition 2:

$$Z_1\left[\frac{\partial u_i(0,t)}{\partial t} - \frac{\partial u_r(0,t)}{\partial t}\right] = Z_2\frac{\partial u_t(0,t)}{\partial t} \tag{2.34}$$

where Z_1 and Z_2 are the characteristic impedances of the section to the left and right of section x = 0 in Figure 2.11. Differentiating equation (2.33) and substituting the resulting equation into equation (2.34), gives:

$$Z_1\left[\frac{\partial u_i(0,t)}{\partial t} - \frac{\partial u_r(0,t)}{\partial t}\right] = Z_2\left[\frac{\partial u_i(0,t)}{\partial t} + \frac{\partial u_r(0,t)}{\partial t}\right] \tag{2.35}$$

which may be expressed as:

$$\frac{\partial u_r(0,t)}{\partial t} = \frac{Z_1 - Z_2}{Z_1 + Z_2}\frac{\partial u_i(0,t)}{\partial t} \tag{2.36}$$

Integrating both sides of equation (2.36) gives:

$$u_r(0,t) = \frac{Z_1 - Z_2}{Z_1 + Z_2}\, u_i(0,t) \tag{2.37}$$

where the constant of integration has been cancelled due to the fact that when $u_i(0,t)$ is zero, $u_r(0,t)$ must also be zero. Equation (2.37) shows how the displacement of the reflected pulse, u_r, must be related to the displacement of the incident pulse, u_i, at the section x = 0 at any time t. It has been shown by Main (Ref. 2.31) that for equation (2.37) to hold for any section along the bar, the reflected pulse has the same shape as the incident pulse, but in the reverse direction along the bar. Equation (2.37) may be expressed as:

$$u_r(0,t) = Ru_i(0,t) \tag{2.38}$$

where,

$$R = \frac{Z_1 - Z_2}{Z_1 + Z_2} \tag{2.39}$$

and R is called the Reflection Coefficient of amplitude. The transmission coefficient of amplitude may be found by considering equations (2.33) and (2.38):

$$u_t(0,t) - u_i(0,t) = Ru_i(0,t)$$

that is,

$$u_t = (1 + R)u_i(0,t) \tag{2.40}$$

It is obvious from equation (2.39) that the reflection coefficient ranges between 1 and -1. A negative coefficient means that the incident pulse has been inverted, that is, has a 180^{o} phase shift. This is a particular case when the bar has a fixed end and $Z_2 = \infty$. Similarly, a free end at section x = 0 may be treated as $Z_2 = 0$. In these two particular cases, the amplitude of the incident and reflected pulses are the same.

From equation (2.40), the transmission coefficient, 1 + R, has a value between 0 and 2. Since the transmission coefficient is always positive, inversion of the transmitted wave never occurs. If Z_2 is larger than Z_1, the displacement of the transmitted pulse is less than that of the incident pulse; if Z_2 is smaller than Z_1, the transmitted pulse is larger. This study has shown that the reflected pulse from an anomaly along the pile may indicate the nature and extent of the anomaly.

2.3.3 Vibration Methods

The vibration methods of pile integrity testing involve the principle of system identification by dynamic methods. The response of the system subjected to an excitation may be expressed as:

$$F(t) = G(t)y(t) \tag{2.41}$$

where F(t) is the excitation; G(t) is the system characteristic which may be in the form of differential operators; and y(t) is the response. The system may also be represented in block diagrams as shown in Figure 2.12. If the response sought is the derivative of y(t), that is $\dot{y}(t)$, the system characteristic will be in the form of a linear differential-integral operator which is the integral of G(t). If the system equation describing the system, equation (2.41), is transformed by means of the Laplace transformation, the relation between the excitation and response will become simple algebraic expression where the differential operators are replaced by a subsidiary variable which may be a complex quantity.

The ratio of the transformed excitation to the transformed response will become an algebraic equation, represented by G(s).

$$\frac{\bar{F}(s)}{\bar{y}(s)} = G(s) \tag{2.42}$$

The ratio is called the Generalised Impedance of the system (Ref. 2.35). The reciprocal of this ratio is called the Admittance of the system (Ref. 2.35). The admittance of a pile-soil system has been employed to interpret the integrity of the pile-soil system tested by the vibration methods (Refs. 2.21, 2.22, 2.23, 2.24, 2.36). For more general applications, the Transfer Function which relates the input and output at various points is defined as:

$$G_{ij}(s) = \frac{L(\text{output at point j due to input at point i})}{L(\text{input at point i})} \tag{2.43}$$

In vibration testing of a foundation pile, the excitation and pile responses are measured, the problem is to determine the system characteristics.

2.3.3.1 Steady State Vibration

A free standing pile may be idealised as a mass-spring system subjected to a continuous periodic applied force as shown in Figure 2.13. The mass, M, is supported by a spring which has stiffness, K. The applied force has maximum value F_0 and varies sinusoidally with time with circular frequency p. The behaviour of the one-dimensional system may be expressed using a differential equation (Ref. 2.31, 2.32):

$$M\ddot{x} + C\dot{x} + Kx = F_0\sin(pt) \tag{2.44}$$

where $M\ddot{x}$ is the inertia force of the mass; $C\dot{x}$ is the damping force due to air resistance etc.; and Kx is the resistance force from the spring.

Equation (2.44) may be expressed as:

$$\ddot{x} + 2b\dot{x} + \omega_0^2 x = P_0 \sin(pt) \tag{2.45}$$

where $2b = C/M$; $\omega_0^2 = K/M$; and $P_0 = F_0/M$. The general solution of equation (2.45) is (Ref. 2.32):

$$\dot{x} = Ae^{bt}\sin(\omega t+\varepsilon) + \frac{P_0\sin(pt-\delta)}{[(\omega_0^2-p^2)^2+4p^2b^2]^{0.5}} \tag{2.46}$$

where

$$\delta = \tan^{-1}[2bp/(\omega_0^2-p^2)] \tag{2.47}$$

and

$$\omega^2 = \omega_0^2 - b^2$$

and A and ε are arbitrary constants. The general solution given in equation (2.46) may be considered as the sum of the complimentary function and the particular integral of equation (2.45). The first term on the right hand side of equation (2.46) is the complimentary function while the second term is the particular integral. The complimentary function describes the behaviour of the free vibration of the mass-spring system where damping is introduced by the damping term e^{bt}. The particular integral has the same circular frequency as the driving force, p, but differs in phase from the driving force by the phase angle δ in equation (2.47).

Assuming that there is no damping, $b = 0$, and at low driving frequencies, $p << \omega_0$, the velocity response of the system is:

$$\dot{x} = A\omega_0\cos(\omega_0 t+\varepsilon) + Bp\cos(pt-\delta) \tag{2.48}$$

where,

$$B = P_0/[(\omega_0^2-p^2)+4p^2b^2]^{0.5} \tag{2.49}$$

which shows that the response is mainly affected by the ω_0 term which in turn depends on the stiffness of the spring. The stiffness of the spring in the idealised system is analogous to the stiffness of the free standing pile. This may explain the interpretation of the mechanical admittance of a pile which indicates the dynamic pile head stiffness in testing concrete foundation pile using the vibration methods of testing (Refs. 2.21, 2.23, 2.36).

Again, considering no damping, the general solution given by equation (2.46) represents a motion in the form of beats. Beats is the type of motion obtained when a particle executes two simple harmonic motion of different frequencies simultaneously. At certain times the two motions are in phase with each other and resulted in a large displacement. Since the frequencies of the two vibrations are different, the motion will gradually become out of phase with each other and tends to cancel each other out. A typical case of this is give in Figure 2.14.

2.3.3.2 Resonance

As the frequency of the applied force is varied, the amplitude of the resulting forced vibration will be changed. The phenomenon of the amplitude taking a maximum value is known as resonance (Ref. 2.32). Consider the second term on the right hand side of equation (2.48):

$$Bp\cos(pt-\delta) = \frac{P_0\cos(pt-\delta)}{\{[(\omega_0^2-p^2)/p]^2+4b^2\}^{0.5}} \tag{2.50}$$

Equation (2.50) is maximum when the denominator on the right hand side is minimum. If:

$$y = \{[(\omega_0^2-p^2)/p]^2+4b^2\}^{0.5}$$

then

$$\frac{dy}{dp} = \{[(\omega_0^2-p^2)/p]^2+4b^2\}^{0.5}(p^4-\omega_0^4)/p^3 = 0 \qquad (2.51)$$

Therefore, y is minimum when $p = \omega_0$. The maximum amplitude will be $P_0/2b$. It is also noted that the resonant frequency is independent of the damping. The damping effect only affects the amplitude of the response.

In fact, the idealisation of a pile using one mass-spring-damper system is crude. The pile-soil system may be idealised using more mass-spring-damper systems. Then each lump mass will have one normal mode of vibration and its natural frequency (Ref. 2.32). The general state of motion of the pile will be a combination of the total number of normal modes corresponding to the mass-spring-damper systems representing the pile-soil system. For a uniform pile, the axial resonant behaviour of the pile is similar to the formation of standing waves in an organ pipe. The resonances appeared in harmonics.

The axial resonances may be used to interpret the vibration testing results at high frequencies (Ref. 2.21, 2.23, 2.36).

2.3.3.3 Transient Vibrations

A sudden blow at the pile head is used in transient vibration test to excite the pile-soil system. The vibrations occur in the pile due to the blow is similar to the vibration of the air enclosed in cylindrical pipes (Ref. 2.37).

The elastic deformation of a bar with longitudinal vibration is that the elongation varies from point to point along the bar. The elongation across any section of the bar is instantaneously the same.

When a long bar is vibrating longitudinally in one of its normal modes, the elongation characteristic of any right section of the bar will vary periodically with time. The period of such variation will be the same for all sections and the instantaneous phase will be the same for all sections. The amplitude of the vibration of elongation will vary from section to section.

To find the variation of the amplitudes along the length of the bar with respect to the normal modes of vibrations, a uniform bar which is free of transverse constraints is considered (Figure 2.15). Consider the segment between P and P′ which are at a distance x and x+dx from O. At any instant, when the bar is vibrating longitudinally in a normal mode, the sections has longitudinal displacements u and u+du respectively. The total normal force across the section through P is:

$$F = AE\frac{\partial u}{\partial x} \tag{2.52}$$

where A is the cross-sectional area of the bar and E is the Young's modulus of the material. The total normal force across the section through P′ may be represented by F+dF where:

$$dF = \frac{\partial F}{\partial x}dx \tag{2.53}$$

$$= AE\frac{\partial^2 u}{\partial x^2}dx \tag{2.54}$$

The mass of the segment of the bar under consideration is ρAdx where ρ is the mass density of the bar material. Instantaneously, the acceleration of the segment is given by:

$$a = \frac{dF}{\rho A dx} = \frac{E}{\rho}\frac{\partial^2 u}{\partial x^2} \quad (2.55)$$

For a simple harmonic motion to occur in the bar, the acceleration of the segment is proportional to its displacement, that is:

$$a = -\mu u \quad (2.56)$$

where μ is a constant which is the same for all sections along the bar when the bar is vibrating in a normal mode. Thus:

$$\frac{E}{\rho}\frac{\partial^2 u}{\partial x^2} = -\mu u \quad (2.57)$$

The general solution of equation (2.57) is:

$$u = A \sin[(\sqrt{(\rho\mu/E)}x + \delta] \quad (2.58)$$

Apply the boundary conditions where the strain, $\partial u/\partial x$, is zero at both ends of the bar which is similar to a free end pile 'floating' in the space. Therefore:

$$\frac{\partial u}{\partial x}\Big|_{x=-L/2} = \frac{\partial u}{\partial x}\Big|_{x=L/2} = 0$$

Thus:

$$\cos[(L/2)\sqrt{(\rho\mu/E)} + \delta] = \cos[\delta - (L/2)\sqrt{(\rho\mu/E)}] = 0$$

which gives two sets of solutions:

1) if $\delta = 0$

then, $(L/2)\sqrt{(\rho\mu/E)} = (n+\frac{1}{2})\pi$ (2.59)

2) if $\delta = \pi/2$

then, $(L/2)\sqrt{(\rho\mu/E)} = n\pi$ (2.60)

Substituting equations (2.59) and (2.60) into equation (2.58) gives:

$$u = A\sin[2(n+\tfrac{1}{2})\pi x/L] \tag{2.61}$$

and

$$u = A\cos(2n\pi x/L) \tag{2.62}$$

respectively, where, in respect of either equation, n is any integer. Equation (2.61) describes a series of normal modes each having a node at the centre of the rod. Equation (2.62) represents a series of modes for each of which the centre of the bar is an anti-node. In both cases, the ends of the bar are anti-nodes. Figure 2.16 shows the first three axial resonant modes of a free end pile 'floating' in the space. Now, consider the bar being fixed at $x = -L/2$ and free at $x = L/2$, where L is the length of the bar, which is similar to a fixed end pile. That is:

$$u|_{x=-L/2} = 0 \tag{2.63}$$

and

$$\frac{\partial u}{\partial x}\Big|_{x=L/2} = 0 \tag{2.64}$$

Substituting equation (2.63) into equation (2.58):

$$u = A\sin[(-L/2)(\sqrt{(\rho\mu/E)}+\delta] = 0$$

that is,

$$\delta - (L/2)\sqrt{(\rho\mu/E)} = 0$$

thus,

$$\delta = (L/2)\sqrt{(\rho\mu/E)} \tag{2.65}$$

Substituting equation (2.64) into equation (2.58):

$$\cos[(L/2)\sqrt{(\rho\mu/E)}+\delta] = 0 \tag{2.66}$$

Substituting δ from equation (2.65) into eqaution (2.66), then:

$$\sqrt{(\rho\mu/E)} = (n + \tfrac{1}{2})\pi/L \tag{2.67}$$

The general equation representing the normal mode shapes may be obtained by substituting equations (2.65) and (2.66) into equation (2.58). Thus:

$$u = A\sin[(n+\tfrac{1}{2})\pi(x/L+1/2)] \tag{2.68}$$

The first three axial resonant modes of this bar are shown in Figure 2.17. The two cases shown are the most common situation in a vibrating pile testing. It is obvious that the frequency of the resonant modes of vibration is related to the length of the pile. Therefore, the frequency response of the pile measured on the pile head could indicate the integrity of the pile under test.

2.4 Conclusions

Methods for assessing the load bearing capacity and integrity of structural members have been reviewed. Particular interest has been shown on Non-Destructive Methods of Testing Pile Foundations. The methods of non-destructive testing of foundation piles may be applied to test other structures or structural members by slight modifications to the methods.

The earth resistance method, sonic echo method and the vibration methods of non-destructive testing were chosen for further studies. The theories behind the operations of these methods were presented. It appeared that the earth resistance method of pile testing may provide qualitative indication of the integrity of the pile-soil system. The sonic echo method of pile testing may also give indications of the integrity of a pile while the location and extent of the defect may be assessed. The vibration methods of pile testing may be used to assess the integrity of a pile while the stiffness of the pile-soil system may also be assessed. Due to the similarity in operation between the sonic echo method of testing and the transient vibration method of testing, the two methods of testing may be combined to provide the engineer with more information about the integrity of a pile under test.

References 2.

1. Weltman, A.J., "Integrity testing of Piles: A Review", DoE and CIRIA, Piling Development Group Report PG4, September, 1977.

2. Savage, R.J., "Review of Non-Destructive Testing of Structures", NDT 83, Proceedings of the International Conference on Non-Destructive Testing, Engineering Technics Press, 124-141, 1983.

3. Tomlinson, M.J., "Pile Design and Construction Practice", Cement and Concrete Association, 1977.

4. Fegen, I., "Testing Concrete Foundation Piles by Sonic Echo", Ph.D. Thesis University of Edinburgh, 1981.

5. Long, A.E., "A Review of Methods of Assessing the In-Situ Strength of Concrete", NDT 83, Proceedings of the International Conference on Non-Destructive Testing, Engineering Technics Press, 56-76, 1983.

6. Keiller, A.P., "An Investigation of Test Methods for the Assessment of Strength of In-Situ Concrete", NDT 83, Proceedings of the International Conference on Non-Destructive Testing, Engineering Technics Press, 45-55, 1983.

7. Chabowski, A.J., Bryden-Smith, D.W., "A Simple Pull-Out Test to Assess the Strength of In-Situ Concrete", Precast Concrete, Vol. 8, No. 5, May, 1977, 243-246, 258. Reprinted as BRE Current paper CP25/77, June, 1977.

8. Chabowski, A.J., Bryden-Smith, D.W., "Assessing the Strength of In-Situ Portland Cement by Internal Fracture Tests", Magazine of Concrete Research, Vol. 32, No. 112, 164-172, September, 1980.

9. Keiller, A.P., "Technical Report 551: A Preliminary Investigation of Testing Methods for the Assessment of Strength of In-Situ Concrete", Wexham Springs, Cement and Concrete Association, September, 1982.

10. Stenho, G., Mall, G., "The Tear-Off Method - A New Way to Determine the Quality of Concrete in Structures on Site", RILEM Symposium: Testing In Situ of Concrete Structures, September, 1977, Budepest, Proceedings Vol. 2, 335-347.

11. Long, A.E., Murray, A., "Pull-Off Test for In-Situ Concrete Strength", Concrete, Vol. 15, No. 12, 23-24, December, 1981.

12. Savage, R.J., "Critical Review and Appraisal of NDT Methods", University of Edinburgh, Symposium on Structural Faults - Inspection and Repair, 22-24, March, 1983.

13. Jones, R., "A Review of the Non-Destructive Testing of Concrete", Symposium on Non-Destructive Testing of Concrete and Timber, The Institution of Civil Engineers, 1970.

14. Jackson, N., "Civil Engineering Material", The MacMillan Press Ltd., 1980.

15. Bobrowski, J., Bardhan-Roy, B.K., Magiera, R.H., Lowe, R.H., "The Structural Integrity of Large Diameter Bored Piles", in 'Behaviour of Piles': Proc. Conf. I.C.E., London, 1971.

16. McCarter, W.J., "Resistivity Testing of Piled Foundations", Ph.D. Thesis, University of Edinburgh, 1981.

17. Paquet, J., "Étude Vibratoire Des Pieux En Béton Réponse Harmonique et Impulsionnelle Application au Controle", Annls. Inst. Tech. Batim., 21st year, No. 245, 789-803, May, 1968.

18. Steinbach, J., Vey, E., "Caisson Evaluation by the Stress Wave Propagation Method", Journal of the Geotechnical Engineering Division, Proceedings of the American Society of Civil Engineers, Vol. 101, No. GT4, 361-378, April, 1975.

19. Byle, R., "Dutch Strike a Blow for Integrity Testing", New Civil Engineer, 26, 11 June, 1981.

20. Paquet, J., Briard, M., "Controle Non Destructif des Pieux en Béton, Carottage Sonique et Méthode de L'impedance Méchanique", Annls. Inst. Tech. Batim., No. 337, 50-80, March, 1976.

21. Davis, A.G., Dunn, C.S., "From Theory to Field Experience with the Non-Destructive Vibration Testing of Piles", Proceedings of The institution of Civil Engineers, Part 2, 571-593, December, 1974.

22. Davis A.G., Robertson, S.A., "Vibration Testing of Piles", Structural Engineer, June, 1976.

23. Higgs, J.S., "Integrity Testing of Concrete Piles by Shock Method", Concrete, 31-33, October, 1979.

24. Stain, R.T., "Integrity Testing", Civil Engineering, 53-73, April, 1982.

25. Kreyszig, E., "Advanced Engineering Mathematics", Third Edition, John Wiley and Sons, Inc., 1972.

26. Koefoed, O., "Geosounding Principles 1: Resistivity Sounding Measurement", Elsevier Scientific Publishing Company, 1979.

27. Grant, F.S., West, G.F., "Interpretation Theory in Applied Geophysics", McGraw-Hill, Inc., 1965.

28. Parasnis, D.S., "Principles of Applied Geophysics", Methuen and Company Limited, London, 1967.

29. Griffiths, D.H., King, R.F., "Applied Geophysics for Engineers and Geologists", Pregamon Press Ltd., 1965.

30. Telford, W.M., Geldart, L.P., Sheriff, R.E., Keys, D.A., "Applied Geophysics", Cambridge University Press, 1976.

31. Mains, I.G., "Vibrations and Waves in Physics", Cambridge University Press,

1978.

32. Gough, W., Richards, J.P.G., Williams, R.P., "Vibrations and Waves", Ellis Horwood Ltd., 1983.

33. Richart, F.E., Hall, I.R.Jr., Woods, R.D., "Vibrations of Soils and Foundations", Prentice-Hall Inc., 1970.

34. Timoshenko, S.P., Goodier, J.N., "Theory of Elasticity", International Student Edition, McGraw-Hill Kogakushe Ltd., 1970.

35. Meirovitch, L., "Analytical Methods in Vibrations", The MacMillan Company, 1967.

36. Ellway, K., Crawford, R., "Vibration Testing Clarified", NDT 83, Proceedings of the International Conference on Non-Destructive Testing, Engineering Technics Press, 158-166, 1983.

37. Feather, N., "An Introduction to the Physics of Vibrations and Waves", Edinburgh University Press, 1961.

Chapter 3

Simulation Methods

3.1 Introduction

The closed form solutions for the three non-destructive testing methods given in Chapter 2 have indicated that the integrity of a pile-soil system may be assessed from the characteristic response of the pile-soil system to a controlled input. To verify these solutions, the idealised conditions which may be made attainable by using analogue models are generally preferred. Analogue models are more attractive to researchers than field experiments because of their lower associated costs and fewer difficulties in preparing the experiments. McCarter (Ref. 3.1) and McCarter et. al. (Ref. 3.2) have undertaken experimental investigation into the earth resistance method using electrical analogues, the conductive sheet analogue and the electrolytic tank. Steinbach et. al. (Ref. 3.3) worked on scaled physical models to establish the application of the theory of stress-wave propagation in a cylinder. Aluminium and concrete bars were used in his studies. The aluminium bar, whose cross sectional area along its length may be modified easily by machining, was also used to show that the stress wave propagation method (sonic echo method) may be used to detect abrupt changes in cross sectional areas in a free bar. Fegen (Ref. 3.4) also employed scaled models for his study of the application of the sonic echo method on testing foundation piles. Electric analogues were used by Paquet (Ref. 3.5), Briard (Ref. 3.6), Davis et. al. (Ref. 3.7) and Swann (Ref. 3.8) in the study of the vibration method of testing foundation piles. A pile-soil system was represented by an electric circuit where the applied current source and the output voltage are equivalent to the applied vibration force and the pile head movements. Ellway et. al. (Ref. 3.9) illustrated the behaviour of regular and defective piles to an axial excitation force applied at the pile head using mechanical analogues. The pile shaft was represented by a series of interconnected masses and springs while the soil effects are simulated by spring elements and dampers.

Observations from the analogue models may also be applied to the interpretation of field data. To a certain extent, the analogue models may be useful in the development of testing methods.

The analogue models employed in the development of the three non-destructive testing methods will be described in this chapter. Some of the shortcomings of using the analogue models and how these problems may be overcome by using the numerical model, finite element method, will also be discussed in this chapter.

3.2 The Use of the Electric Analogue for the Study of the Earth Resistance Method of Pile Testing

3.2.1 The Conductive Sheet

McCarter (Ref. 3.1) and McCarter et. al. (Ref. 3.2) used a conductive sheet analogue to study two dimensionally the electric field distribution around a reinforced pile and the disturbing effects which are associated with pile defects and other anomalies. The commercially available graphitised paper, which is also known by its trade name, Teledeltos, was used. The paper has a resistivity in the region of 1000 ohms per square.

3.2.1.1 The Specification of Conductive Sheet

In specifying the resistivity of a conductive sheet, it is customary to measure the resistance across opposite faces of a square of the material by employing two strip electrodes extending over the entire length of the specimen. The resistivity is defined as the ratio of the voltage difference between the electrodes to the current which flows as a result. It is directly proportional to the distance between the two faces and inversely proportional to the length of these faces. Therefore, the dimensions of the square do not affect the resistivity, and this parameter has the units of ohms per square.

3.2.1.2 The Resistance Paper - Teledeltos

Teledeltos paper, which was originally developed as a recording medium for telegrams, is formed by adding carbon black to paper pulp in the pulp-beating stage of the paper-manufacturing process (Ref. 3.10). The paper thus formed has a uniform dispersion of carbon which acted as a conductive material. This conductive paper is then coated on one side with a lacquer, which acts as an electrical insulator, and on the other side with a layer of aluminium paint. An enlarged cross-section of the Teledeltos paper is given in Figure 3.1.

The application of the Teledeltos paper to the two dimensional study of the earth-resistance response of a reinforced concrete pile consists of three basic steps (Refs. 3.1, 3.10). The conductive paper is prepared in such a way that it has the same geometrical shape as the field under study. Then, the boundary conditions of the particular field are simulated in the scaled analogue system by means of suitable current sources and sinks. Finally, the voltage distribution within the conductive sheet is measured and recorded by means of a suitable sensing equipment.

3.2.1.3 Change of Resistivity in the Conductive Sheet Analogue

The simulation of local changes in the resistivity in the conductive sheet analogue may be achieved by perforating the paper, by applying several layers of a graphite solution, or by extending the scaled dimensions of the medium of higher resistivity. The reason for these effects may be explained by the following relationship:

$$R = \frac{\rho L}{A} \tag{3.1}$$

where R is the resistance of the paper in ohms; ρ is the resistivity of the paper in ohm-m; L is the length of the paper in m; and A is the cross-sectional area of the paper in m^2. Therefore, punching holes in the paper reduces the cross-sectional area for conduction and thus increases the resistance of the paper. The application of several layers of graphite solution and the scaled dimensions directly increase the resistance in equation (3.1).

3.2.1.4 Boundary Conditions

Boundary conditions involved in the electrical analogue investigation of the earth-resistance response of a reinforced concrete pile are specified potentials along certain boundaries. The specified potential along a boundary is equivalent to an equipotential. Silver paint, a conducting paint containing a high percentage of finely divided silver, is preferred as the electrode material for equipotential boundaries (Ref. 3.10) and may be applied using a small brush. Connections to the equipotential boundary may be made by embedding the copper wire into the paint and over the full length of the boundary and using the paint as an adhesive.

A termination of the conductive sheet represents a flow line in the analogue system. Therefore, the simulation of an infinite media by terminating the Teledeltos paper at a certain distance is bound to introduce errors. The errors may be minimised by terminating the Teledeltos paper at a sufficiently large distance relative to the region interested.

3.2.1.5 Plotting the Equipotentials

After the Teledeltos paper has been prepared to have similar geometrical shape as the prototype and the boundary conditions are applied, the equipotential distributions in the system may be plotted. A schematic layout of the application of the Teledeltos analogue to the study of the earth-resistance response of a reinforced concrete pile is given in Figure 3.2.

The source and sink in the system is firstly checked for as the 100% and 0% equipotentials. Then the potentiometer is set successively to 90%, 80%, ... and the corresponding equipotential lines are plotted using a null balance technique. The technique is to locate points on the Teledeltos paper which has the same percentage of voltage drop from the source as that set on the potentiometer. The points will be found as a balance of the scale when the probe is touching a point having the same voltage drop from the source as the potentiometer.

When required, the current flow lines may be sketched by hand such that they cut the equipotential lines orthogonally forming squares.

3.2.1.6 Advantages and Disadvantages

The advantages of using the Teledeltos paper is that it is easy to operate and convenient to use in the simulation of two dimensional field problems.

There are also some disadvantages of using the Teledeltos paper. The paper may be easily damaged by the probe or by bending. In addition, the paper absorbs moisture which may make the simulation sensitive to temperature variation.

In general, the application of the conductive-sheet analogue suffers from the defect that it does not simulate correctly the properties of the original field; it may not simulate the boundary conditions correctly and errors may be introduced during sensing and plotting of the equipotentials. These problems are due to the nonuniformity, inhomogeneity and anisotropicity of the sheet. In addition, the conduction properties of paper may be changed due to a change in the moisture content or the temperature of the paper. Perhaps the errors due to the instruments and during the application of the boundary conditions will also affect the final results.

3.2.2 The Electrolytic Tank

The two dimensional conductive-sheet analogue enables qualitative studies on the earth-resistance response of a reinforced concrete pile and the disturbing effects due to a defect or an anomaly in a pile. However, the conductive-sheet analogue is restricted to the simulation of situations where the resistivity of concrete is higher than the surrounding soils (Ref. 3.1). For problems which can be formulated only in three dimensions such as the application of the earth-resistance method of non-destructive testing in the field, three dimensional conductive analogues are required (Ref. 3.10). One of such three dimensional analogues which is convenient to use is the electrolytic tank.

The basic principles underlying the operation of the electrolytic tank and the conductive-sheet analogue system are similar (Ref. 3.10). For the simulation of the application of the earth-resistance method of non-destructive testing in the field, a tank of suitable dimensions and filled with an electrolyte is required to represent the ground. The electrolyte used by McCarter (Ref. 3.1) and McCarter et. al. (Ref. 3.2) is brine solution. The advantages of using brine solution as the electrolyte are that the resistivity of the electrolyte may be adjusted by adjusting the proportion of the solute and solvent; the isotropy and homogeneity of the electrolyte are more certain; the longitudinal profile may be measured; and good electrical contact can be obtained between the electrodes and the electrolyte.

Perfect and typical defective pile scaled models were used to study the disturbing effects on the resistance measurements due to a defect in a pile. Unlike the qualitative information which can be obtained using the conductive-sheet model, the electrolytic tank analogue allows a quantitative study of the earth-resistance method of testing in a field.

The fibre reinforced plastic tank used by McCarter (Ref. 3.1) and McCarter et. al. (Ref. 3.2) simulated a streamline boundary. Therefore, some errors may be expected due to this termination of the boundary to simulate an infinite boundary. McCarter (Ref. 3.1) and McCarter et. al. (Ref. 3.2) attempted to minimise this error by using a relatively small model compared to the dimensions of the tank.

The choices of the probe and the applied current source may affect the measurement of the potential in the electrolyte. The probe should be as small as possible to ensure that the introduction of the electrolyte will not distort the potential field. On the other hand, the probe should be stiff enough so that it will not bend while traversing the electrolyte. The material used for the probe should not react with the electrolyte chemically nor should it be dissolved by the electrolyte. The probe used by McCarter (Ref. 3.1) and McCarter et. al. (Ref. 3.2) was made of graphite. The polarisation effects in the immediate vicinity of the electrode (model pile and the return electrode) may be minimised by choosing a suitable combination of electrolyte and electrodes

(Refs. 3.10, 3.11). However, McCarter (Ref. 3.1) has suggested the use of a square wave excitation in his electrolytic tank analogue to reduce the polarisation effects. In addition, Karplus (Ref. 3.10) also suggested that the signals at the probe and the potentiometer arm should be in phase with each other to obtain a true null indication of the potentiometer.

McCarter (Ref. 3.1) and McCarter et. al. (Ref. 3.2) used this analogue model to study qualitatively the disturbing effects on the earth-resistance measurements due to anomalies in a model pile by comparing the earth-resistance curves between a perfect pile model and a defective pile model. The analogue can simulate a real field situation where the soil is homogeneous and the conductivity of the soil is isotropic in all directions.

In a real site, however, the soil may be layered and the conductivity of the soils may be different in different directions. In these cases, the application of the electrolytic tank analogue becomes inappropriate. The size of the analogue is restricted by the size of the tank. The model piles, which are also restricted by the size of the tank, are not flexible to changes so that a model pile has to be casted for different cases considered. For variations in the relative resistivity between the pile and the soil, the casting of a different model pile may be avoided by changing the resistivity of the background medium, the electrolyte, to provide the required relative resistivity between the pile and the soil. The measurement of the potentials below the surface of the electrolyte is difficult and the immersion of the probe into the electrolyte is bound to introduce error in the measurement. Although the errors introduced during the measurement of potentials in the analogue may happen in a field test, the scale of the error may be different in the two cases. Owing to the close spacing of the electrodes and the probes required in a limited size electrolytic tank, measurements of the field strength may be difficult. This effect is significant when electric field measurements are required near to an electrode.

3.3 A Scaled Model for the Study of the Sonic Echo Method of Testing

One of the most popular type of analogue model used in fluid mechanics and structures is the scaled model. It is usually more economical to construct a scaled model and carry out tests on the model in order to predict the behaviour of the prototype in a similar situation. In a scaled model, every element of the prototype is reproduced, only different in size. The excitation applied to the model should also be scaled accordingly. It is essential to have the dimensional conformity between the scaled model and the prototype retained. That is, the relationships between the characteristics of the scaled model and the prototype must be dimensionally correct. However, this has restricted its application to model prototypes where mass is involved because the gravitational constant g cannot be scaled down. Another difficulty in applying scaled model technique is the difficulty in making accurate measurements at points within the field. Frequently, it is physically impossible to insert a suitable measuring device into a three dimensional field.

The first restriction mentioned above, however, does not restrict its application to the investigation of pulse propagation along a rod. The difficulties in applying the scaled model to study the sonic echo method of testing are the choices of suitable measuring device and a suitable material for the model. Fegen (Ref. 3.4) found that the use of short laboratory specimens of metal or concrete (Ref. 3.3) resulted in small time separation between the input and reflected pulses. He tackled the problem by constructing a larger scaled model (Plate 3.1) in an attempt to provide a systematic analysis under close controlled conditions while retaining some of the realities of full size operations. In fact, the small time separation between the signals may be increased by choosing a different combination of material properties for the model pile as well as that for the hammer head used to apply the pulse. These material properties governed the contact time between the hammer head and the pile head. And this in turn governed the wavelength of the input pulse. The material property of the model pile determines the speed at which the pulse may propagate along the model pile. These are the factors which may be considered in order to improve the results from the scaled model without building a full size model which is expensive, time consuming and requires space for its construction and storage.

3.4 An Electric Analogue for the Study of the Steady State Vibration Method of Testing

It is a common approach to study the pile drivability using the finite difference method by idealising the soil as massless medium providing frictional resistance alone, while the pile is modelled as a discrete assembly of mass elements interconnected by springs. The model was first developed by Smith (Ref. 3.12) and was used by Ellway et. al. (Ref. 3.9) to study the response of a pile-soil system to an applied axial vibration at the pile head using a similar mass-spring-damper system. The pile was idealised as a series of interconnected mass and springs (Figure 3.3). The masses (M_p) represented the mass per unit length of the pile shaft. The spring (K_p) represented the spring stiffness of the pile shaft. The soil effects were idealised as springs in parallel with dampers. The springs (K_s) represent the shear stiffness of the soil surrounding the shaft. The dampers (D_s) are related to the amount of vibrational energy dissipated from the pile shaft into the soil as shear waves. The end bearing support at the toe of the pile is represented by a spring (K_t)

which corresponds to the effective ground stiffness at the toe of the pile.

The basic reason for the existence of analogy is rooted in the fact that the same principles were used in setting up the differential equations which describe the behaviour of systems in most areas of physics (Ref. 3.10). These principles are the laws of conservation of energy and continuity. Since the same laws are applicable to a mechanical system and an electrical system, the characteristic equations are similar in form. Therefore, the response of a pile-soil system may be predicted by making use of the analogue which exists between mechanical wave propagation and an electrical transmission line (Refs. 3.5, 3.6, 3.7). The analogy between these two systems may be demonstrated by noting the similarities between the characteristic equations of the two systems. Figure 3.4 shows a mechanical circuit while Figure 3.5 illustrates an electric circuit.

3.4.1 The Mechanical Circuit

The equation for the deflection x of the spring in Figure 3.4 may be found by means of Newton's second law, which states that the sum of all external forces acting upon a mass is equal to the inertia response of the mass. The statement may be summarised as follows for quiescent initial condition:

Inertia force of mass + Damping force of dashpot + Spring force = Upward force acting as source

$$M\frac{d^2x}{dt^2} + D\frac{dx}{dt} + Kx = F(t) \tag{3.2}$$

3.4.2 The Force-Voltage Analogue

The electric circuit shown in Figure 3.5 consists of a resistance, R, an inductance, L, a capacitance, C, and a time dependent voltage source e(t) connected in series. If i(t) denotes the loop current, from Kirchhoff's law, which states that the sum of the voltage drops around a closed loop is equal to zero, the equation for electric circuit is:

Voltage drop across inductaor + Voltage drop across resistor + Voltage drop across capacitor = Voltage source

or

$$L\frac{d^2q}{dt^2} + R\frac{dq}{dt} + \frac{q}{C} = e(t) \tag{3.3}$$

where $q(t) = \int i(t)dt$

The analogy is often called the 'force-voltage analogy' (Ref. 3.13) and is the most widely mentioned analogy between mechanical and electrical systems (Refs. 3.14, 3.15, 3.16). The electric circuit in Figure 3.5 is thus an analogous system of the spring-mass-damper system shown in Figure 3.4 in the sense that a time-dependent voltage source will produce a current in the circuit in an analogous way as a time-dependent force imparts a velocity to the mass of the spring-mass-damper system.

3.4.3 The Force-Current Analogue

An electrical analogue for the same mechanical system is given in Figure 3.6. This circuit consists of a capacitance, C, a resistance, R, and an inductance, L, connected in parallel to a time-dependent current source i(t). If e(t) is the voltage drop across the three parallel elements, the branch currents flowing in these elements are:

$$i_c = C\dot{e} \tag{3.4}$$

$$i_r = \frac{e}{R} \tag{3.5}$$

$$i_l = \frac{1}{L}\int e\,dt \tag{3.6}$$

Since the sum of the branch currents must be equal to the current from the current source, thus:

$$C\dot{e} + \frac{1}{R}e + \frac{1}{L}\int e\,dt = i(t) \tag{3.7}$$

Putting $q(t) = \int e(t)dt$, equation (3.7) may be expressed as:

$$C\ddot{q} + \frac{1}{R}\dot{q} + \frac{1}{L}q = i(t) \tag{3.8}$$

This analogy is called a 'force-current analogy' (Ref. 3.13). Hence, the voltage response to a current source is analogous to the velocity response of a mechanical system to an applied force.

3.4.4 The Relationships between Analogues

The mechanical circuit in Figure 3.4 could be studied or simulated by the electric circuit shown in Figures 3.5 and 3.6. The corresponding variables in the analogies may be summarised in Table 3.1:

Mechanical System	Force-Voltage Analogue	Force-Current Analogue
Force (F)	Voltage (e)	Current (i)
Mass (M)	Inductance (L)	Capacitance (C)
Spring Constant (K)	Reciprocal Capacitance (1/C)	Reciprocal Inductance (1/L)
Damping (D)	Resistance (R)	Conductance (1/R)
Displacement (x)	Charge (q)	Integral of Voltage ($\int vdt$)
Velocity ($\dot{x}$, v)	Current (i)	Voltage(e)
Acceleration ($\ddot{x}$)	Derivative of Current ($\dot{i}$)	Derivative of Voltage ($\dot{e}$)

Table 3.1

3.4.5 A Simulation for Vibration Method of Testing

The analogue model employed by Paquet (Ref. 3.5), Briard (Ref. 3.6) and Davis et. al. (Ref. 3.7) is shown in Figure 3.7. The approach was the force-current analogue. The applied force, F_t, is regarded as analogous to the applied current, I_t. The velocity at the pile head is analogous to the voltage, e_t. The mass of the pile per unit length is represented by a capacitance, C_p. The stiffness per unit length of pile is represented by the inductance, L_p. The resistance per unit length due to soil is represented by the inductance, L_s. The damping effect due to the soil is represented by the resistance, R_s. The stiffness at the base of the pile is represented by another inductance, L_b. The mechanical admittance |V/F| required for the interpretation of the vibration tests may be obtained from the corresponding electrical impedance |e/I|. Electric impedance is defined by Rocard (Ref. 3.14) as the quotient of a potential difference by the intensity of current created in a circuit system. In fact, the electric circuit analogue models mentioned by Paquet (Ref. 3.5), Briard (Ref. 3.6) and Davis et. al. (Ref. 3.7) were not built in their studies for the vibration method of testing and the electrical admittance was not measured directly from the analogue model. The electrical admittance was determined by solving sets of equations, which described the electric circuit, using a computer. The general form of the equations may be derived by considering the circuit in Figure 3.7 in blocks. The derivation of the general equation is due to Ref. 3.17. Considering the block between 1 and 2 in Figure 3.7:

$$e_2 = \left(1 + \frac{Z_2}{Z_1}\right)e_1 - Z_2 i_1 \tag{3.9}$$

and

$$i_2 = i_1 - \frac{e_1}{Z_1} \tag{3.10}$$

where,

$$Z_1 = j\omega L_p \tag{3.11}$$

and,

$$Z_2 = \frac{1}{j\omega C_p + \frac{1}{R_s} + \frac{1}{j\omega L_p}} \tag{3.12}$$

in which ω is the applied freqency from the source and j equals $\sqrt{(-1)}$.

Expressing equations (3.9) and (3.10) in matrix form:

$$\begin{pmatrix} e_2 \\ i_2 \end{pmatrix} = \begin{bmatrix} 1+\frac{Z_1}{Z_2} & -Z_2 \\ -\frac{1}{Z_1} & 1 \end{bmatrix} \begin{pmatrix} e_1 \\ i_1 \end{pmatrix} \tag{3.13}$$

$$\begin{pmatrix} e_2 \\ i_2 \end{pmatrix} = [A_1] \begin{pmatrix} e_1 \\ i_1 \end{pmatrix} \tag{3.14}$$

In fact, the output at 2 may be considered as an input for the block between 2 and 3. Thus, equations (3.13) and (3.14) may be considered as a general relationship for each block. Applying this general equation to each block and the general equation for the system is:

$$\begin{pmatrix} e_{n+1} \\ i_{n+1} \end{pmatrix} = [A_n] \text{ .... } [A_2][A_1] \begin{pmatrix} e_1 \\ i_1 \end{pmatrix} \tag{3.15}$$

where $[A_n]$ is the matrix relating the output voltage and output current to the input voltage and input current for block n. The ratio of $|e_n/i_n|$, which is equivalent to the mechanical admittance of the pile, may be found for each applied frequency for a known end condition, e_1 or i_1.

3.5 The Finite Element Method

Karplus (Ref. 3.10) reviewed that any problem solvable by analogue models can be solved by numerical models and with greater accuracy. Numerical modelling can duplicate and refine any analogue process to sufficient magnitude and complexity. Therefore, numerical models must be regarded as a more powerful research tool than the analogue models. Thus, the application of the finite element technique to the study of the non-destructive methods of testing, which has been studied by using analogue models, should be appropriate. Perhaps, analogue models and field tests are also required to validate the finite element models. Using the finite element approach can greatly reduce the cost and time for building a large number of analogue models for both qualitative and quantitative studies of the testing methods.

The finite element method is an approximating technique where a continuum is idealised into a finite number of elements. The elements may be polygons in two dimensional space or polyhedral brick in three dimensional space. The behaviour of the elements due to an applied cause may be expressed as a general matrix relationship. The general matrix relationship for each element may be combined throughout the continuum according to the law of continuity between the finite elements. A complete solution may be obtained by the solution of the combined matrix equations.

In the simulation of stratified ground, where the earth resistance test was applied, a finite element model would be more suitable than the electrolytic tank model because the properties of each finite element can be defined differently. In addition, both the resistivity of the pile concrete and the soil may be changed as required for different pile-soil systems. It may be expensive and time consuming to prepare different pile models for a qualitative study of the testing method. The choice of a suitable pair of electrode and electrolyte is not required in the finite element approach. The results from the finite element analysis are reproducible and are not subjected to change due to the variation of the ambient temperature or moisture as it would be in the conductive sheet analogue.

The shape of the input signal may be varied by using the finite element method. The pulse width, which is the contact time between the hammer and the pile head when the pulse is applied, is also variable. These are very useful in the development of the testing method in choosing a suitable means to apply the pulse. The pile size and the type and size of a defect may be simulated by the finite element method. The response at any point in the pile-soil system may be investigated in the finite element analysis.

The pile-soil interaction may also be simulated by the finite element technique. Again, the effects due to the soil properties may be understood by varying the elastic properties of the soil. The possible signal processing techniques may also be studied by computer modelling. That is, the whole procedure for testing may be understood and any shortcomings in any of the process may be revealed.

Both the steady state and the transient state vibration testing methods may be studied using the same finite element idealisation. It may be expensive to use the finite element method to simulate the steady state vibration test as the analysis may have to be repeated for each applied frequency if time domain analysis is used. For the transient state vibration test, the process is similar to the sonic echo test except for the method used for signal processing. Apart from the computing costs, the finite element technique has many advantages over the analogue models as variation in the models may easily be taken care of by changing the input data. Therefore, a wide range of case studies may be undertaken.

3.6 Conclusions

The analogue approaches to the study of the earth resistance method, the sonic echo method and the vibration methods of pile testing were reviewed. A numerical method, the finite element technique is proposed as an alternative of the analogue models. For the purpose of research, the finite element technique is suitable because a controlled, idealised situation may be studied and compare with closed form solutions and analogue model results. Complicated situations may be simulated by changing the shape or material properties with the idealised finite element domain. Only a few physical or analogue models are required for the validation of the finite element simulations. This greatly reduced the expenses and difficulties in preparing physical and analogue models. In addition, the finite element technique may produce more accurate measurements than the analogue models. The material properties in the finite element simulation tests may be kept constant while the material properties in an analogue model may vary due to a change in the ambient temperature or humidity. The use of the finite element simulation can also avoid the difficulties in choosing some suitable measuring equipment and no error will be introduced by measuring the response. The finite element approach can also reduce the problem in converting the measurements between two analogue systems.

Engineers are more familiar with the finite element analysis than the electric analogues. Therefore, the interpretation of the non-destructive testing methods using finite element approach would be easily accepted by engineers. Since the finite element method is a computer based technique, the required signal processing on the measured responses from the system may also be simulated by using additional computer programmes. The finite element simulation results are more readily presented in a table or graphical form for comparison with the field test results. Since large amounts of simulated test results may be stored in the computer, the interpretation of the field test results by comparing the simulation results with the field test results is made easier. The same finite element idealisation may be used to interpret results from different tests. The finite element method may be developed so that the same programme may be used for the interpretation of test results from different tests.

Although the finite element simulation has been shown to be a good alternative to the analogue models, its appropriateness for modelling should be judged by the availability of adequate computer resources and the adequate knowledge of the material properties to be simulated. Handling of input data for finite element analysis has been simplified by using automatic mesh generation programmes. However, the analysis itself still requires a large amount of computer resources which depend on the size of the problem and the fineness of the finite element mesh required. Therefore, the finite element analysis will not be possible if these resources are inadequate or the computing time allowed for an analysis is not long enough. As a tool for the qualitative studies in the development and feasibility assessment of the application of the non-destructive testing methods, typical material properties may be used in the analysis. More precise material properties are required as input data to the finite element analysis when it is to interpret field test results. Therefore, the ability of the finite element analysis to interpret field test results is dependent on the availability of data on the material properties to be simulated.

References 3.

1. McCarter, W.J., "Resistivity Testing of Piles Foundation", Ph.D. Thesis, University of Edinburgh, 1981.

2. McCarter, W.J., Whittington, H.W., Forde, M.C., "An Experimental Investigation of the Earth-Resistance Response of a Reinforced Concrete Pile", Proceedings of the Institution of Civil Engineers, Vol. 70, Part 2, 1101-1129, 1981.

3. Steinbach, J., Vey, E., "Caisson Evaluation by the Stress Wave Propagation Method", Journal of the Geotechnical Engineering Division, Proceedings of the American Society of Civil Engineers, Vol. 101, No. GT4, 361-378, April, 1975.

4. Fegen, I., "Testing Concrete Foundation Piles by Sonic Echo", Ph.D. Thesis, University of Edinburgh, 1981.

5. Paquet, J., "Étude Vibratoire Des Pieux En Béton Réponse Harmonique et Impulsionnelle Application au Controle", Annles. Inst. Tech. Matim., 21st year, No. 245, 789-803, May, 1968.

6. Briard, M., "Controle Des Pieux Par La Méthode Des Vibrations", Annles. Inst. Tech. Batiment, Vol. 23, Part 270, 105-107, June, 1970.

7. Davis, A.G., Dunn, C.S., "From Theory to Field Experience with the Non-Destructive Vibration Testing of Piles", Proceedings of the Institution of Civil Engineers, Part 2, 571-593, December, 1974.

8. Swann, L.H., "The Use of Vibration Testing for the Quality Control of Driven Cast In-Situ Piles", NDT 83, Proceedings of the International Conference on Non-Destructive Testing, Engineering Technics Press, 113-123, 1983.

9. Ellway, K., Crawford, R., "Vibration Testing Clarified", NDT 83, Proceedings of the International Conference on Non-Destructive Testing, Engineerig Technics Press, 158-166, 1983.

10. Karplus, W.J., "Analog Simulation", McGraw-Hill Book Company, Inc., 1958.

11. Sander, K.F., Yates, J.G., "The Accurate Mapping of Electric Fields in an Electrolytic Tank", Proc. Inst. Elect. Engrs., Part II, Vol. 100, 167-183, 1953.

12. Smith, E.A.L., "Pile Driving Analysis by the Wave Equation", Journal of the Soil Mechanics and Foundation Division, Proceedings of the American Society of Civil Engineers, Vol. 86, No. SM4, 35-61, 1960.

13. Tong, K.N., "Theory of Mechanical Vibration", John Wiley and Sons, Inc., 1960.

14. Rocard, Y., "General Dynamics of Vibrations", Crosby Lockwood and Son, Ltd., 1960.

15. Jones, D.S., "Electrical and Mechanical Oscillations", Routledge and Kegan

Paul Ltd., 1961.

16. Main, I.G., "Vibrations and Waves in Physics", Cambridge University Press, 1978.

17. Lam, S.C.K., University of Edinburgh, Private Communication, 1986.

Chapter 4

Finite Element Formulation

4.1 Introduction

This chapter will briefly describe the formulation of the Finite Element Analysis for static and dynamic problems. The simulation of the Earth Resistance Method of Non-Destructive Testing may be considered as a field problem. The simulation of the Sonic Echo Method and the Vibration Methods of Non-Destructive Testing may be treated as a dynamic problem. The finite element method is a very popular tool used for structural analysis and the formulation of the method has been widely published (Refs. 4.1, 4.2, 4.3, 4.4, 4.5, 4.6, 4.7). The finite element formulation for a two dimensional field analysis will be presented. The system of equations will be modified for two dimensional plane stress or plane strain analysis and a time dependent applied load is used to simulate the Sonic Echo Method and the Vibration Methods of Testing. The application of an energy absorbing boundary in the simulation of the response of a pile-soil system under an applied impulse will be illustrated. Finally, some pre- and post-processing data techniques are also discussed.

4.2 The Static Field Problem

The basis of the finite element method is to represent the actual continuum by an approximate structural idealisation consisting of a finite number of individual elements. The elements are connected at their nodes and along common element sides according to the nature of the structure. A solution for the field problem is sought at the nodes.

The continuum structure shown in Figure 4.1 is subjected to an applied source $\{P\}$. The applied source may be the applied current in an electricity flow problem or the applied loading in a structural analysis problem. The applied source may be concentrated as a point source or uniformly distributed on the edge or over the surface of the element as traction. The domain of the structure is denoted by Ω and the boundary by Γ. Along the boundary, there are some parts which are specified and denoted by ϕ_s. These parts may be a region of fixed potential for an electricity flow problem or a structural support in a structural analysis. In the discretised structure, the sub-domains are denoted by Ω_e and the sub-boundaries by Γ_e. The behaviour of the overall structure is thus the sum of the behaviour of each of the sub-domains.

Different approaches such as the energy methods and the residual methods are available for the formulation of the finite element relationships. In this chapter, a method equivalent to the principle of virtual displacement will be applied to the formulation of the Admittance Relations for the Finite Element Analysis of the electricity flow in a continuum. The admittance relations express the relationship between the distribution of the electrical potential in a medium under the constraints of the applied current and the boundary potential conditions. Three node triangular finite elements will be used for the derivation of the admittance relations. These elements will also be used to derive the stiffness relations for the dynamic analysis. Desai (Ref. 4.6) suggested that the formulation and application of the static finite element analysis may consist of eight basic steps. The formulation of the admittance relations for the electricity flow problem has been undertaken following the same steps which are described in sections 4.2.1 to 4.2.7.

4.2.1 Discretisation

Discretisation involves the idealisation of the structure by a series of discrete, finite, elements. Their size is arbitrary; they may be all of the same size or all different. The intersection of the sides of the elements are called nodes (nodal points). Interfaces between elements are called nodal lines for two dimensional analysis and nodal planes for three dimensional analysis (Figure 4.2).

4.2.2 The Shape Functions

The three node finite element as shown in Figure 4.3 has constant potential gradient over the element. The potential function which describes the variation of the potential within an element is:

$$\phi(x,y) = \alpha_1 + \alpha_2 x + \alpha_3 y \tag{4.1}$$

$$= [1 \;\; x \;\; y]\begin{Bmatrix}\alpha_1\\ \alpha_2\\ \alpha_3\end{Bmatrix} \tag{4.2}$$

where $\phi(x,y)$ is the potential at point (x, y) in the element. The potentials therefore vary linearly along any side of the triangle. Since the potential of nodes at the ends of the common side of a triangle must be equal. The variation of potential, which must be linear, is the same along the common side of each element. This automatically guarantees continuity of potentials between adjacent elements.

The α's in equation (4.1) may be evaluated in terms of the nodal potentials by solving three simultaneous equations:

$$\begin{aligned}\phi_1 &= \alpha_1 + \alpha_2 x_1 + \alpha_3 y_1\\ \phi_2 &= \alpha_1 + \alpha_2 x_2 + \alpha_3 y_2\\ \phi_3 &= \alpha_1 + \alpha_2 x_3 + \alpha_3 y_3\end{aligned} \tag{4.3}$$

which give:

$$\begin{matrix}\alpha_1 \\ \alpha_2 \\ \alpha_3\end{matrix} = \frac{1}{2\Delta}\begin{bmatrix}(x_2y_3-x_3y_2) & (x_3y_1-x_1y_3) & (x_1y_2-x_2y_1) \\ (y_2-y_3) & (y_3-y_1) & (y_1-y_2) \\ (x_3-x_2) & (x_1-x_3) & (x_2-x_1)\end{bmatrix}\begin{Bmatrix}\phi_1 \\ \phi_2 \\ \phi_3\end{Bmatrix} \tag{4.4}$$

where:

Δ = area of the element

$$= 0.5(x_2y_3 + x_1y_2 + y_1x_3 - x_2y_1 - x_3y_2 - y_3x_1) \tag{4.5}$$

Substituting equation (4.4) into equation (4.2), the potential function becomes:

$$\{\phi\} = [N_1\ N_2\ N_3]\begin{Bmatrix}\phi_1 \\ \phi_2 \\ \phi_3\end{Bmatrix} \tag{4.6}$$

$$= [N]\{\phi^e\} \tag{4.7}$$

where [N] is a set of interpolation functions called Shape Functions and $\{\phi^e\}$ is the vector of nodal potentials for the element. The shape functions express the pattern of the distribution of the unknown quantity, in this case the potential, over the element. N_i is the shape function of the element at node i where:

$$\begin{aligned} N_1 &= \frac{1}{2\Delta}[(x_2y_3-x_3y_2) + (y_2-y_3)x + (x_3-x_2)y] \\ N_2 &= \frac{1}{2\Delta}[(x_3y_1-x_1y_3) + (y_3-y_1)x + (x_1-x_3)y] \\ N_3 &= \frac{1}{2\Delta}[(x_1y_2-x_2y_1) + (y_1-y_2)x + (x_2-x_1)y] \end{aligned} \tag{4.8}$$

4.2.3 Definition of Electric Field Relationships

4.2.3.1 The Electric Field - Potential Relationship

For the two dimensional electricity flow problem, the electric field vector at any point within an element may be described by two components which contribute to the internal power consumption:

$$E_x = -\frac{\partial \phi}{\partial x}$$
$$E_y = -\frac{\partial \phi}{\partial y} \tag{4.9}$$

where E_x, E_y are the potential gradient in the x and y directions respectively. Substituting the expression for potential from equation (4.7) into equation (4.9) gives:

$$\{E^e\} = \begin{Bmatrix} E_x \\ E_y \end{Bmatrix} = \begin{bmatrix} -\frac{\partial N_1}{\partial x} & -\frac{\partial N_2}{\partial x} & -\frac{\partial N_3}{\partial x} \\ -\frac{\partial N_1}{\partial y} & -\frac{\partial N_2}{\partial y} & -\frac{\partial N_3}{\partial y} \end{bmatrix} \begin{Bmatrix} \phi_1 \\ \phi_2 \\ \phi_3 \end{Bmatrix}$$
$$= [B]\{\phi^e\} \tag{4.10}$$

Thus, the element potential gradients are expressed directly in terms of the nodal potentials by means of the [B] matrix which defines the electric field - potential relationship.

4.2.3.2 The Constitutive Law

Before a procedure equivalent to the virtual displacement method may be applied, an additional quantity, the current density, must be defined by expressing its relationship with the potential gradient. Using this constitutive law, the power consumed within a medium may be found when a virtual fluctuation of potential is applied to the medium. The relationship between the current density flow through a conductor and the potential gradient along the conductor is dictated by the Ohm's Law:

$$\{J^e\} = [s]\{E^e\} \tag{4.11}$$

where $\{J^e\}$ is the current density (Ampere/Unit area) flowing through the element and [s] is the conductivity matrix of the element. For anisotropic conductors, the conductivity properties may be different in different directions, thus:

$$[s] = \begin{bmatrix} s_x & 0 \\ 0 & s_y \end{bmatrix} \tag{4.12}$$

where s_x and s_y will be equal for isotropic conductors.

4.2.4 The Admittance Relations

Appropriate admittance equations may be obtained by an approach equivalent to the principle of virtual displacement. The principle applied to a structural problem may be expressed as follows. If a system which is in equilibrium under the action of a set of forces is subjected to a virtual displacement, that is any displacement compatible with the system constraints, the total work done by the force will be zero (Ref. 4.8). From sections 4.2.2 and 4.2.3, the similarity between the electricity flow problem and the structural displacement analysis problem is obvious. In fact, there are equivalent variables between the two types of problems which are given in Table 4.1.

Electricity Flow Problem			Structural Displacement Analysis	
Potential	$\{\phi\}$	$\equiv$	Displacement	$\{\delta\}$
Applied Current	$\{I\}$	$\equiv$	Applied Load	$\{F\}$
Admittance	$[S]$	$\equiv$	Stiffness	$[K]$
Current Density	$\{J\}$	$\equiv$	Stress	$\{\sigma\}$
Potential Gradient	$\{E\}$	$\equiv$	Strain	$\{\varepsilon\}$
Ohm's Law		$\equiv$	Hooke's Law	

Table 4.1

Using the electric field - potential relationship (equation (4.10)) and the Ohm's Law (equation (4.11)), the current density vector $\{J^e\}$ may be expressed in terms of the nodal potential vector $\{\phi^e\}$ thus:

$$\{J^e\} = [s][B]\{\phi^e\} \tag{4.13}$$

The elemental admittance properties may be derived by considering the virtual fluctuation in the potential of the field. This fluctuation would result in virtual power δP_i being delivered to the element thus:

$$\delta P_i = \{\phi^{e*}\}^T\{I^e\} \tag{4.14}$$

where δP_i is the virtual power delivered to the element in Watts (Joule/sec); $\{\phi^{e*}\}$ is the virtual fluctuation of potential components in Volts; and $\{I^e\}$ is the corresponding applied current components in Amperes.

The virtual power δP_c dissipated by the element is given by:

$$\delta P_c = \int_{\Omega^e} -\{E^{e*}\}^T\{J^e\}d\Omega^e \tag{4.15}$$

where $\{E^{e*}\}$ is the vector of corresponding elemental virtual fluctuation in electric field intensity (potential gradient); and $\{J^e\}$ is the vector of the elemental current density. The negative sign in equation (4.15) is required to ensure that the correct sign for electric potential is used. Substitutingthe expression for $\{J^e\}$ from equation (4.13) into equation (4.15) gives:

$$\delta P_c = \int_{\Omega^e} -\{E^{e^*}\}[s][B]\{\phi^e\}d\Omega^e \tag{4.16}$$

And substituting the expression for $\{E^{e^*}\}$ from equation (4.10) in equation (4.16) for δP_c gives:

$$\delta P_c = \int_{\Omega^e} -\{\phi^{e^*}\}^T[B]^T[s][B]\{\phi^e\}d\Omega^e \tag{4.17}$$

Provided that no power is lost within the element, the power delivered to the element should equal to the power dissipated by the element thus:

$$\{\phi^{e^*}\}^T\{I^e\} = -\int_{\Omega^e} \{\phi^{e^*}\}^T[B]^T[s][B]\{\phi^e\}d\Omega^e \tag{4.18}$$

This statement is analogous to the principle of virtual work in structural analysis. Equation (4.18) may be rearranged to give:

$$\{I^e\} = -\int_{\Omega^e} [B]^T[s][B]\{\phi^e\}d\Omega^e = -[S^e]\{\phi^e\} \tag{4.19}$$

where $[S^e]$ is the elemental admittance matrix ($[S^e] = \int [B]^T[s][B]d\Omega^e$); $\{I^e\}$ is the vector of the nodal applied current; and $\{\phi^e\}$ is the vector of nodal potential of the element. A brief derivation of the elemental admittance matrix for a 20-node isoparametric element is given in Appendix A.

4.2.5 The Global Admittance Equations and Solution of the Equations

Steps 5 and 6 described by Desai (Ref. 4.6) are combined in this section. The two steps may be separated in most finite element applications where the overall stiffness equations will be formed and stored in core. Then boundary conditions such as nodal applied current and prescribed nodal potential are applied to render the system of stiffness equations non-singular before they may be solved by the Direct Elimination Method or Iterative Methods.

The generic relationship given by equation (4.19) is applied to each element and the equations describing the behaviour of the domain Ω is obtained by summing the elemental equations describing the behaviour of individual element Ω^e. The assembly process is based on the law of continuity while ensuring that the potentials at the element nodes is satisfied. The continuity between adjacent elements is satisfied during the derivation of the shape functions. The compatibility condition may be satisfied by giving the same global node number to a node which is shared by two or more elements.

In numerical computation, a correspondence between the element and the overall degrees of freedom is first established, then elemental admittance matrices are added to their locations in the overall admittance matrix. The electrical admittance equations of the field are then given by the Admittance Relation:

$$\{I\} = -[S]\{\phi\} \tag{4.20}$$

where $\{I\}$ is the vector of overall applied electricity current ($\{I\} = \sum\{I^e\}$); $[S]$ is the overall admittance matrix ($[S] = \sum[S^e]$); and $\{\phi\}$ is the vector of overall nodal potentials ($\{\phi\} = \sum\{\phi^e\}$). And the appearance of the full matrix is:

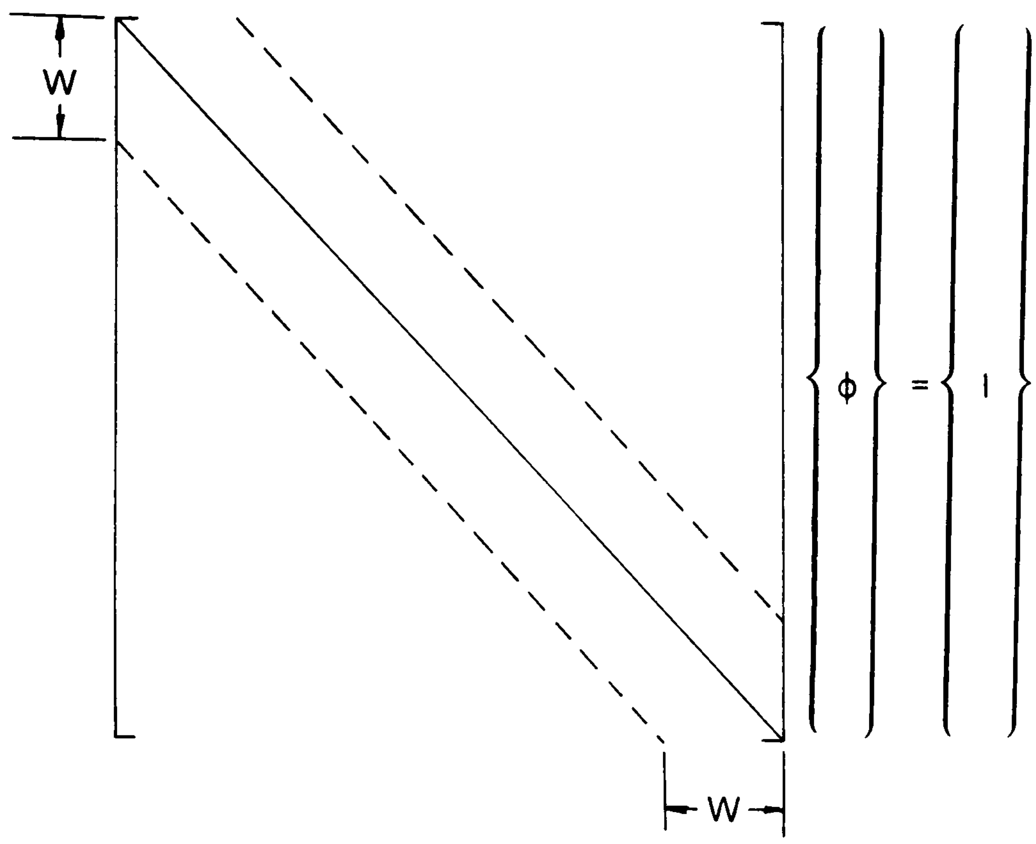

(4.21)

The admittance matrix [S] is sparse and also symmetric about the leading diagonal. The nonzero coefficients are clustered within a bandwidth. The width, W in equation (4.21) is called the semi-bandwidth (including the diagonal term) of the matrix.

The system of equations as shown in equation (4.20) may be solved using Gaussian Elimination. The system of equations may be stored in core for solution or by taking the advantage of the symmetry about the leading diagonal and only the semi-bandwidth of the matrix need be stored in core. The amount of core storage required is thus much reduced. The size of problem which may be solved in this way is limited by the available core storage of the computer. In this research, a pile-soil system of the field was idealised by a large number of two-dimensional three node finite elements. The twenty node isoparametric elements used for the three dimensional pile-soil electrical simulation also demand a large storage space if a Gaussian band solver is used. Therefore, the Frontal Solution, which it has been suggested in many finite element texts (Ref. 4.1, 4.4, 4.7) is a very efficient direct solution process for a large number of finite elements, was used in this research. The technique will be described briefly in this section while detail explanations and computer implementations may be found in finite element texts (Ref. 4.1, 4.4, 4.7, 4.9).

4.2.5.1 The Frontal Solution

The Frontal Technique differs from the direct elimination method in that with the frontal technique assembly and reduction of the equations occurs at the same time. A variable will be eliminated as soon as the coefficients of that equation have completely assembled from all the relevant elements. During this assembly/elimination process, the elements in the domain are considered in turn according to their element number prescribed. Therefore, the first step in the frontal technique is to search through the element list to find out in which element a node number appears for the last time. Then the node number where it appears for the last time in the element definition list is given a negative sign which indicates that the variable is ready for elimination at that stage.

Whenever a new element admittance is formed, its elememtal admittance coefficients will be added to existing equations if the node is already active. If the node first appears, activated, the equation will take up a free space in the front. If the node appears for the last time, the corresponding equation will be eliminated and stored on a disc file and thus deactivated. In this case, the boundary conditions incorporated in an element are also considered at this stage. It should be noted that the equation being used to reduce the other equations may not be at the top of the equations being considered. After an equation is deactivated from the front, free spaces become available in the front which may be employed during the assembly of the next element. When the elimination reaches a prescribed variable, such as fixed potential at a node, the coefficients of other equations in the global admittance matrix will not be reduced. The remaining coefficients in the global applied current vector, {I}, will be modified by subtracting from the product the value of the prescribed potential and the appropriate column term of the global admittance matrix [S] (Figure 4.4). In addition to the eliminated variables are written to a disc file, the position of the variable in the front at the time of elimination and its corresponding global degrees of freedom are also written in the same record in the disc file. This extra information may be useful in the backsubstitution phase.

After all the equations have been eliminated, backsubstitution may commence starting with the last eliminated variable and moving upwards through the equations. The coefficients stored in the disc file are recalled by backspacing the disc file by one record each time. Each new equation introduces only one unknown quantity which may be calculated directly. In case where an applied potential is prescribed, the equivalent applied current at the node may be found by subtracting the products of the corresponding admittance coefficient with the known applied currents at other nodes from the calculated nodal applied current (Figure 4.5).

The efficiency of the frontal technique thus depends on the order of element numbering. Therefore, pre-processing programs are required to rearrange the node numbers and element numbers to improve the efficiency of the solution method. The pre-processing programs used to optimise the front width will be described in section 4.5.1.

4.2.6 Secondary Quantities

In section 4.2.5, the nodal applied currents and nodal potentials were found. The quantity, Earthing Resistance of the pile to a particular point between the pile and the return current electrode as defined in section 2.2.4.8, is required for the interpretation of the results from the earth resistance method of integrity testing. The earth resistance may be computed at this stage from the nodal potentials and the total applied current found from section 4.2.5:

$$R = (\phi_P - \phi_C)/I \tag{4.22}$$

where R is the earth resistance between P and C (Figure 1.1); ϕ_P, ϕ_C are the potentials at P and C (Figure 1.1); and I is the total applied current.

This computed earth resistance may be used for qualitative study of the earth resistance method using two dimensional analysis. The computed results from a three dimensional analysis may be applied to field data interpretations.

4.2.7 Display of Finite Element Analysis Results

The nodal potentials found for a finite element idealisation due to an applied potential may be presented as an equipotential plot. In addition, the computed earth-resistance values between nodal points may be converted into an earth-resistance curve for the interpretation of field test results as described in section 2.2.4.8. The computer programs for post-processing of data will be discussed in section 4.5.2.

4.3 Dynamic Finite Element Analysis

4.3.1 Static Plane Strain/Plane Stress Problem

A method equivalent to the virtual displacement approach has been used in section 4.2 to obtain the admittance relationship for a three node triangular finite element. The use of the same type of finite element will also be used for the simulation of the application of the Sonic Echo Method of Integrity Testing on Civil Engineering Structures or a structural member. The formulation of the relations for a three node triangular finite element is straightforward and similar to that shown in section 4.2 and details will not be presented here. The equivalent parameters between the electricity flow problem and a structural displacement analysis has been given in Table 4.1. Perhaps, some points about the formulation should be mentioned here.

The simulation of the Sonic Echo Method may be considered as a Plane Strain/Plane Stress problem. Each node of the triangular element as shown in Figure 4.3 has two degrees of freedom. The displacement function corresponding to equation (4.1) is:

$$\{\delta\} = \begin{Bmatrix} \delta_x \\ \delta_y \end{Bmatrix} = \begin{bmatrix} 1 & x & y & 0 & 0 & 0 \\ 0 & 0 & 0 & 1 & x & y \end{bmatrix} \begin{Bmatrix} \alpha_1 \\ \alpha_2 \\ \alpha_3 \\ \beta_1 \\ \beta_2 \\ \beta_3 \end{Bmatrix} \tag{4.23}$$

The α's and β's may be found by substituting the nodal coordinates into the equations (4.23). Two sets of three equations each set similar to equation (4.3) may be obtained. A similar set of shape functions (equation 4.8) will be obtained, thus:

$$\{\delta\} = [N]\{\delta^e\} = \begin{bmatrix} N_1 & 0 & N_2 & 0 & N_3 & 0 \\ 0 & N_1 & 0 & N_2 & 0 & N_3 \end{bmatrix} \begin{Bmatrix} \delta_{1x} \\ \delta_{1y} \\ \delta_{2x} \\ \delta_{2y} \\ \delta_{3x} \\ \delta_{3y} \end{Bmatrix} \tag{4.24}$$

The strain at any point within the element is described by three components which contributes to internal work:

$$\{\varepsilon^e\} = \begin{Bmatrix} \varepsilon_x^e \\ \varepsilon_y^e \\ \gamma_{xy}^e \end{Bmatrix} = \begin{Bmatrix} \dfrac{\partial \delta_x}{\partial x} \\ \dfrac{\partial \delta_y}{\partial y} \\ \dfrac{\partial \delta_x}{\partial y} + \dfrac{\partial \delta_y}{\partial x} \end{Bmatrix} \tag{4.25}$$

$$= \begin{bmatrix} \dfrac{\partial N_1}{\partial x} & 0 & \dfrac{\partial N_2}{\partial x} & 0 & \dfrac{\partial N_3}{\partial x} & 0 \\ 0 & \dfrac{\partial N_1}{\partial y} & 0 & \dfrac{\partial N_2}{\partial y} & 0 & \dfrac{\partial N_3}{\partial y} \\ \dfrac{\partial N_1}{\partial y} & \dfrac{\partial N_1}{\partial x} & \dfrac{\partial N_2}{\partial y} & \dfrac{\partial N_2}{\partial x} & \dfrac{\partial N_3}{\partial y} & \dfrac{\partial N_3}{\partial x} \end{bmatrix} \begin{Bmatrix} \delta_{1x} \\ \delta_{1y} \\ \delta_{2x} \\ \delta_{2y} \\ \delta_{3x} \\ \delta_{3y} \end{Bmatrix} \tag{4.26}$$

$$= [B]\{\delta^e\} \tag{4.27}$$

In choosing the Constitutive Law for the stiffness relations, an assumption has to be made as to whether the finite element should be a plane strain element or a plane stress element. The stress/strain relationship for an isotropic elastic material, in the absence of initial strains, may be written as:

$$\{\sigma^e\} = [D]\{\varepsilon^e\} \tag{4.28}$$

where [D] is the matrix of elastic constants (equivalent to [s] in the electricity flow problem). The matrix [D] is given in finite element analysis and elasticity texts (Ref. 4.1, 4.2, 4.4, 4.10) as:

$$[D] = \frac{E}{1-\nu^2}\begin{bmatrix} 1 & \nu & 0 \\ \nu & 1 & 0 \\ 0 & 0 & \frac{1-\nu}{2} \end{bmatrix} \tag{4.29}$$

for plane stress condition and:

$$[D] = \frac{E(1-\nu)}{(1+\nu)(1-2\nu)}\begin{bmatrix} 1 & \frac{\nu}{1-\nu} & 0 \\ \frac{\nu}{1-\nu} & 1 & 0 \\ 0 & 0 & \frac{1-2\nu}{2(1-\nu)} \end{bmatrix} \tag{4.30}$$

for plane strain condition. Both plane strain and plane stress elements were useful in idealising a three dimensional problem into a two dimensional problem. The choice of plane strain and plane stress element for an analysis has implications for the practical situations. For the plane strain situation, it is assumed that the normal strain in the z-direction, ε_z, is zero. A plane strain element therefore represents a solid whose thickness is large in comparison with the representative x and y dimensions. Or, the ends of the solid are constrained from moving in the z-direction. For example a section through a long earth dam.

For the plane stress condition, the normal stress in the z-direction, σ_z, is zero. This is an approximate theory where the variation of the ε_z strain over the x-y plane is neglected. A plane stress element therefore represents a solid which is very thin in comparison with the representative x and y dimensions.

For example a thin shear wall subject to in plane loads axially.

In both cases, it is assumed that the only nodal displacement components and applied loads are those in the x and y directions.

If such a plane strain or plane stress element is now subjected to an arbitrary virtual displacement, $\{\delta^{e*}\}$, and the strain distribution is $\{\varepsilon^{e*}\}$, then the principle of virtual displacement requires that (Refs. 4.1, 4.4, 4.7):

$$\int_{\Omega^e} \{\varepsilon^{e*}\}^T \{\sigma\} d\Omega^e = \{\delta^{e*}\}^T \{P^e\} \tag{4.31}$$

where $\{P^e\}$ is the vector of elemental nodal applied loads. The external virtual work is on the right hand side of equation (4.31) and is equal to the actual applied forces multiplied by the virtual displacements. The internal virtual work is on the left hand side of the equation and is equal to the actual stresses multiplied by the virtual strains of the field. Substituting equations (4.24), (4.27), (4.28) into equation (4.31), the elemental stiffness equations may be obtained thus:

$$\int_{\Omega^e} \{\delta^{e*}\}^T [B]^T [D][B] \{\delta^e\} d\Omega^e = \{\delta^{e*}\}^T \{P^e\}$$

and

$$\left[\int_{\Omega^e} [B]^T [D][B] d\Omega^e \right] \{\delta^e\} = \{P^e\} \tag{4.32}$$

or in matrix form:

$$[K^e]\{\delta^e\} = \{P^e\} \tag{4.33}$$

The global equilibrium equations become:

$$[K]\{\delta\} = \{P\} \tag{4.34}$$

where [K] is the global stiffness matrix ($[K] = \sum[K^e]$); $\{\delta\}$ is the vector of nodal displacements ($\{\delta\} = \sum\{\delta^e\}$) and {P} is the global vector of applied loads ($\{P\} = \sum\{P^e\}$). $\{P^e\}$ may include effects due to point loads, $\{P_f^e\}$, and body forces, $\{P_b^e\}$, and surface tractions, $\{P_q^e\}$:

$$\{P^e\} = \{P_f^e\} + \{P_b^e\} + \{P_q^e\} \tag{4.35}$$

where:

$$\begin{aligned} \{P_f^e\} &= [N]^T\{f^e\} \\ \{P_b^e\} &= \int_{\Omega^e} [N]^T\{b^e\}d\Omega^e \\ \{P_q^e\} &= \int_{\Gamma^e} [N]^T\{q^e\}d\Gamma^e \end{aligned} \tag{4.36}$$

in which $\{f^e\}$ is the vector of elemental nodal applied force due to point loads; $\{b^e\}$ is the vector of the amplitude of body force per unit volume; and $\{q^e\}$ is the amplitude of the surface traction per unit area on the element. A brief description of the formulation of the stiffness relationship for the eight node isoparametric finite element is given in Appendix B.

The derivatives for the admittance relationships (sections 4.2.1 to 4.2.4) and the stiffness relationships (section 4.3.1) for the finite element analysis were given briefly since the finite element method has been very well developed and details about the derivatives may be found from many standard finite element element texts (Refs. 4.1, 4.2, 4.3, 4.4, 4.5, 4.6, 4.7).

The assembly and solution of the global stiffness equations is the same as shown in section 4.2.5 using the frontal technique. In this application, one global degree of freedom will be eliminated at a time instead of one nodal equation in the case of electricity flow problem because in the two dimensional plane strain/plane stress analysis, there are two degrees of freedom at each node.

4.3.2 Formulation of the Equation of Motion

Equation (4.33) represents the static equilibrium state of a finite element. When the applied force $\{P^e\}$ varies with time, the displacements in the element, $\{\delta^e\}$ also vary with time. Two sets of additional forces must be considered when the displacements of an elastic body vary with time (Ref. 4.1). These forces are inertia forces and damping forces. Bathe et. al. (Ref. 4.2) showed that both of these forces may be included as part of the body force, $\{P_b^e\}$.

Using the d'Alembert's principle, that a mass develops an inertia force proportional to its acceleration and opposing it (Ref. 4.10), the inertia force is $-\rho\,\partial^2\{\delta\}/\partial t^2$. Thus, the total body force becomes:

$$\{P_b^e\} = \int_{\Omega^e} [N]^T\{b^e\}d\Omega^e + \int_{\Omega^e} [N]^T\rho[N]\{\ddot{\delta}^e\}d\Omega^e \qquad (4.37)$$

where $\{b^e\}$ is the body force excluding the inertia force; ρ is the mass density of the element; and $\{\ddot{\delta}\}$ is the vector of the nodal accelerations assuming that the element acceleration may be idealised in the same way as element displacement ($\{\ddot{\delta}\} = [N]\{\ddot{\delta}^e\}$).

The damping force may be considered to be the resistance due to microstructure movements, air resistance etc. (Ref. 4.1). For simplicity, linear, viscous type damping is considered, $-\mu\partial\{\delta\}/\partial t$.

Therefore, the total applied load is:

$$\{P^e\} = \{P_f^{\,e}\} + \{P_b^{\,e}\} - \int_{\Omega^e}[N]^T\rho[N]\{\ddot{\delta}^e\}d\Omega^e - \int_{\Omega^e}[N]^T\mu[N]\{\dot{\delta}^e\}d\Omega^e + \{P_q^{\,e}\} \quad (4.38)$$

where $\{P_b^{\,e}\}$ is the elemental body force vector excluding the inertia force and the velocity dependent damping force. The elemental equilibrium equation becomes:

$$[K^e]\{\delta^e\} + [C^e]\partial\{\delta^e\}/\partial t + [M^e]\partial\{\delta^e\}/\partial t = \{P^e\} \quad (4.39)$$

where $\{P^e\}$ is the elemental time dependent load vector excluding the inertia force and the velocity dependent damping force. In matrix form:

$$[K^e]\{\delta^e\} + [C^e]\{\dot{\delta}^e\} + [M^e]\{\ddot{\delta}^e\} = \{P^e\} \quad (4.40)$$

If the damping factor in matrix $[C^e]$ and the mass densities in matrix $[M^e]$ are time independent, the global damping matrix $[C]$ and global mass matrix $[M]$ may be assembled in the same way as the global stiffness matrix, thus:

$$[K]\{\delta\} + [C]\{\dot{\delta}\} + [M]\{\ddot{\delta}\} = \{P\} \quad (4.41)$$

where: $[K] = \sum[K^e]$;

$$[C] = \sum[C^e] = \int_{\Omega^e}[N]^T\mu[N]d\Omega^e;$$

$$[M] = \sum[M^e] = \int_{\Omega^e}[N]^T\rho[N]d\Omega^e$$

Both the elemental damping matrix and the elemental mass matrix are considered to have the damping factor and mass density distributed over the element (not lumped at the nodes), they are called the Consistent Elemental Damping Matrix and Consistent Elemental Mass Matrix (Ref. 4.2).

4.3.3 Time Integration

Equation (4.40) represents the equilibrium for a finite element in motion. The response of the element, such as the time history of the accelerations, velocities, displacements stresses and strains at the nodes and the elements, may be found by integrating equation (4.40) forward in time. The three most popular techniques for integrating equation (4.40) with respect to time (Refs. 4.11, 4.12) are the Modal Superposition Technique, the Direct Integration Technique and the Complex Response Technique.

The disadvantage of using the Modal Superposition Technique is that the damping property has to be applied to the whole idealisation (Ref. 4.11, 4.12). This constant damping property has restricted its general application to the analysis of pile-soil systems and the simulation of an energy absorbing boundary where the damping properties for the boundary elements may be different from the other elements.

The Complex Response Technique can handle problems where the damping properties of the elements are not uniformly distributed over the whole system. In addition, this method preserves the frequency dependence of the damping properties (Ref. 4.11, 4.12). However, a general non-harmonic applied force function has to be converted to equivalent harmonic components in the frequency domain before solutions for each component can be found. The solutions are then re-synthesised by converting back to time domain.

Smith (Ref. 4.11) noted that the Complex Response Technique is not suitable for a large finite element system nor when the input force has a range of frequencies.

The Direct Integration Technique will be considered in this chapter for its similarity between the analysis of the idealised and actual Sonic Echo Tests where time domain data are discretised into discrete time points.

4.3.3.1 Direct Integration

With the Direct Integration Technique, no transformation of the equation (equation 4.40) is required prior to the numerical integration. The direct integration techniques may be physically interpreted as the iterative attempts to satisfy the equilibrium equation (equation 4.40) at discrete time intervals Δt apart. In addition, it is assumed that there is a variation of displacements, velocities and accelerations within each time interval Δt. The direct integration techniques may be divided into Explicit Procedures and Implicit Procedures (Ref. 4.11, 4.13). With the explicit procedures, the solution of the displacement, $\{\delta_{t+\Delta t}\}$, at time $t+\Delta t$ is obtained by satisfying the equilibrium equation, $([M]\{\ddot{\delta}_t\} + [C]\{\dot{\delta}_t\} + [K]\{\delta_t\} = \{F_t\})$, at time t. On the other hand, the implicit procedures require that the solution of the displacements, $\{\delta_{t+\Delta t}\}$, at time $t+\Delta t$ being obtained by satisfying the equilibrium equation, $([M]\{\ddot{\delta}_{t+\Delta t}\} + [C]\{\dot{\delta}_{t+\Delta t}\} + [K]\{\delta_{t+\Delta t}\} = \{F_{t+\Delta t}\})$, at time $t+\Delta t$.

The most widely used explicit time integration procedure is the Central Difference Method. The central difference method is only conditionally stable. That is, the integration scheme requires the use of a time step Δt which must be smaller than a critical time step, Δt_{cr}. The critical time step may be found from the properties of the finite element assemblage (Ref. 4.2):

$$\Delta t_{cr} = \frac{T}{\pi} \tag{4.42}$$

where T is the smallest period of the finite element assemblage.

There are a great variety of implicit time integration procedures; for example Houbolt's Method, Wilson-θ Method and Newmark's Method. Key (Ref. 4.13) showed that both Houbolt method and Wilson method have greater frequency distortion when compared with the results of the Newmark method. In addition, both of these methods possess large amount of damping which cannot be controlled independent of time step as with the Newmark method. Bathe et. al. (Ref. 4.2) also showed that the Newmark method is the most stable time integration procedure among the three procedures reviewed. The Newmark method of time integration will be described in section 4.3.3.2.

4.3.3.2 Newmark Integration Method

Newmark (Ref. 4.14) proposed a general procedure for the solution of problems in structural dynamics. The method is suitable for analysing structures for their elastic behaviour, inelastic behaviour or plastic response, up to failure due to any type of dynamic loading such as shock or impact, vibration, and earthquake motions (Ref. 4.14). The method is a step-by-step method of integration of the equation of motion. The method determines the "static" behaviour of the structure at each time step during the integration process. The procedure may predict the nodal displacements, velocities and accelerations at time $t+\Delta t$ from the known nodal displacements, velocities and accelerations at time t by assuming that:

$$\{\dot{\delta}_{t+\Delta t}\} = \{\dot{\delta}_t\} + (1-\gamma)\{\ddot{\delta}_t\}\Delta t + \gamma\{\ddot{\delta}_{t+\Delta t}\}\Delta t \tag{4.43}$$

and

$$\{\delta_{t+\Delta t}\} = \{\delta_t\} + \{\dot{\delta}_t\}\Delta t + [(½-\alpha)\{\ddot{\delta}_t\}+\alpha\{\ddot{\delta}_{t+\Delta t}\}]\Delta t^2 \tag{4.44}$$

where parameters γ and α are related to the damping of the motion and the assumption for the nodal acceleration between each time interval. To solve for the nodal displacements, velocities and accelerations at time $t+\Delta t$, the equilibrium equation (4.41) at time $t+\Delta t$ must also be considered:

$$[K]\{\delta_{t+\Delta t}\} + [C]\{\dot{\delta}_{t+\Delta t}\} + [M]\{\ddot{\delta}_{t+\Delta t}\} = \{P_{t+\Delta t}\} \tag{4.45}$$

Expressing $\{\ddot{\delta}_{t+\Delta t}\}$ in terms of $\{\delta_{t+\Delta t}\}$ in equation (4.44), thus:

$$\{\ddot{\delta}_{t+\Delta t}\} = a_0[\{\delta_{t+\Delta t}\}-\{\delta_t\}] - a_2\{\dot{\delta}_t\} - a_3\{\ddot{\delta}_t\} \tag{4.46}$$

where,

$$a_0 = \frac{1}{\alpha\Delta t^2};$$

$$a_2 = \frac{1}{\alpha\Delta t};$$

$$a_3 = \frac{1}{2\alpha} - 1$$

Substituting for $\{\ddot{\delta}_{t+\Delta t}\}$ into equation (4.43):

$$\{\dot{\delta}_{t+\Delta t}\} = \{\dot{\delta}_t\} + a_6\{\ddot{\delta}_t\} + a_7(a_0\{\delta_{t+\Delta t}\}-a_0\{\delta_t\}-a_2\{\dot{\delta}_t\}-a_3\{\ddot{\delta}_t\}) \tag{4.47}$$

where

$$a_6 = \Delta t(1-\gamma);$$

$$a_7 = \gamma\Delta t$$

It is obvious from equations (4.46) and (4.47) that by substituting for $\{\dot{\delta}_{t+\Delta t}\}$ and

$\{\ddot{\delta}_{t+\Delta t}\}$ into equation (4.45), the equilibrium equations may be solved for $\{\delta_{t+\Delta t}\}$ provided that the applied load at time $t+\Delta t$, $\{P_{t+\Delta t}\}$ is known. The general form of the equilibrium equation at time $t+\Delta t$ may be expressed as:

$$[\hat{K}]\{\delta_{t+\Delta t}\} = \{\hat{P}_{t+\Delta t}\} \tag{4.48}$$

where $[\hat{K}]$ is the Global Effective Stiffness Matrix and $\{\hat{P}_{t+\Delta t}\}$ is the Global Effective Load Vector. The global effective stiffness matrix is:

$$[\hat{K}] = [K] + a_0[M] + a_1[C] \tag{4.49}$$

where,

$$a_1 = \frac{\gamma}{\alpha \Delta t};$$

and [K] is the global stiffness matrix; [M] is the global mass matrix and [C] is the global damping matrix.

The global effective load vector is:

$$\begin{aligned}\{\hat{P}_{t+\Delta t}\} &= \{P_{t+\Delta t}\} + [M](a_0\{\delta_t\}+a_2\{\dot{\delta}_t\}+a_3\{\ddot{\delta}_t\}) \\ &\quad + [C](a_1\{\delta_t\}+a_4\{\dot{\delta}_t\}+a_5\{\ddot{\delta}_t\})\end{aligned} \tag{4.50}$$

where

$$a_4 = \frac{\gamma}{\alpha} - 1$$

$$a_5 = \frac{\Delta t}{2}\left(\frac{\gamma}{\alpha} - 2\right)$$

and $\{\hat{P}_{t+\Delta t}\}$ is the global effective load vector.

The derivation of the general equilibrium equations has been based on reference 4.2, thus, the constants a_0, ..., a_7 has been put in such an order so that they conforms with the constants given in the reference.

Newmark (Ref. 4.14) proposed that for the case of no damping the parameter γ should be assigned a value of 0.5 for the integration. It was also shown that a system may become self-excited if γ is taken as zero while the magnitude of response may be reduced during the time integration if γ is greater than 0.5 (Ref. 4.14). It was also shown that the selection of different values of α corresponds to a different assumption of the acceleration of the particles between two time points t and t+Δt of the vibration. Figure 4.6 illustrates the variation of acceleration between two time points for three assumed values of α while γ is kept constant at 0.5 (Ref. 4.14). The choice of α = 1/6 corresponds to a linear variation of acceleration in the interval which is the same as the Wilson-θ method when $\theta = 1$. A constant-average-acceleration approach is obtained by using α = 1/4. In this case, the nodal accelerations during a time interval between t and t+Δt are constant and that the accelerations are equal to the mean value of the nodal accelerations at time t and t+Δt, that is, $(\frac{1}{2}\{\ddot{\delta}_t\} + \frac{1}{2}\{\ddot{\delta}_{t+\Delta t}\})$. A choice of α = 1/8 corresponds to a step function with a uniform value equal to the initial value for the first half of the time interval and a uniform value equal to the final value for the second half of the time interval.

For the computer implementation, the effective stiffness matrix and the effective load vector are assembled from their elemental contributions and eliminated according to the frontal solution process during the first time point integration. The elemental mass matrices and the elemental damping matrices are written into a disc file at the first time point integration. These matrices will be recalled at the subsequent time point integrations to form the global load vector. Taking advantage that the global effective stiffness matrix is unchanged throughout the time integration processes, the equations needed reduced once at the first time point integration.

At each time step, the effective load vector is formed from the known nodal applied forces at time $t+\Delta t$, nodal displacements, velocities and accelerations at time t and the corresponding mass matrix and damping matrix. The effective load vector is modified using the coefficients of the reduced global stiffenss matrix. The nodal displacements at time $t+\Delta t$ are obtained by back substitution. The nodal velocities and accelerations are computed using equations (4.43) and (4.44).

4.3.4 Boundary Conditions

It was shown in section 4.2.5 that prescribed potentials at some nodes or applied nodal currents at other points are required to solve the system of equations to obtain the resultant potential distribution within the finite element idealisation. These prescribed values of potentials and applied currents are called the boundary conditions of the finite element idealisation. In a static Plane Strain or Plane Stress analysis, equivalent boundary conditions (applied loads and prescribed displacements) are required. The boundary conditions may be geometric or force boundary conditions. The geometric boundary conditions are the fixed displacement type at fixed nodal supports. The force boundary conditions are sometimes referred to as the Natural Boundary Conditions (Ref. 4.2). The natural boundary conditions correspond to prescribed boundary forces. When the applied load at a node is zero, it implies that the strain at that node is always zero provided that the displacement at the node is not specified.

The boundary conditions where the displacements are prescribed are called the Dirichlet boundary conditions while the no strain boundary is called the Neumann boundary condition (Ref. 4.4). In static displacement analysis of a structure, there must be a structural support to maintain the stability of the structure under the applied loading. Therefore, most of the time, the Dirichlet boundary condition is required. Both Dirichlet boundary condition (Fixed end) and Neumann boundary condition (Free end) may exist in dynamic analysis. Due to the inertia terms in the system of equations, the transient state of the structure may be found even if the structure under consideration is "floating" in the space (without any fixed support).

4.4 The Transmitting Boundary

In the static finite element displacement analysis of a large continuum, the finite element idealisation is simply truncated with various boundary nodal conditions at a distance which is considered to be sufficient to prevent incurring significant errors at the zone of interest. In dynamic analysis, for example, a wave is radiated from a source in an infinite medium, the wave encounters an increasingly larger volume of material as it travels outward from the source. The energy density in the wave is thus decreased with distance from the source. The decrease in the energy density in the wave is called the geometrical damping. In a finite element analysis of a dynamic problem, the geometrical damping effect may be simulated by an energy absorbing boundary. The wave energy arriving at the energy absorbing boundary is absorbed such that the wave energy within the finite element model is decreased similar to the geometrical damping effect. A simply truncated boundary used in a dynamic finite element analysis may cause reflections of wave fronts from the boundary which may not be able to simulate the geometrical damping effect. The reflections from the boundary may also lead to spurious response at the area of interest. The simply truncated boundary may be adequate for dynamic finite element analysis under certain circumstances. For instance, in the pile-soil system shown in Figure 4.7:

1. when the frequency of excitation is below the natural frequency of a soil stratum the problem of wave propagation does not arise;

2. when the internal damping of the soil is adequate to efficiently removed the reflected wave before its return to the pile;

3. when the time-span under consideration is shorter than that required for a wave to return to the pile or area to be considered.

Bayo et. al. (Ref. 4.12) reviewed some methods of solving the problem of reflection from a simply truncated boundary. He considered:

1. extending the finite element mesh as much as necessary in order to prevent the reflected wave from reaching the pile (Figure 4.7) during the time of the analysis;

2. prolonging the finite element mesh with elements whose size gradually increase with increasing distance from the pile. The zone of growing grid is made dissipative with internal viscous damping, and terminates at a large distance from the pile. (Ref. 4.15);

3. averaging independently computed solutions with different boundary conditions (Superposition Boundary) (Ref. 4.16);

4. prescribing a set of normal and tangential stress on the boundary in such a way that the effect of these stresses

and the stresses due to any incident stress wave will produce zero energy being reflected back from the model. (Viscous Boundary) (Ref. 4.17)

Bayo et. al. (Ref. 4.12) also noted that the effectiveness of the method suggested by Day (Ref. 4.15) depends on the rate of grid growth and viscous damping. The superposition boundary and the viscous boundary will be described in the following sections.

4.4.1 The Superposition Boundary

The technique of the superposition boundary proposed by Smith (Ref. 4.16) will be illustrated by a one-dimensional wave-propagation problem (Figure 4.8). The incident wave displacements are given by:

$$\delta_I = A\{\exp[i\omega(t-x/c)]\} \tag{4.51}$$

The reflected wave equation is:

$$\delta_R = B\{\exp[i\omega(t+x/c)]\} \tag{4.52}$$

Summing the incident and reflected wave equations subjected to a fixed boundary condition (Dirichlet boundary), $\delta|_{x=0} = 0$, gives:

$$\delta_{FIXED} = A\{\exp[i\omega(t-x/c)] - \exp[i\omega(t+x/c)]\} \tag{4.53}$$

and for a free boundary condition (Neumann boundary), $\partial\delta/\partial x|_{x=0} = 0$ gives:

$$\delta_{FREE} = A\{\exp[i\omega(t-x/c)] + \exp[i\omega(t+x/c)]\} \tag{4.54}$$

For a Neumann boundary the form of the reflected wave (free of the incident wave) at any distance x′ from the boundary will be the same as that for a wave propagating through the boundary x = 0 as:

$$\underbrace{\exp[i\omega(t+x'/c)]}_{\text{reflected wave at } x = x'} \quad = \quad \underbrace{\exp[i\omega(t-[-x'/c])]}_{\text{incident wave at } x = -x'} \tag{4.55}$$

so that for no boundary the displacements to the right of x = 0 are given by:

$$\delta_{RIGHT} = A\{\exp[i\omega(t+x/c)]\} \tag{4.56}$$

The displacement to the left of x = 0 for no boundary are given by the incident wave equation:

$$\delta_{LEFT} = A\{\exp[i\omega(t-x/c)]\} \tag{4.57}$$

It can be seen from equation (4.53) and (4.54) that the displacements for no boundary may be recovered from the solutions to the fixed and free boundary conditions as follows:

$$\delta_{LEFT} = 0.5(\delta_{FREE} + \delta_{FIXED}) \tag{4.58}$$

$$\delta_{RIGHT} = 0.5(\delta_{FREE} - \delta_{FIXED}) \tag{4.59}$$

Thus, by combining the individual solutions to the Dirichlet (fixed) and Neumann (free) boundary conditions the solution for the corresponding unbounded situation is obtained.

The formulation may be applied to both body and surface waves and is independent of frequency and angle of incidence. However, it requires 2^n complete dynamic solutions if n reflections occur during the time-span of interest (Ref. 4.18).

Simons et. al. (Ref. 4.18) demonstrated that the technique of superposition boundary is more expensive to implement than the viscous boundary because a greater number of nodes is required for the superposition boundary. The method of superposition will not be applied to the simulation of an infinite boundary in a pile-soil system. A simple example will be shown in Chapter 6, section 6.8 to indicate the inadequacy of the method to apply to a pile-soil system.

4.4.2 The Viscous Boundary

Viscous dampers may be used in the frequency or in the time domain (Refs. 4.19, 4.20). Chow (Ref. 4.21) noted that although more accurate transmitting boundaries are available, they are mainly confined to linear analysis in the frequency domain. The simulation of the Sonic Echo Method of Non-Destructive Testing requires the analysis in the time domain. Therefore, the frequency independent energy absorbing boundary is considered in this section.

Lysmer et. al. (Ref. 4.20) found that an energy absorbing boundary may be modelled by prescribing a set of normal and tangential stresses on the boundary in such a way that all energy at the boundary is absorbed. The proposed expressions for the stresses are:

$$\sigma_n = a\rho c_p \dot{\delta}_n \qquad (4.60)$$

and

$$\sigma_t = b\rho c_s \dot{\delta}_t \qquad (4.61)$$

where σ_n and σ_t are the normal and shear stress, respectively; $\dot{\delta}_n$ and $\dot{\delta}_t$ are the normal and tangential particle velocities respectively; ρ is the mass density; c_s and c_p are the velocities of compressional waves and shear waves, respectively; and a and b are dimensionless parameters. Lysmer et. al. (Ref. 4.20) also found that unit values for both constants, a and b, would yield a nearly perfect absorber of harmonic elastic waves. The absorption characteristics in equations (4.60) and (4.61) are independent of frequency, therefore, the boundary can absorb both harmonic and nonharmonic waves. The viscous boundary defined by equations (4.60) and (4.61) are referred by Lysmer et. al. (Ref. 4.20) as the Standard Viscous Boundary.

The Unified Boundary Condition introduced by White et. al. (Ref. 4.17) is an extension of the Standard Viscous Boundary applied to anisotropic materials. The Unified Boundary Condition represents an improvement of the absorption efficiency of the Standard Viscous Boundary. This is accomplished by varying the constants a and b in equations (4.60) and (4.61) for any given Poisson's ratio. The two dimensional dynamic finite element analyses considered in Chapter 6 and Chapter 8 will incorporate this type of energy absorbing boundary to simulate the geometrical damping effect in the infinite soil mass. A two dimensional formulation of the method is presented here. The formulation of the Unified Boundary Condition in this section is mainly due to White et. al. (Ref. 4.17).

The general equation for the propagation of plane wave in a general anisotropic medium is given by Synge (Ref. 4.22) as:

$$\{\delta\} = A\{n\}\exp[i\omega(\{k\}^T\{r\}-t)] \tag{4.62}$$

where $\{\delta\}$ is the vector of particle displacement; $\{n\}$ is the vector of direction cosines of the particle displacements; $\{k\}$ is the vector of the horizontal wave number vector; $\{r\}$ is the vector of particle coordinates; A is the amplitude of the wave; $i = \sqrt{(-1)}$; ω is the circular frequency of the wave; and t is the time. In a two dimensional plane case, equation (4.62) has two independent solutions for $\{k\}$ and for $\{n\}$ for any given circular frequency, ω. Therefore, in a given direction ($\{n_1\}$ or $\{n_2\}$), there may be two waves propagated with different velocities ($\{k_1\}$ or $\{k_2\}$). Hence, the total movement may be written as:

$$\{\delta\} = \{\delta_1\} + \{\delta_2\} \tag{4.63}$$

and

$$\{\delta\} = \sum_{m=1}^{2} A_m\{n_m\}\exp[i\omega(\{k_m\}^T\{r\}-t)] \tag{4.64}$$

From the displacements in equations (4.64), the strains may be found using:

$$\varepsilon_x = \frac{\partial\{\delta_x\}}{\partial x} = i\omega\sum_{m=1}^{2} A_m n_{mx} k_{mx}\exp[i\omega(\{k_m\}^T\{r\}-t)] \tag{4.65a}$$

$$\varepsilon_y = \frac{\partial\{\delta_y\}}{\partial y} = i\omega\sum_{m=1}^{2} A_m n_{my} k_{my}\exp[i\omega(\{k_m\}^T\{r\}-t)] \tag{4.65b}$$

$$\gamma_{xy} = \frac{\partial\{\delta_x\}}{\partial y} + \frac{\partial\{\delta_y\}}{\partial x}$$

$$= i\omega A_m(n_{mx}k_{my}+n_{my}k_{mx})\exp[i\omega(\{k_m\}^T\{r\}-t)] \tag{4.65c}$$

The particle velocities are obtained by differentiating equation (4.64) with respect to time, thus:

$$\{\dot{\delta}_x\} = -i\omega\sum_{m=1}^{2} A_m n_{mx} \exp[i\omega(\{k_m\}^T\{r\}-t)] \tag{4.66a}$$

$$\{\dot{\delta}_y\} = -i\omega\sum_{m=1}^{2} A_m n_{my} \exp[i\omega(\{k_m\}^T\{r\}-t)] \tag{4.66b}$$

The strains in equations (4.65) may be expressed in terms of velocities by using equations (4.66), thus:

$$\{\varepsilon\} = [B_c]\{\dot{\delta}\} \tag{4.67}$$

where $[B_c]$ was found by White et. al. (Ref. 4.17) to be:

$$[B_c]^T = \frac{-1}{\lambda}\begin{bmatrix} n_{2y} & -n_{1y} \\ -n_{2x} & n_{2y} \end{bmatrix}\begin{bmatrix} n_{1x}k_{1x} & n_{1y}k_{1y} & n_{1x}k_{1y}+n_{1y}k_{1x} \\ n_{2x}k_{2x} & n_{2y}k_{2y} & n_{2x}k_{2y}+n_{2y}k_{2x} \end{bmatrix} \tag{4.68}$$

where,

$$\lambda = n_{1x}n_{2y} - n_{1y}n_{2x}$$

Such a wave (equation (4.62)) incident on a boundary (Figure 4.9) will cause normal and tangential stresses at the boundary:

$$\{\sigma\} = [D_c][B_c]\{\dot{\delta}\} \tag{4.69}$$

where $\{\sigma\}$ is the vector of normal and tangential stresses; and $[D_c]$ is the matrix defining the stress-strain relationship. If tractions are applied to the boundary which have equal magnitude as the incident wave and in opposition direction, then the energy at the boundary will be absorbed. It can be noted from equation (4.68) that the matrix $[B_c]$ is dependent on the direction of wave propagation. Therefore, if the direction of propagation of a given wave is known, a perfect energy absorbing frequency independent mechanism may be obtained by satisfying the boundary condition:

$$\{\sigma\} = -[D_c][B_c]\{\dot{\delta}\}$$

However, the direction at which a wave may impinge on a boundary is unknown. Therefore, White et. al. (Ref. 4.17) introduced another matrix $[C^*]$ to approximate the elements of $-[D_c][B_c]$ by direction independent terms. By optimising the matrix $[C^*]$ to obtain the maximum obsorption efficiency, White et. al. (Ref. 4.17) expressed the energy absorbing boundary condition for isotropic materials in terms of the normal and tangential velocities at the boundary in a form similar to Lysmer et. al. (Ref. 4.20):

$$\sigma_n = a\rho c_p \dot{\delta}_n$$
$$\sigma_t = b\rho c_s \dot{\delta}_t$$

where a, b are constants which may be altered to maximise the efficiency of the boundary for any given Poisson's ratio; ρ is the density of the material; c_p, c_s are the velocities of compression wave and shear waves respectively; and $\dot{\delta}_n$ and $\dot{\delta}_t$ are the normal and tangential velocities at the boundary. The values of a and b which give maximum efficiency are given by White et. al. (Ref. 4.17) and listed in Table 4.2:

Poisson's ratio	a	b
0.00	0.959	0.769
0.05	0.967	0.761
0.10	0.975	0.756
0.15	0.982	0.751
0.20	0.986	0.747
0.25	0.986	0.744
0.30	0.986	0.742
0.35	0.992	0.740
0.40	1.007	0.746
0.45	1.011	0.773

Table 4.2 Values of a and b for Unified Boundary Condition

4.4.3 The Damping Matrix

In a finite element, the velocity vector may be written as:

$$\{\dot{\delta}\} = [N]\{\dot{\delta}^e\} \tag{4.70}$$

where $[N]$ is the shape function matrix; and $\{\dot{\delta}^e\}$ is the vector of nodal velocities for an element.

The equivalent nodal forces due to the boundary stresses are:

$$\{P_c^e\} = -\int [N]^T\{\sigma\}d(\text{area}) \tag{4.71}$$

The consistent damping matrix may be written as:

$$[C_c^e] = \int [N]^T[D^*][N]d(\text{area}) \tag{4.72}$$

where,

$$[D^*] = \rho \begin{bmatrix} ac_p & 0 \\ 0 & bc_s \end{bmatrix}$$

and the integration is evaluated over the boundary area. The lumped damping matrix is:

$$[C_c^e] = \int [N]^T[D^*][I]d(\text{area}) \tag{4.73}$$

where [I] is the identity matrix.

The overall damping matrix for the geometrical damping of the structure may be obtained by assembling those elemental damping matrices for geometrical damping for the boundary elements:

$$[C_c] = \sum[C_c^e] \tag{4.74}$$

The overall damping matrix for the geometrical damping is added to the overall damping matrix in equation (4.41) to incorporate the geometrical damping effect.

Although it was suggested by White et. al. (Ref. 4.17) and Chow (Ref. 4.21) that the difference in the results obtained using the consistent matrix or lumped matrix is insignificant, the consistent damping matrix will be used in this study for the simulation of an infinite domain in a pile-soil system.

4.5 Data Processing

The application of the Finite Element Technique requires the manipulation of a large amount of data input and output. One of the most time consuming processes in finite element analysis is to input the data sets of the node numbers and their coordinates as well as the element numbers and their definitions. If this data was prepared by hand, human error would no doubt be introduced. If the computed results of a finite element analysis is presented as pages of numerical figures then these are difficult to comprehend. Therefore, pre- and post-processor computer programs were used to generate the input data and to present the computed results in an appropriate form for easy interpretation.

4.5.1 Pre-Processor Computer Programs

The pre-processor programs are the mesh generation program and the renumbering programs. The renumbering programs are used to rearrange the orders of the nodes and the elements in the generated mesh so as to improve the efficiency of the soultion method. The two-dimensional mesh generation program (Refs. 4.5, 4.23) generates the node number and their coordinates together with the element numbers and their definitions automatically from the basic control data provided. The basic control data are those require to describe the overall shape of the domain and how the domain should be discretised. The program may be used to generate two-dimensional 3-node and 8-node finite elements and produce a graphical presentation of the discretised domain. The author has modified the program to generate three dimensional 20-node isoparametric brick elements and to produce a graphical presentation of the discretised domain at a chosen horizontal section of the domain.

Since the mesh generation program is a general purpose one, it does not arrange the node numbers and element numbers so as to optimise the efficiency for a particular equation solving technique. Pre-processor programs (Ref. 4.24, 4.25) are then used to rearrange the node and element numbering to improve the efficiency of the frontal solution technique for the soultion of the admittance equations or the stiffness equations. Sloan et. al. (Ref. 4.24) proposed the use of a direct method to renumber the higher order finite elements to optimise the efficiency of the solution of such finite element system by using the frontal solution method. It was suggested that the frontwidth will be optimised when the order of the corner nodes are optimised. A direct method renumbers the finite element nodes using the minimum front growth criteria to obtain an optimal elimination sequence. The method proposed by Sloan et. al. (Ref. 4.24) renumbers the corner nodes of the finite element mesh to optimise the elimination sequence. Then the method reorders the element numbers. Both of the node numbers and the element numbers have to be rearranged because of the nature of the frontal solution method which assembles the variables in an element-by-element basis and eliminates the variables node by node. The advantage of using this program is that it chooses the starting node automatically and search through the whole domain to obtain the optimised frontwidth. The selection of the starting nodes for the optimisation process is based on some conceptes of the graph theory (Ref. 4.24).

The approach proposed by Sloan et. al. (Ref. 4.24) is suitable for the optimisation of the frontwidth for the higher order finite elements such as isoparametric elements. For the 3-noded simplex finite element meshes, the author of this thesis has developed another program to optimise the frontwidth of the 3-node finite element meshes. The program may be considered as an indirect method for optimising the frontwidth of a finite element mesh. This indirect method is based on the technique described by Sloan et. al. (Ref. 4.24) where the maximum frontwidth is reduced indirectly by minimising the bandwidth, by using the condition that the maximum frontwidth must always be less than, or equal to, this quantity. The program uses the Bandwidth

Reduction algorithm proposed by Collins (Ref. 4.25) to optimis the bandwidth for the finite element mesh. The element numbers are then rearranged to an ascending sequence of their lowest numbered nodes. This ensures that the new elimination order is preserved as closely as possible.

Although it may found that the time taken to pre-process the data is very long, the savings on the computation time and total file storage during the main analysis make it worthwhile. The savings are more significant when the same structure is analysed more than once.

4.5.2 Post-Processor Computer Program

The post-processor programs are used to present some chosen parameters from the finite element analysis results in a graphical form for interpretation. The software GPCP (A General Purpose Contouring Program) (Ref. 4.26) which is available in the mainframe computer (ICL 2900 model) at Edinburgh University was used to plot the equipotential contours for the simulation of the earth-resistance method of non-destructive testing. The equipotential contour plots may be used for qualitative assessment of the non-destructive method of testing the integrity of a pile-soil system. Before using the GPCP program, it is required to prepare the data in a format suitable for the program input. Again, to prepare such a large amount of data, it is tedious, time consuming and prone to error. Hipkin (Ref. 4.27) has developed a computer program to convert geophysical data sets into a format suitable for the GPCP program. His program was used to convert the data from the finite element analysis to a format suitable for the GPCP program. For the interpretation of earth-resistance test results using finite element method, the E-R curves are required. The E-R curves for the field data and the finite element simulations can be drawn using the Easygraph package (Ref. 4.28) which is also available in the mainframe computer at Edinburgh University. This kind of comparative E-R curves are most suitable for interpretation of earth-resistance testing results.

The easygraph package can also be used to plot the displacement, velocity or acceleration traces for the finite element idealisation in the time domain for the simulation of the sonic echo testing on a civil engineering structure. Although the deformed shape of the structure may be plotted using the ERCC Graphics Package to illustrate physically the wave propagation in a structure, the large amount of file spaces required to store all the data at each time step has made it impossible. The stress and strain distributions in the idealised structure, which may also be plotted as stress or strain contours in the structure, are not included because a large storage space is required again. In fact, they are not used for data interpretation in a real test.

4.6 Finite Elements Used and Programming Techniques

The problems to be studied in this research are the simulation of the the Earth-Resistance Method and the Sonic Echo Method and the Vibration Methods of Non-Destructive Testing of Civil Engineering Structures and Structural Members. The Earth-Resistance Method of Testing is an Electricity Flow problem at steady state. The Sonic Echo Method and the Vibration Methods of Integrity Testing are dynamic situations in which the structure responds to a time dependent applied force. Three node triangular finite elements are used for the two-dimensional study of the electricity flow problem while 20-node isoparametric elements are used for the three-dimensional analysis. Three-dimensional dynamic analysis is not practical due to the large amount of computing time required for the time integration. Therefore, the simulation of the Sonic Echo Method and the

Vibration Methods of Integrity Testing is undertaken by two-dimensional finite element analysis. The analysis is undertaken using 3-node triangular elements and 8-node isoparametric elements.

A considerable proportion of the time spent on this research was spent on computer programming. The computer programs were developed for two and three dimensional electricity flow problem and for the two-dimensional dynamic analysis of a structure in transient state and steady state. The computer program for electricity flow problem analysis was developed based on a computer program which was used to analyse a two dimensional plane frame using the Stiffness Method. The program was also modified to handle three-dimensional analysis using the 20-node isoparametric finite elements. The computer program for dynamic analysis is a modified version of the computer program in Reference 4.3 which uses triangular elements for the static analysis of two-dimensional planes. Since the program is divided into subprograms, it may easily be modified for the dynamic analysis of two-dimensional planes using either 3-node or 8-node finite elements.

The computer programs are developed using the mainframe computer at Edinburgh University. The computer is the ICL 2900 model and the operating system is called EMAS 2900 which is a general-purpose and multi-access system developed by ERCC (Edinburgh Regional Computing Centre). Each user of the system is allocated with a processor and shares the computer with other users. The processor used consisted of 30 megabytes of virtual memory which is sufficient to run both static and dynamic finite element analysis programs. The programs were written in Fortran 77 and double precision was used for the analyses. ERCC also provided a compiler which optimised the object code of the source program. This feature was used during the compilation and is found very useful in improving the efficiency in both static and dynamic finite element analysis.

A relatively large finite element system has been used throughout this research and therefore frontal solution has been used for both static and dynamic finite element analysis. Advantage has been taken of the symmetry nature of the stiffness matrix and only the upper half of the matrix is written into the disc files. The type of plane finite elements to be used in the analyses, plane strain elements or plane stress elements, will be mentioned in Chapters 6, 7 and 8 when they are applied to the analyses. In the dynamic analysis, the effective stiffness matrix, which is the same throughout, is only solved once at the first time step and the displacements at each time step is computed by modification and backsubstitution of the load vectors at each time point. Only displacements, velocities and accelerations at chosen degrees of freedom are output and stored in a file to reduce the file spaces required to store all the output data. For the same reason, the stress and strain distributions within the structure are not computed to save both computer time and file storage unless they are required.

The computer program listings are not given in the thesis because they are lengthy. Instead, flowcharts for the main analysis programs are given in Appendix C to show the main differences in the analysis procedures.

References 4.

1. Zienkiewicz, O.C., "The Finite Element Method in Engineering Science", McGraw-Hill Publishing Company Limited, 1971.

2. Bathe, K., Wilson, E.L., "Numerical Methods in Finite Element Analysis", Prentice-Hall Inc., 1976.

3. Segerlind, L.J., "Applied Finite Element Analysis", John Wiley and Sons Inc., 1976.

4. Hinton, E., Owen, D.R.J., "Finite Element Programming", Academic Press Inc., (London) Ltd., 1977.

5. Hinton, E., Owen, D.R.J., "An Introduction to Finite Element Computations", Pineridge Press Limited, 1979.

6. Desai, C.S., "Elementary Finite Element Method", Prentice-Hall Inc., 1979.

7. Cheung, Y.K., Yeo, M.F., "A Practical Introduction to Finite Element Analysis", Pitman Publishing Limited, 1979.

8. Clough, R.W., Penzien, J., "Dynamics of Structures", McGraw-Hill Inc., 1975.

9. Irons, B., Ahmad, S., "Techniques of Finite Elements" Ellis Horwood Limited, 1980.

10. Chen, W., Saleeb, A.F., "Constitutive Equations for Engineering Materials", John Wiley and Sons, Inc., 1982.

11. Smith, I.M., "Programming The Finite Element Method", John Wiley and Sons Ltd., 1982.

12. Bayo, E., Wilson, E.L., "Numerical Techniques for the Evaluation of Soil-Structure Interaction Effects in the Time Domain", Earthquake Engineering Research Centre, Report No. UBC/EERC - 83/04, University of California, Berkeley, California, February, 1983.

13. Key, S.W., "Transient Response by the Time Integration: Review of Implicit and Explicit Operators", in 'Advanced Structural Dynamics', Edited by J. Donea, Applied Science Publishers Ltd., London, 71-96, 1986.

14. Newmark, N.M., "A Method of Computational for Structural Dynamics", Journal of the Engineering Mechanics Division, Proceedings of the American Society of Civil Engineers, Vol. 85, No. EM3, 67-94, July, 1959.

15. Day, S.M., "Finite Element Analysis of Seismic Scattering Problems", Ph.D. Thesis, University of California, San Diego, 1977.

16. Smith, W., "A Non-Reflecting Plane Boundary for Wave Propagation Problems", Journal of Computational Physics, Vol. 15, 492-503, 1974.

17. White, W., Valliapan, S., Lee, I.K., "Unified Boundary for Finite Dynamic

Models", Journal of the Engineering Mechanics Division, Proceedings of the America Society of Civil Engineers, Vol. 103, No. EM5, 949-964, October, 1977.

18. Simons, H.A., Randolph, M.F., "Short Communication: Comparison of Transmitting Boundaries in Dynamic Finite Element Analysis using Explicit Time Integration", International Journal for Numerical and Analytical Methods in Geomechanics, Vol. 10, 329-342, 1986.

19. Lysmer, J., Waas, G., "Shear Waves in Plane Infinite Structures", Journal of the Engineering Mechanics Division, Proceedings of the American Society of Civil Engineers, Vol. 98, No. EM1, 85-105 February, 1972.

20. Lysmer, J., Kulemeyer, R.L., "Finite Dynamic Model for Infinite Media", Journal of the Engineering Mechanics Division, Proceedings of the American Society of Civil Engineers, Vol. 95, No. EM4, 859-877, August, 1969.

21. Chow, Y.K., "Accuracy of Consistent and Lumped Viscous Dampers in Wave Propagation Problems", International Journal for Numerical Methods in Engineering, Vol. 21, 723-732, 1985.

22. Synge, J.L., "Elastic Waves in Anisotropic Media", Journal of Mathematics and Physics, Vol. 35, 323-334, 1956.

23. Abu Kassim, A.M., University of Edinburgh, Private Communication, 1984.

24. Sloan, S.W., Randolph, M.F., "Automatic Element Reordering for Finite Element Analysis with Frontal Solution Scheme", International Journal for Numerical Methods in Engineering, Vol. 19, 1153-1181, 1983.

25. Collins, R.J., "Bandwidth Reduction by Automatic Renumbering", International Journal for Numerical Methods in Enhineering, Vol. 6, 345-356, 1973.

26. Calcomp, "GPCP A General Purpose Contouring Program" User's Manual, California Computer Products, Inc., August, 1983.

27. Hipkin, R., University of Edinburgh, Private Communication, 1984.

28. Stroud, N., "Easygraph on EMAS 2900", User Note 12, Edinburgh Regional Computing Centre, March, 1983.

Chapter 5

A Finite Element Simulation of the Resistivity Method for Non-Destructive Testing of Reinforced Concrete Piles

5.1 Introduction

The Electrical Earth-Resistance Method of Non-Destructive Testing of reinforced concrete piles proposed by McCarter (Ref. 5.1) and McCarter et. al. (Ref. 5.2) is illustrated in Figure 5.1. McCarter (Ref. 5.1) demonstrated a theoretical approach to the study of the variations to be expected and how the earthing resistance is related to the physical dimensions of the pile in the ground. McCarter (Ref. 5.1) also studied: the effect of the mutual resistance of the return current electrode, when it is placed at a more practical distance from the pile; the effects that a defective pile may have on the earthing-resistance; and how the resistance may be measured in the field. The closed form solution for these studies on the earth resistance method of testing concrete pile has been reviewed in section 2.3.1. McCarter (Ref. 5.1) and McCarter et. al. (Ref. 5.2) also employed electrical analogues; electrolytic tank and conductive paper simulations to establish the validity of his theoretical predictions; to study the methodology of testing and to highlight the problem that may encounter in the interpretation of field data. The electric analogue models used by McCarter (Ref. 5.1) and McCarter et. al. (Ref. 5.2) for these studies have been described in section 3.2 where the advantages and disadvantages of using the electric analogue models have also been discussed.

This chapter is concerned with the study of the earth resistance method of testing using the finite element approach. Two dimensional finite element analysis will be applied to study qualitatively: the interrelationship between the system variables; the effects on the measured earth-resistance when any of the parameter is changed; and the effects on the resistance measurements when there are some typical faults in a pile. The significance of these effects on the interpretation of the results of the earth-resistance technique of non-destructive testing is also discussed. These studies will be enhanced by the use of three dimensional finite element models. The limits of application of the earth-resistance method will be revealed. The application of the three dimensional finite element analysis to the interpretation of field test results will also be demonstrated. Some possible modifications to the testing method will also be discussed.

The finite element technique which has been applied to many structural problems and field problems may be applied equally to the analysis of electrical engineering problems (Refs. 5.3, 5.4, 5.5). The electric current flow in a conductor may be treated as a potential flow in a porous medium using the finite element analysis technique (Ref. 5.6). An advantage of applying the finite element model over the closed form theoretical approach and the electric analogue model studies on the non-destructive method of resistivity testing is that a wide range of relative resistivities between the pile concrete and soil may be simulated and the influence of this factor on fault detection may be made with relatively simple operations. The two dimensional finite element analysis may be used for qualitative studies on the testing method while the three dimensional finite element finite element analysis may be used for both qualitative and quantitative studies on the testing method. Since the finite elements in a domain may be defined to have different material and geometric properties in order to simulate a more realistic pile-soil system, the finite element technique is more attractive in the interpretation of resistivity field test results.

5.2 Model Verification

In the two-dimensional finite element analysis, three node triangular finite elements are used. The finite elements used are equivalent to three node triangular constant stress elements used in structural analysis. In an electric current flow problem, however, it is assumed that the potential gradient in each element is constant. This analysis would approach the exact solution if the element sizes in the domain were reduced to a sufficiently small size.

A regular finite element mesh will be used to verify the response of the pile-soil system due to an applied electric current as studied by McCarter (Ref. 5.1). Figure 5.2 shows a typical 100 element finite element idealisation of one half of the plan of the problem studied. The domain is also divided into smaller triangular elements to test the analysis convergence as the élement sizes became finer. A potential of 10 V was applied between the lower left hand corner and the lower right hand corner and the computed applied current at the lower left hand corner was plotted against the total number of finite elements in the domain. This graph, which is shown in Figure 5.3 shows that the analysis gives an upper bound solution of the applied current. This may be explained for an increased in the element size means an increased conductivity which is equivalent to the increased stiffness or too-stiff element when a coarse finite element mesh is used for structural analysis. It is obvious in Figure 5.3 that the analysis has converged reasonably well when the domain is discretised into 6400 three node elements, that is, the right angled triangular elements have perpendicular edges of 0.125 m length.

5.3 Typical Responses of the Resistivity Method of Pile Testing

5.3.1 The Response Curves

In the interpretation of geophysical methods of ground explorations, response curves may be used. A response curve as defined by Beck (Ref. 5.7) as "a plot of position versus the abnormal response of a detector to the physical property anomaly in a body of interest". The electrical resistivity technique of non-destructive testing investigated by McCarter (Ref. 5.1) and McCarter et. al. (Ref. 5.2), which is based on standard geophysical method, may be interpreted in a similar manner. The Earth Resistance curve (E-R curve) defined in reference 5.1 may be considered as the response curve for the earth resistance method of non-destructive testing. The E-R curve as defined in reference 5.1 is the plot of apparent resistance Voltage Drop from the Pile Head/Applied Current Ratio against the distance from the centre line of the pile head. This E-R curve has been used for the interpretation of the earth resistance method of testing for pile-soil systems (Ref. 5.1).

Using the conductive paper model, McCarter (Ref. 5.1) and McCarter et. al. (Ref. 5.2) studied the variation of electric field distribution around a pile and its variations due to a change of relative resistivity between the pile material and soil. This method of interpretation is similar to the method of equipotential maps (Refs. 5.7, 5.8) in the geophysical technique.

In this chapter, earth-resistance curves will be used for the interpretation of the simulated test results and the electric field distribution will be provided for reference when necessary.

5.3.2 Finite Element Models

In the field, piles may be of different shapes and sizes. Here, it is only possible to determine the field characters of a number of typical piles. However, the size of the domain to be considered is limited by the number of finite elements used. In the following two dimensional finite element simulations, a pile has been considered to have a square cross-sectional area and so is the reinforcement cage. For these studies, the piles are considered to have square cross sectional areas so that regular finite element meshes can be used while the ratio of the size of the pile to the size of the reinforcement cage may be controlled. In addition, due to the use of the regular finite element mesh, the results for different simulations may be compared because the effects due to a sudden change in finite element sizes when an irregular finite element mesh is used may be avoided.

Since the pile to be considered in the two dimensional simulations are of 5.0 m long, the return current electrode may be placed 5.0 m from the centre of the pile for the earth resistance tests. Then, the finite element mesh as shown in Figure 5.2 for a 10.0m x 5.0m domain may not be required. To optimise a finite element mesh for the two dimensional simulation of the earth resistance method of testing foundation piles, the distortion of the potential distribution in the domain due to the truncation at the boundary has to be minimised. Figure 5.4 shows a 5.0m x 5.0m domain which has been divided into 5000 regular triangular elements. The finite elements used here have 0.1 m long perpendicular edges. This has an advantage over the finite element size mentioned in section 5.2, where the corresponding edges are 0.125 m long in that the change in the size of the pile or the reinforcement cage may be in steps of 0.1 m, which is more realistic. A point source, which has a potential of 10.0 V, is applied at the bottom left hand corner while the point sink at 0.0 V is situated at the bottom right hand corner. The main purpose of the simulations is to observe the distortion on the earth resistance measurement due to truncation at the boundary. Therefore, the earth resistance curves between the source and the sink were plotted for different sizes of the domain to search for an appropriate finite element mesh where the truncation at the boundary cause the least distortion on the earth resistance measurements between the source and the sink.

Figure 5.5 shows the E-R curves between the source and the sink when the lateral dimension of the domain has been reduced from 5.0 m to 3.0 m and 2.0 m. It is obvious from Figure 5.5 that the distortion on the earth resistance readings are negligible when the lateral dimension of the domain is greater than 3.0 m. The variation in the longitudinal dimension of the domain is then considered by terminating the domain at 0.5 m, 1.0 m, 2.0 m and 3.0 m from the source and the sink. Figure 5.6 shows the E-R curves for each case where it may be concluded that if the source and the sink are placed at 1.0 m from the boundaries, the distortion on the E-R curve will be negligible.

The two dimensional finite element idealisation used in these studies are shown in Figures 5.7 and 5.8. The finite element mesh shown in Figure 5.7 represents one half of the problems studied where the hatched area indicates the cross section of a typical idealised pile. The position of the return current electrode is marked R in Figure 5.7. The thickness of the elements are 5.0 m to simulate a 5.0 m pile in a site where there is a non-conducting layer at 5.0 m.

Figure 5.8 shows half of the elevation of the problem studied. Again, the hatched area shows the pile under consideration and the return current electrode is again marked R in Figure 5.8. Here, the element thickness is 0.2 m to simulate a quarter of the square pile which has a cross sectional area of 0.4m x 0.4m.

5.3.3 Electrical Properties of Concrete and Soil

In this study, particular interest has been shown to the application of the resistivity method on cast in-situ piles. Therefore, the electrical properties of the concrete and soil are required in the simulation of the earth-resistance method of pile testing. In addition, the resistivity of concrete at different ages is also required. It was suggested by McCarter (Ref. 5.1) that the earth-resistance method of pile testing should be carried out when the reflection coefficient, k (equation 2.16), is large. Such a large reflection coefficient may be obtained when the concrete is first poured, where $\rho_2 >> \rho_1$, or when the concrete has hardened, where $\rho_1 >> \rho_2$ (ρ_1 = resistivity of concrete; ρ_2 = resistivity of soil).

The resistivity of a 1:2:4 mix was studied by McCarter et. al. (Ref. 5.9) and Whittington et. al. (Ref. 5.10). It was shown in both references that the resistivity of the 1:2:4 mix, which has 0.7 w/c ratio, has a resistivity of 10.0 Ωm about three hours after pouring and 30.67 Ωm after about thirty days since it was poured.

The resistivity of minerals, rocks and sediments may be found in a number of geophysics texts. Some of the typical resistivity values of minerals and sediments given in reference 5.11 are summarised in Tables 5.1 and 5.2.

Mineral	Resistivity Range (Ωm)	Resistivity Average (Ωm)
Meteoric waters	$30 - 10^3$	
Surface waters (ign. rocks)	$0.1 - 3x10^3$	
Surface waters (sediments)	10 - 100	
Soil water		100
Natural waters (ign. rocks)	0.5 -150	
Natural waters (sediments)	1 - 100	
Sea water		0.2
Saline waters, 3%		0.15
Saline waters, 20%		0.05

Table 5.1

Sediments	Resistivity Range (Ωm)
Unconsolidated wet clay	20
Marls	3 - 70
Clays	1 - 100
Alluvium and sands	10 - 800
Oil sands	4 - 800

Table 5.2

5.3.4 Simulated Testing of Reinforced Concrete Piles

Figure 5.9 shows the percentage equipotential contours when the resistivity of the concrete pile is the same as the soil at 1.92 Ωm while Figure 5.10 shows the equivalent E-R curve. This model is hereafter referred to as the 'reinforcement model' since it could correspond to a reinforcement cage being placed directly in the soil. The soil considered in this study is clay with a resistivity of 1.92 Ωm.

5.3.4.1 Testing of Mature Reinforced Concrete Pile

Figure 5.11 illustrates the percentage equipotential contour for a pile where the concrete to soil relative resistivity is 19/1 ($k = -0.9$). This represents pile concrete with a high resistivity, a situation which may be considered to correspond to concrete that has been cured for over 30 days. The effect of this is to increase the relative resistance of the pile and thereby group the equipotential contours closer around the pile reinforcement.

5.3.4.2 Testing of Fresh Reinforced Concrete Pile

By way of contrast, when the concrete has lower resistivity than the soil, as in the example with a concrete to soil relative resistivity of 1/19 ($k = +0.9$) shown in Figure 5.12, the percentage equipotential contour will move away from the pile and there will be a decrease in the measured resistance.

5.3.4.3 Interpretation of Test Results

The reinforcement model is the case where $k = 0$. If the resistivities of pile concrete and the soil surrounding it are the same, the integrity of the pile may not be assessed by the earth-resistance method.

Figure 5.13 shows the E-R curves for the reinforcement model, the mature concrete pile model and fresh concrete pile model. The increase in relative resistivity, resulting from the relatively lower conductivity of the old concrete, increases the potential difference between the pile reinforcement and any point outwith the nominal pile periphery. This, in turn, will result in an increase in measured resistance and hence an upward displacement of the E-R curve. In contrast with the fresh concrete, which has a relatively higher conductivity, there is a reduction in resistivity and a consequent downward displacement of the E-R curve as shown in Figure 5.13.

Figures 5.14 and 5.15 show graphically the relationship between the disturbing effects due to the soil and the variation in the width/length ratio of the pile (p/h) for different resistivity coefficients as given in Equation (2.14). From this, McCarter (Ref. 5.1) suggested that a pile should be tested when the relative resistivity ratios have a large magnitude, that is large ρ_2/ρ_1 or ρ_1/ρ_2 ratios. However it should be noted in Figures 5.14, 5.15 that the disturbing effects due to the soil are much greater in Figure 5.14 when $k > 0$. When $k < 0$, the disturbing effects are smaller. Therefore, if $k > 0$, the disturbing effects due to the soil may become so great that a variation in the pile section or concrete resistivity may become insignificant in the interpretation of the resistivity tests. That is, a fault in a pile which has $k > 0$ may not be detected by the resistivity method.

The same conclusion may be drawn from Figures 5.9 to 5.13 where the disturbing effects is more significant when the concrete is old rather than fresh. The earth resistance method of testing is suitable for sites where the resistivity of the pile concrete is greater than the resistivity of the surrounding soil. In the following studies, examples will concentrate on mature concrete pile models. The application of the E-R curves in the interpretation of earth-resistance method of integrity testing is illustrated in Figure 5.13 where the slopes of the concrete portion and the soil portion of the E-R curves could give an indication of the relative resistivity between the concrete and its surrounding soil. A steep slope means a large potential drop in that region indicating the existence of a high resistance material. Similarly, a gentle slope indicates a low resistance material.

5.4 Case Studies

It has been shown in section 5.3 that in the application of resistivity techniques to pile testing, the earth resistance measurements are affected by the resistivities of both the pile concrete and the surrounding soil. The effects on the measured earth-resistance when: the cross-sectional area of the pile; the size of the reinforcement cage; or the location of the return current electrode is changed, will be studied in this section. The finite element idealisation shown in Figure 5.7 will be used for these studies. Again, the domain has been considered to be 5 m deep.

5.4.1 Variation of the Return Current Electrode Distance/Pile Length (L/h) Ratio

Figure 5.16 shows the E-R curves for the perfect pile model where the return current electrode has been placed at a distance of 0.5h, 1.0h, 1.5h and 2.0h away from the axis of the pile (h is the length of the pile). It is clear that the measured resistance near the pile head, which was shown in Figures 5.9 to 5.13 to indicate the integrity of the pile-soil system, was not affected by the position of the return current electrode relative to the pile. Therefore, the location for the return current electrode will not affect the resistance measurement in the field and the interpretation of the pile-soil system in a relatively homogeneous ground will not be affected. For a quick interpretation of field data, McCarter (Ref. 5.1) suggested that the piles be tested with a constant distance between the centre of the pile and the return current electrode so that anomalies in the group may be spotted by comparing the E-R curves without further data processing.

5.4.2 Variation of the Pile Width/Pile Length (p/h) Ratio

Figure 5.17 shows the E-R curves for a series of 5 m idealised piles where the widths of the reinforcement cages are half the width of the pile. In general, the soil portion of the E-R curves are similar and the differences in the measured earth-resistance are small. Therefore, if the soil in a site is reasonably homogeneous and the ratio of the width of the reinforcement cage to that of the pile is constant, the measured earth-resistance for different sizes of piles would be similar. Hence, a similar E-R curve may be expected from different lengths of piles if the ratio of the width of the pile to the width of the reinforcement cage of the pile is kept constant.

5.4.3 Variation of the Reinforcement Cage Width/Pile Width (a/p) Ratio

Figure 5.18 shows the E-R curves for the 1.0m x 1.0m x 5m idealised pile model where the width of the reinforcement cage has increased from 0.2 times that of the pile width to 0.8 times in steps of 0.2. This figure indicates that in the case of a cast-in-situ pile, differences in the cross sectional dimensions may be detected by the resistivity method of testing. For a mature concrete pile, decreasing the ratio of a/p or a/h, that is using a smaller pile or a shorter pile than specified, will result in an increase in the measured resistance and an upward displacement of the E-R curve from the reference pile. The soil portion of the E-R curves in Figure 5.18 are parallel indicating that the change in the a/p ratio is independent of the soil resistivity which agrees with equation (2.14).

In Figures 5.17 and 5.18, the slopes of the concrete portion of the E-R curves are different when the position of the reinforcement cages are varied. This illustrates that the potential drop in the concrete is also dependent on the width of the reinforcement cage.

5.4.4 Variation of the Reinforcement Cage Length

To investigate the effects when the length of the pile reinforcement is reduced or the soil is stratified using a two-dimensional finite element model, vertical sections of the problem are considered.

Figure 5.8 shows the idealisation of the vertical section of the problem. Figure 5.19 illustrates the apparent resistances measured on the ground surface when the length of the reinforcement cage in the pile is reduced. This indicates that the method of integrity testing can be used to check the length of reinforcement in a perfect pile. A decrease in the reinforcement length in a concrete pile will result in an increase in resistance and hence resultant upward displacement of the E-R curve.

5.5 Sensitivity of the Resistivity Tests

The load bearing capacity of a pile depends on the concrete strength and the cross-sectional area of the pile. Necking in a cast-in-situ pile could seriously reduced the load bearing capacity of the pile. Particular interest has been shown in the sensitivity of the resistivity method of integrity test to locate necking in a pile. The effects of defects in a pile on the percentage equipotential distributions and the measured earth-resistance during a resistivity test may also be simulated using the finite element method. Through these studies, some guidelines in the interpretation of the results from earth-resistance technique of integrity testing and its limits of application may be revealed.

5.5.1 Necking Piles

In a necking pile, the void may be filled by the surrounding soil or honeycombed concrete. Depending on the relative conductivity between the pile concrete and the infill material, the equipotentials near the fault may move away or nearer to it. In Figure 5.20, the defect, shown by a dotted rectangle, is idealized as if it were full of soil of the same resistivity as the surrounding soil. In this case, as would be expected, the equipotentials have moved nearer to the return current electrode. The void, shown in Figure 5.21, is filled with gravel which may be a result of the cement being washed away during concreting and leaving honeycombed concrete in the void. The gravel is assumed to have a higher resistivity than the concrete with a resistivity of 20000.0 Ωm (k = 0.99). The resulting shift of the percentage equipotentials is towards to the necking.

The E-R curves shown in Figure 5.22 indicate that a lower resistivity material in the void results in a downward shift of the E-R curve relative to the original pile model and vice versa. In addition, the example illustrates that the earth-resistance method of pile testing is more sensitive to the detection of necking filled by a less resistant material than the pile concrete. In the following studies, the voids will be considered to be filled by the surrounding soil. It should be noted that in the above simulation, the pile has been considered to have a reduced cross-sectional area along its whole length.

5.5.2 Defects Inside the Reinforcement Cage

The resistivity method of integrity testing of pile proposed by McCarter (Ref. 5.1) measured the apparent resistance of the soil between the electrodes, that is the reinforcement cage and the return current electrode. It was assumed that this measured earth-resistance would reveal any anomalies that existed in the pile and the soil between the electrodes. Figure 5.23 shows that the method would not be able to locate faults inside the reinforcement cage. Here, the pile core was considered to be soil and there was no consequent shift in the E-R curve when compared with a perfect pile.

5.5.3 Position of the Fault Relative to the Line of Resistance Measurement

Figure 5.24 shows the E-R curves for the resistivity method of testing when the necking was considered to be along the measurement line and at 90° from the line. This indicates that the integrity of the pile-soil system in each direction may be assessed by the resistivity method of testing. The distortion of the E-R curve is most significant near the pile head.

5.5.4 Position of the Fault Relative to the Pile Head

Two dimensional finite element analysis may also be used to study the variations of the measured earth-resistance due to the change in the relative position between the necking and the pile head by considering a vertical idealisation of the problem as shown in Figure 5.8. Figure 5.25 gives the percentage equipotential contours of a non-defective mature concrete pile in a vertical section. A necking void at mid-depth of the pile was considered to be filled by the surrounding soil or gravel. Figure 5.26 shows the distribution of percentage equipotential contours when the necking is filled by the surrounding soil. If the void is filled by gravel, the distribution of percentage equipotentials is as shown in Figure 5.27. These equipotential distributions confirm that a different infill material in the necking void has resulted in a change in the position of the equipotentials at the ground surface. This implies that the E-R curve, which is a measure of the potential drop on the ground surface, is suitable for the interpretation of the earth-resistance method of pile testing.

Figure 5.28 shows the E-R curves for the simulated tests on an idealised perfect pile and idealised necking piles. The figure again illustrates that a higher resistance infill material in the necking displaced the corresponding E-R curve upwards compared to a non-defective pile model. In contrast, the E-R curve for a lower resistance infill material is displaced downwards. The necking void considered has a volume of 10% of the total volume of the pile.

Instead of having a necking at mid-depth of the pile, necking voids situated at 1/4 depth and 3/4 depth of the pile are also considered. Figure 5.29 shows the E-R curves for the simulated tests on an idealised perfect pile and the idealised necking piles where the necking voids are at different depths from the pile head. The necking voids of these idealised necking piles are considered to have a volume equal to 10% of the total volume of the pile. It may be concluded from Figure 5.29 that the faults near to the pile head may be detected easily by the earth-resistance method of pile testing. Although the apparent resistances near the return current electrode are similar for different positions of the necking, the deviation of the measured earth-resistance from the perfect pile is most significant for the case where the necking is nearest to the pile head. This gives an indication that a fault near to the pile head may be detected easily and confirms that the resistance measurements near to the pile head are more important in determining the integrity of the pile-soil system in the resistivity method of testing.

5.5.5 Size of Fault in the Pile

The necking pile model with a necking at its mid-depth is used again. This time, the simulated necking has a volume 5% of the total volume of the pile. In addition, the fault is assumed to be filled by the surrounding soil. Two cases are considered, one where the void is in contact with the surrounding soil (Case a) and the other when it is in touch with the reinforcement (Case b) as shown in Figure 5.30.

The E-R curves shown in Figure 5.31 indicate that a fault in a pile may be detected if it is between the reinforcement cage and the return current electrode and that the sensitivity of the method in detecting the anomaly in the pile soil system is independent of the distance of the fault from the reinforcement. It is also shown that the sensitivity of the resistivity method in detecting a fault in a pile is also a function of the size of the fault.

5.5.6 Length of Reinforcement in the Pile

The ability of the earth-resistance method of integrity testing to detect necking in a partially reinforced pile is shown in Figure 5.32 where the E-R curve for a faulty pile with shortened reinforcement cage is considered. It may be concluded that if the reinforcement does not extend into or beyond the defect in the pile, then the integrity of the pile-soil system cannot be assessed using the earth resistance technique since the E-R curves for a perfect pile and the defective pile is indistinguishable.

5.5.7 Stratified Ground

In this section, the 5 m pile is considered to be buried in layered ground which consists of three horizontal layers of soil. One of the interfaces appears at the mid-depth of the pile while the other is located at 0.10 m above the toe of the pile. The bottom layer may be considered to have a high resistivity to simulate a rock base such as granite which has a resistivity range between 3×10^3 Ωm and 6×10^6 Ωm (Ref. 5.11). Conversely, it may be considered to have a low resistivity to simulate the existence of saline water in the layer which has an average resistivity of 0.05 Ωm (Ref. 5.11). The effects of different types of soil on the measured earth-resistance may be interpreted from the E-R curves shown in Figure 5.33. This figure illustrates that the measured resistance of the pile-soil system increases or decreases depending on the resistivity of the soil layers as well as its level relative to the toe of the pile. Figures 5.34 and 5.35 show that the response of the pile-soil system is dominated by the resistivity of the top soil. In Figure 5.34, the top soil is given a low resistivity value of 0.05 Ωm, and the response of the system will be similar to that if the return current electrode has been moved to an infinite distance from the pile. In contrast, if the top soil has high resistivity (3.0×10^3 Ωm), the measured resistance is similar to that of the whole soil mass consists of the high resistivity soil. In Figure 5.35, the high resistivity soil has been marked as rock. It may be concluded that if the resistivity of soil is lower than the concrete, a flatter E-R curve will result and vice versa.

Although McCarter (Ref. 5.1) suggested that piles should be tested as a group and an abnormal response of a pile from the group would be suspicious, for more reliable interpretation of the test results using finite element analysis, the E-R curves shown in Figure 5.33 suggest that accurate soil data should be used. This also suggests that the earth-resistance method of integrity testing is most effective in homogeneous ground.

5.6 Three Dimensional Analyses

The two dimensional finite element analysis has been shown to be suitable for the qualitative studies on the earth resistance method of testing for foundation piles. The case studies given in sections 5.3 to 5.4 have shown that the earth resistance method of testing may be used for assessing the integrity of foundation piles. Some limitations of the application of the testing method have been revealed in section 5.5.1 to 5.5.7 using finite element studies. The two dimensional finite element analysis is particularly suitable for qualitative studies on non-destructive testing methods due to its lower computing cost compared to a three dimensional finite element analysis. The two dimensional finite element analysis can also be considered to provide guidelines for the interpretation of field test results. The application of the two dimensional analysis to field data interpretation cannot give any prediction on the properties of the pile-soil system because the idealisation used cannot represent the actual field test situation. The horizontal section idealisations used in sections 5.3 to 5.5 may be considered as testing a pile-soil system between an infinitely long pile and an infinitely long return current electrode. Similarly, the vertical section idealisations may be considered as the testing of an infinitely long wall between the reinforcements in the wall and an infinitely long line of current electrode placed on the ground surface.

For a more realistic representation of the pile-soil system, three dimensional finite element idealisations may be used. The three dimensional finite element idealisations may be used for qualitative and quantitative studies of non-destructive testing methods as well as for the interpretation of field test results. In sections 5.6.1.1 to 5.6.1.3, some case studies will be used to confirm the results obtained using two dimensional analysis. The application of the three dimensional analysis to the interpretation of field test results will be illustrated in section 5.6.2.

5.6.1 Case Studies

The finite element idealisation of one half of the three dimensional pile-soil system is given in Figure 5.36. The pile has a diameter of 0.3 m while the diameter of the reinforcement cage is 0.15 m. The pile is marked P and the return current electrode is marked R in Figure 5.36. The domain has been considered symmetrical about the line A-B and, therefore, only one half of the domain is analysed. The pile is 5.0 m long and the return current electrode is placed 5.0 m from the pile head. In these studies, the return current electrode is assumed to be inserted into the ground to a depth of 0.20 m which corresponds to field practice (Ref. 5.2).

Figure 5.37 shows the E-R curve for a reinforcement model together with the E-R curves for the simulated tests on an old concrete pile and a fresh concrete pile. Similar to the results obtained from a two dimensional analysis (section 5.3.4.3), the displacement of the E-R curve for the old concrete pile from that for the reinforcement model is greater than the displacement for the fresh concrete pile. This also demonstrates the guideline provided by using the two dimensional analysis to interpret real site results. It is confirmed that the testing method is more suitable for testing foundation piles where the resistivity of the surrounding soil is lower than the resistivity of the pile concrete.

5.6.1.1 Test on a Necking Pile

A necking pile is shown in Figure 5.38. The loss of concrete in the necking section has a volume approximately 12% of the total volume of the pile. In this study, the necking void in the pile has been filled by the surrounding soil. Figure 5.39 shows the E-R curves for the perfect pile model and the necking pile model obtained from the simulations. It is obvious that the E-R curve for the necking pile model has displaced downwards compared to the perfect pile model due to the inclusion of the surrounding soil which has a lower resistivity.

5.6.1.2 Test on a Partially Reinforced Concrete Pile

Figure 5.40 shows the simulated test results on a partially reinforced perfect pile, a partially reinforced necking pile and a perfect pile which is reinforced for its whole length. The partially reinforced pile has one third of its whole length reinforced. The E-R curves shown in Figure 5.40 illustrate that the earth resistance method of testing cannot locate a necking in the unreinforced part of the pile. This confirmed that the earth resistance method of non-destructive testing can only detect defects lying between the electrodes, the pile reinforcement and the return current electrode.

5.6.1.3 Test on a Layered Ground

In this study, the lower third of the pile is considered to have embedded into soil which has a resistivity twice that of the top soil. The resistivity of the top soil is the same as the resistivity of the soil in other case studies. Simulated tests on a perfect pile and a necking pile in such layered ground has been undertaken. The resultant E-R curves for such simulations are given in Figure 5.41. Also shown in Figure 5.41 is the E-R curve for the perfect concrete pile embedded in a homogeneous ground. The resistivity of the homogeneous ground is the same as the top layer of the layered ground model.

It may be concluded from Figure 5.41 that the electrical properties of the soil surrounding the pile must be known, since the interpretation of the earth resistance results based on the electrical properties of the top soil is not acceptable. If the electrical properties of the soil surrounding the pile is known, the finite element simulation is suitable for the interpretation of such test results.

5.6.2 Interpretation of Field Test Results

Three dimensional finite element analysis has been used to confirm the results obtained from the two dimensional qualitative studies on the earth resistance method of testing (sections 5.6.1.1 and 5.6.1.2). The three dimensional finite element analysis may also apply to the interpretation of field test results by comparing the simulated test results with the field test results. Therefore, the soil profile in the site and the electrical properties of the soil and the pile concrete must be known before the finite element analysis may be used to analyse the field test results.

Two examples will be shown to demonstrate the application of the three dimensional finite element analysis to interpret field test results. Both the field tests were undertaken by McCarter (Ref. 5.1). The tests were carried out on two different sites and the electrical properties of the soil and the pile concrete were given. The first test was carried out on a site when the concrete was still fresh while the second test was carried out on another site six weeks after the concrete was poured, which may be regarded as old concrete. Both piles were reinforced for their whole length which has made them suitable for testing by the earth resistance method.

A plan of the idealisation used during simulations for the first site is given in Figure 5.36. The pile was tested using the resistivity technique when the concrete was still fresh. The site test data is shown in Figure 5.42 together with two simulations. The first simulation is undertaken using resistivity values of 6.5 Ωm and 62.0 Ωm respectively for the concrete and boulder clay as measured by McCarter (Ref. 5.1). The result of the first simulation does not match the field data exactly and a further simulation is undertaken using an adjusted resistivity value of 55.0 Ωm for the boulder clay. This second simulation, shown in Figure 5.42, is a reasonable match for the field data indicating that a defect in the pile is unlikely.

The plan for the idealisation used for the second example is shown in Figure 5.43. The position of the pile and the return current electrode are marked P and R respectively in the figure. The problem is again assumed to be symmetrical about the line A-B and only half of the domain is analysed. The pile is 6 m long with 400 mm diameter and is constructed using a concrete mix of 1:1.5:3 with 0.6 w/c ratio. The pile is continuously reinforced with a 200 mm diameter reinforcement cage. The electrical resistivity of the compact clay fill and concrete are 15.0 Ωm and 70.0 Ωm. The concrete is assumed to be hardened, being more than six weeks old. The site space available for test limited the pile-current electrode spacing to 2 m. A typical test result is shown in Figure 5.44 together with the finite element simulation. The fit between the two E-R curves is particularly good near the pile head indicating that the pile is unlikely to have any significant defect.

5.7 Modifications to the Testing Method

It was shown in sections 5.5.1 to 5.5.7 that the earth-resistance method of pile testing may not be effective in some situations. In some cases, extra resistance measurements may be made to improve the reliability of the non-destructive testing technique while in some other cases, the earth-resistance method should be avoided.

The earth-resistance method will become ineffective if the resistivities of the pile concrete and the soil are the same. Therefore, the method should not be applied to test the integrity of a pile on sites where the resistivities of the pile concrete and the soil are very similar.

5.7.1 Faults Inside the Reinforcement Cage

It was shown in section 5.5.2. that a defect inside the reinforcement cage of a pile may not be detected when the return current electrode is placed outside the pile periphery. It was also shown in section 5.5.4 that a fault in a pile may be assessed by the earth-resistance technique if the fault is lying between the electrodes.

Figure 5.45 shows the E-R curves of the models studied in section 5.5.2 where the return current electrode is placed at the centre of the pile head. It seems obvious from Figure 5.45 that the fault can be detected easily by placing the return current electrode at the centre of the pile head.

5.7.2 Faults Relative to Survey Line

It was suggested by McCarter (Ref. 5.1) that the acceptance or rejection of a pile should be based on the relative displacement of earth-resistance curves between neighbouring piles. However, it was found in section 5.5.3 that the significance of the test is also dependent on the position of the fault relative to the measurement line. Therefore, reliable non-destructive testing to produce a clear picture of the resistivity property of the pile-soil system outside the reinforcement cage may be usefully undertaken by taking readings from the pile in either four or eight directions.

5.7.3 Neighbouring Pile as Return Current Electrode

It has been shown in sections 5.5.7 and 5.6.1.3 that the earth resistance test results may be difficult to interpret when a pile is embedded in layered ground. This may be overcome by forming the electrical circuit between neighbouring piles. For layered ground where the soil layers are reasonably uniform and the layers are approximately horizontal, forming a circuit between neighbouring piles may simplify the situation into a two dimensional problem which is similar to the two dimensional horizontal section idealisations. Provided that the soil layers are uniform across the piles, the layered soil effect may be disregarded. The E-R curve, thus obtained gives direct indication on the integrity of the pile-soil system. In addition, anomalies lying between the two piles may be revealed. This kind of anomaly lying between the pile under test and the return current electrode could have affected the test results for the earth resistance test and made the interpretation difficult.

A horizontal section analysis has been undertaken to demonstrate the interpretation of the earth resistance method of testing by forming an electric circuit between neighbouring piles. A voltage is applied between the reinforcing cages of the neighbouring piles. Figure 5.46 shows the half plan view of the two 0.4m x 0.4m x 8.0m neighbouring reinforced concrete piles embedded in soil. A series of studies on the application of the earth resistance method to identify the defects in the piles have been undertaken and the resultant E-R curves are given in Figure 5.47. The E-R curves shown in Figure 5.47 illustrate that the E-R curve near to each pile gives an indication on the integrity of that pile. Direct comparison of the E-R curves between the neighbouring piles may reveal the integrity of the piles while finite element models and analogue models may be used to confirm the test results.

5.8 Conclusions

The system variables of the earth-resistance method of integrity testing of reinforced concrete pile have been analysed using the two-dimensional finite element method. The finite element analysis has been shown to be suitable for this study since both the resistivities of the pile concrete and the soil can be varied conveniently. Comparative E-R curves can be produced on the same ground using the finite element technique.

The electric field distribution around a reinforced concrete pile has been simulated using the two-dimensional finite element technique. Although the simulation cannot be used for accurate comparison with field tests, the simulation being two-dimensional, the characteristic E-R curve produced for a pile gives qualitative indications of the integrity of the pile-soil system. A defective pile will have its E-R curve displaced from that of a non-defective pile; the magnitude of this displacement is dependent upon the resistivity of the material in the defective section and the extent of the defective section. It is also shown that the resistance readings taken close to the pile head are of more significance in determining the pile integrity than are those taken some distance away.

Through the studies, the limits of application of the non-destructive testing method have been shown and some modifications to the method have been proposed so that more information about the integrity of the pile-soil system may be obtained. The application of the testing method to test a pile embedded in layered ground may be possible provided the soil layers are uniform and are approximately horizontal. The integrity test is most suitable in a homogeneous ground where the pile concrete has a much higher resistivity than the surrounding soil.

The horizontal section idealisation used in this study in fact represents a 0.4m x 0.4m x 5.0m square pile placed in the ground where an electric potential is applied between the 5.0 m long pile and a 5.0 m long return current electrode in the ground. It may also be considered as an potential applied between an infinitely long reinforcement cage and an infinitely long return current electrode. The vertical section represents a 0.2 m thick pile-soil system where the current is applied between the 0.2 m reinforcement and the 0.2 m long return current electrode. This may also be considered as a potential applied between an infinitely long reinforcement and an infinitely long return current electrode placed on the ground surface.

For quantitative studies of the method, three-dimensional finite element analysis may be used. The three dimensional analysis has confirmed the results obtained from the qualitative studies using two dimensional finite element analysis. In addition, the three-dimensional analysis may also be used for field data interpretation. It has been shown in the examples that the finite element technique is suitable for the interpretation of field data obtained by the earth-resistance method of pile testing.

References 5.

1. McCarter, W.J., "Resistivity Testing of Piled Foundation", Ph.D. Thesis, University of Edinburgh, 1981.

2. McCarter, W.J., Whittington, H.W., Forde, M.C., "An Experimental Investigation of the Earth-Resistance Response of a Reinforced Concrete Pile", Proceedings of the Institution of Civil Engineers, Vol. 70, Part 2, 1101-1129, December, 1981.

3. Zienkiewicz, O.C., Bahrani, A.K., Arlett, P.L., "Solution of Three-Dimensional Field Problems by the Finite Element Method", The Engineer, Vol. 224, 547-550, October, 1967.

4. Coggon, J.H., "Electromagnetic and Electrical Modeling by the Finite Element Method", Geophysics, Vol. 36, No. 1, 132-152, February, 1971.

5. Chari, M.V.K., Silvester, P.P., "Finite Elements in Electrical Magnetic Field Problems", John Wiley and Sons, Limited, 1980.

6. Owen, D.R.J., Hinton, E., "A Simple Guide to Finite Elements", Pineridge Press Limited, 1980.

7. Beck, A.E., "Physical Principles of Exploration Methods", The MacMillan Press, London, 1981.

8. Kunetz, G., "Principles of Direct Current Resistivity Prospecting", Gebrüder Borntraeger, 1 Berlin 38, 1966.

9. McCarter, W.J., Forde, M.C., Whittington, H.W., "Resistivity Characteristics of Concrete", Proceedings of the Institution of Civil Engineers, Vol. 71, Part 2, 107-117, March, 1981.

10. Whittington, H.W., McCarter, W.J., Forde, M.C., "The Conduction of Electricity Through Concrete", Magazine of Concrete Research, Vol. 33, No. 114, 48-60, March, 1981.

11. Telford, W.M., Geldart, L.P., Sheriff, R.E., Keys, D.A., "Applied Geophysics", Cambridge University Press, 1976.

Chapter 6

Finite Element Modelling of the Sonic Echo Method of Testing Reinforced Concrete Structural Members

6.1 Introduction

It has been shown in Chapter 5 that the Finite Element Method is suitable for the verification of the theory applied on the Resistivity Method of Integrity Testing. In addition, it has also been shown through qualitative studies that the Finite Element Technique could aid in the development or in the modification of the methodology for the integrity testing method and the interpretation of field test results. It was concluded in Chapter 5 that the Resistivity Method would only be effective when the resistivity of the soil is much lower than that of the pile concrete and that only the integrity of the pile-soil system between the electrodes may be detected. Furthermore, the E-R curves obtained from the Resistivity Method of testing do not give a direct indication of the location of the defect.

One of the alternatives to the Earth-Resistance Method of integrity testing is the Sonic Echo Method. The method will be investigated in this chapter using the Finite Element Method. The Sonic Echo Method of Non-Destructive Testing (sometimes referred to by proprietary names such as the T.N.O. method or the Stress Wave Propagation Method) (Refs. 6.1, 6.2, 6.3, 6.4, 6.5, 6.6, 6.7, 6.8) was described in sections 2.2.4.9 and 2.3.2. The objective of the method is to check the integrity of a structure or a structural member by observing the reflected pulses recorded on the same side of the structure or structural member where the impact signal is applied by a hammer blow. An applied pulse may be reflected inside a structure or structural member at the discontinuities of acoustic impedance. A pulse applied to the pile head via a hammer blow will travel down a free standing pile at a speed, c, which is dependent on the elastic properties of the pile concrete as given in section 2.3.2.1:

$$c^2 = E_p/\rho_p \qquad (6.1)$$

where E_p is the Young's modulus of the pile concrete and ρ_p is the density of the pile concrete. The reflection from a defect in the pile will result in a shorter reflection time than the expected reflection from the base. The length from the pile head to the reflection surface may be estimated from the measured reflection time:

$$t_R = 2L/c \qquad (6.2)$$

where t_R is the measured reflection time and L is the length from the pile head to the reflection surface. Since the pile may not have attained a steady state of vibration while the response data is being recorded, the modelling of the Sonic Echo Method using the Finite Element Method requires a transient dynamic model. A transient process may be defined as a time dependent variation in behaviour, of limited duration, spanning between two steady states of much longer duration (Ref. 6.9).

The field test results obtained during site testing are usually stored as time domain data which may be subsequently compared with the results of a step by step integration analysis using a finite element idealisation. Recent developments have simplified the process by recording the signals on a tape recorder and analysing the signal by a micro-computer (Ref. 6.10). The analogue signals are digitised before the signals may be analysed by the micro-computer. These digitised signals in the time domain may also be compared with the results of the finite element analysis. A large domain has to be employed for the simulation of the Earth-Resistance Method of pile testing. However, this is impossible in the simulation of the Sonic Echo

Method of integrity testing, where a step by step time integration process is used, due to the large amount of computer resources that would be required. These resources include the amount of file storage to store the simultaneous equations and the CPU time used in the solution of the simultaneous equations and the step by step time integration. In addition, a fixed boundary at a small distance compared to the pile length will reflect the applied pulse and give misleading results. Therefore, an energy absorbing boundary (Ref. 6.11, 6.12, 6.13, 6.14, 6.15 and 6.16) was incorporated in the computer program to simulate the pile embedded in an infinite soil medium.

In this chapter the effects of the physical and elastic properties of a structural member on pulse propagation will be investigated. The type of input pulse and the position for the response to be recorded on the pile head will also be studied. Subsequently the application of the sonic echo method to assess the integrity of a structural member will be studied. The use of the finite element idealisations to interpret the results from Sonic Echo Method of Non-Destructive Testing on structural members will be shown and the procedures to predict the load bearing capacity of the pile will be discussed. In addition, the pile-soil system will be considered and how the soil properties will affect the sonic echo measurement will be investigated.

6.2 Idealisation Verification

Before commencing the Finite Element Studies, it is necessary to determine the mesh size and idealisation to give satisfactory results. The maximum stresses in the structural member may be used as an indication as to whether an elastic or a plastic finite element analysis should be used. The material damping properties of the concrete are used to decide which damping coefficients are included in the analysis.

6.2.1 Mesh Sizes

A series of numerical tests are carried out using the 3-node triangular element and the 8-node rectangular isoparametric element (with 3 by 3 Gaussian integration points). Plane stress finite elements are used to represent the free standing pile where lateral strain is allowed. A two-dimensional 0.4 m x 0.4 m x 8.0 m finite element pile idealisation is used for these and further studies. The beam is divided into four vertical columns of triangular elements or two vertical columns of 8-node rectangular elements as shown in Figures 6.1a and 6.1b.

Figure 6.2 shows the effects on the maximum displacement at the quarter point of the pile head as the number of vertical divisions along the pile is increased when triangular elements are used. The result indicates that the analysis converges to a solution when the pile is divided into 60 vertical divisions, that is 480 triangular elements. Similar convergence test results for the 8-node rectangular element are given in Figure 6.3. At least 20 vertical divisions, that is 40 elements, are required in this case. However, the mesh size may be halved with no loss of accuracy when the beam has an axis of symmetry.

In these studies, the half wavelength of the applied pulse is 3.49 m, which is the product of the contact time of the hammer blow and the sonic velocity of the pile concrete. The input pulse is half a cycle of a sine function as shown in Figure 6.1c. It is concluded in this study that the maximum dimension of a triangular finite element should not exceed 1/25 of the half wavelength of the pulse under consideration. The maximum dimension of a 8-node rectangular finite element should not exceed 1/9 of the half wavelength of the pulse under consideration.

6.2.2 The Use of Irregular Mesh

Irregular finite element meshes may be used to idealise a large area. It is obvious that finite elements near to a source should be finer while those further away may be coarser. However, it has been found that the rate of change of element dimensions between adjacent elements should not be greater than a factor of 1.2. Changes greater than this result in additional noise in the simulated test results.

6.2.3 Stresses in Structural Member

Figures 6.4a and 6.4b show respectively the compressive stress and shear stress experienced at the Gaussian point nearest to the point where the hammer blow is applied. The maximum compressive stress is just below 10^5 Nm^{-2}, about 1/300 the strength of grade 30 concrete. It is shown by Neville (Ref. 6.17) that the stress-strain relationship of concrete is linearly proportional up to approximately 30 per cent of the ultimate strength of grade 30 concrete. Therefore, the pile concrete should be in its elastic range and an elastic finite element analysis would be adequate.

6.2.4 Damping Properties of Concrete

Goldsmith et. al. (Ref. 6.18) carried out static and dynamic tests on concrete specimens. The dynamic load used in reference 6.18 is applied through a longitudinal impact which is similar to the sonic echo test. It is found that the wave-propagation process in the specimen occurred without dispersion and relatively little attenuation, indicating that the material damping can be represented on a macroscopic scale as an 'elastic' substance with a small structural-damping coefficient. In addition, Ashbee et. al. (Ref. 6.19) showed that the difficulty in measuring the damping of concrete may result from the relatively low damping in a stiff material such as concrete.

Through a comparison between a finite element simulation and a set of field test data on a free beam, the damping in the concrete is found to be very small. Therefore, material damping due to concrete will not be included in the following studies. These results will be discussed in section 6.6.2.

6.3 The Applied Pulse

It has been shown by Steinbach et. al. (Ref. 6.1) and Lilley (Ref. 6.20) that significant surface waves detected by a transducer during a sonic echo test may be reduced by applying a lower frequency pulse. The desired lower frequency applied signal may be obtained by hitting the pile head by a longer steel bar (Refs. 6.1 and 6.20). A finite element approach to the search of a suitable applied pulse for the Sonic Echo Test will be considered later in this study.

6.3.1 An Experimental Approach

Recent studies by Chan (Ref. 6.10) showed that different frequency input signals may be obtained by using different materials on the hammer head. The contact time between the hammer head and the pile head is dependent upon the elastic properties of the hammer head and the pile head. In addition, the contact time is also dependent upon the approaching velocity of the hammer before it is in contact with the pile head. A typical input pulses and a test result for a 5.5 m straight shaft are illustrated in Figures 6.5 and 6.6 (Ref. 6.10). It is suggested that the maximum amplitude of the applied pulses range from 4 KN to 10 KN and the contact time between the hammer head and pile head (pulse width) ranges from 0.5 ms to 1.5 ms (Ref. 6.10). The dotted line shown in Figure 6.5 represents a half sine function which has the same amplitude and pulse width 1.4 ms as the typical input pulse. This indicates that a half sine function which has the same amplitude and frequency may be used to simulate the applied pulse in the finite element simulations.

6.3.2 The Finite Element Approach

The Finite Element Method may be used to investigate the use of input pulses of different frequencies. In addition, the method may be used to simulate different forms of input pulses such as the application of a plane wave to the pile head or the use of a square wave instead of a half sine wave. These simulations are useful in helping to select or design a suitable piece of equipment for the Non-Destructive Testing in the field.

6.3.2.1 Pulse Frequency

The 8 m pile shown in Figures 6.1a and 6.1b, without skin friction, has a density (ρ_1) of 2400.00 kgm^{-3}, a Young's modulus (E_1) of 29.23x10^9 Nm^{-2} and a Poisson's ratio (ν_1) of 0.24, and an effective fixed supports at its base. The sonic echo method of testing usually applied to this pile is simulated and the response curves are shown in Figures 6.7, 6.8, and 6.9. The contact time between the hammer and the pile head is assumed to be 1.0 ms. In this chapter, the displacement, velocity and acceleration response curves represent the time plots of the particle displacements, velocities and accelerations at the point where the signals are measured. Figure 6.7 corresponds to the signal which may be measured by a displacement transducer placed at the quarter point of the pile head. Similarly, Figures 6.8 and 6.9 correspond to the signals that may be measured by a velocity transducer and accelerometer respectively at the same point.

Substituting the above material properties in equation (6.1), it is found that the compression wave will travel at a speed of 3490 ms^{-1} in the concrete pile. The first reflected pulse from the fixed end may therefore be detected at the pile head 4.585 ms after the pulse is applied. In Figures 6.7, 6.8 and 6.9, R marked the time the first reflected pulse is detected at the pile head. From measurement, R corresponds to approximately 4.56 ms and indicated that the simulation may be suitable for quantitative as well as qualitative studies of the Non-Destructive Method of Pile Testing.

The pile head movement may be inferred from the displacement trace from the sonic echo tests. In Figure 6.7, the initial positive displacement corresponds to a downward movement of the pile head. It is also shown in Figure 6.7 that the pile head remained downward displaced after the pulse is applied until the first reflected pulse arrives at the pile head, displacing it in an upward direction by a similar amount. This also indicates that the simulation models the material as perfectly elastic and there is no energy loss during the propagation and reflection of the compression wave.

Figure 6.8 shows the velocity response at the quarter point of the pile head. The amplitude of the reflected velocity signal is shown to be approximately twice that of the applied velocity pulse. This has been described in section 2.3.2.2 as a particle response at a fixed end or a free end where the pulse is reflected. Since the nodal response from the finite element analysis is the same as the response of a particle measured by a transducer in the field test, both the finite element analysis and the field tests conform with the closed form solution as mentioned in section 2.3.2.2. It is also observed in Figure 6.7 that the gradient of the displacement curve, at reflection, is double that of the displacement at input. It must also be noted that there is a change of phase in the velocity signal upon the first reflection from the fixed end of the pile. These response curves (Figures 6.7, 6.8 and 6.9) may be considered as typical responses for a fixed end pile.

Figure 6.9 shows the acceleration response curve where significant noise is found between each pulse reflection. In field testing, the integration of this acceleration signal to give velocity and displacement signals provides clean traces. In most applications, the velocity data is used for interpretation. The results of the case studies undertaken using the Finite Element Analysis will therefore be presented as plots of velocity and displacement response curves.

It is concluded that the velocity response may be a suitable parameter to be measured in the field tests since further integration to the displacement data increases the error due to the integrator.

The response of the pile head due to an applied pulse (half sine function) of 0.1 ms duration is shown in Figures 6.10, 6.11 and 6.12. Again R marks the time the first reflected pulse is detected at the pile head.

The displacement response curve given in Figure 6.10 shows that after the pulse is applied, the pile head remains stationary at some mean position but some minor vibrations still occur. These minor vibrations may be due to surface wave travelling back and forth across the pile head.

Figure 6.11 shows the velocity response curve. In this case, the surface wave effects become significant compared to the reflected pulse. It is shown to be difficult to distinguish between surface wave and longitudinal wave signals in terms of velocity (Figure 6.11) and they are almost impossible to distinguish in an acceleration trace (Figure 6.12).

It may be concluded that to apply the Sonic Echo Method for testing structural members, the applied pulse must have sufficient contact time to ensure that the noise due to the surface wave is low in comparison to the longitudinal wave. Therefore in the following case studies, the contact time of the pulse will be assumed to be 1.0 ms.

6.3.2.2 Positions for Pulse Application

In these simulations, the pulse was applied to a smooth pile head; at the edge, at the quarter point and at the center. The particle velocity at other points on the pile head represented by the finite element nodes are recorded. It is found that certain placements of the applied pulse and detection point gives better traces for interpretation. For example velocity traces that are difficult to interpret may be generated by applying the load at the edge of the pile head and tracing the particle velocity at the opposite quarter point (as shown in Figure 6.13). Another confusing velocity trace is obtained when the load is applied at the quarter point and tracing the particle velocity on the opposite edge as shown in Figure 6.14.

It may be concluded that for best results, a pulse should be applied at the centre of a smooth pile head and signals recorded at quarter points. Alternatively, the pulse may be applied at any other point on the pile head while the signals are recorded at the centre of the pile head. In the following case studies, the hammer blow will be applied at the centre of a smooth pile head and the signals will be recorded at the quarter point.

6.3.2.3 An Applied Planar Pulse

Simulations have been undertaken to investigate if a pulse applied over a plane would have any advantage over one applied at a point. In the first case, a pulse is applied as a uniformly distributed load across the pile head. The displacement and velocity traces at the quarter point of the pile head, when a pulse is applied over a plane, are given in Figures 6.15 and 6.16. The particle displacement and velocity responses at the same position when a pulse is applied as a point load at the centre of the pile head are shown in Figures 6.17 and 6.18. It is concluded from these figures that since the return signals are identical, no advantage is gained by applying a pulse which is uniformly distributed over the pile head over applying the pulse at the centre of the pile as a point.

6.3.2.4 A Square Wave Input

In the above studies, a half sine wave input pulse is used. The effect of a square wave input as shown in Figure 6.19 is investigated. This pulse is applied at the centre of the pile head. Figures 6.20 and 6.21 show the displacement and velocity responses measured at the quarter point of the pile head. Although the displacement data (Figure 6.20) is shown to be similar to the data obtained by an applied half sine wave pulse, it is shown in Figure 6.21 that the square wave input introduced serious noise on the velocity trace. This trace is usually used for interpretation. Therefore, the application of a half sine wave input by the impact by a hammer blow has been shown to be most appropriate for the Sonic Echo Method of integrity testing.

6.4 Case Studies

In these case studies, the effects of discontinuities in acoustic impedance in the pile on the response signals of a sonic echo test will be investigated. The amount of pulse energy reflected from a discontinuity may be found by considering the reflection coefficient, R, as shown in section 2.3.2.3, equations (2.32) and (2.39):

$$R = \frac{[A_1\sqrt{(E_1\rho_1)}-A_2\sqrt{(E_2\rho_2)}]}{[A_2\sqrt{(E_1\rho_1)}+A_2\sqrt{(E_2\rho_2)}]} \tag{6.3}$$

where A_1, E_1 and ρ_1 are the cross-sectional area, Young's modulus and density for medium 1 and A_2, E_2 and ρ_2 are the cross-sectional area, Young's modulus and density for medium 2 as shown in Figure 6.22, where the pulse is assumed to travel from medium 1 to medium 2.

6.4.1 Changes in the Cross-Sectional Area

For this study the 3 node triangular finite element pile idealisation shown in Figure 6.1a is now divided into two parts. The top 4 m has Young's modulus of 29.23 x 10^9 Nm^{-2}, bulk density of 2400.00 kgm^{-3}, Poisson's ratio of 0.24 and cross-sectional area of 0.4m x 0.4m. The lower 4 m of the pile has a cross-sectional area equal to half that of the upper section. Figures 6.23 and 6.24 show the displacement and velocity responses of the pile at the quarter point of the pile head.

In practice, the pulse will propagate along the pile at a constant speed, given by equation (6.1). The reflection coefficient at each discontinuity may be calculated using equation (6.3). The reflections are illustrated in Figure 6.25. Also shown in the figure are the fractions of the applied pulse energy, which are reflected and transmitted across the discontinuities. The corresponding times are shown at the top of Figure 6.25 and marked on the traces in Figures 6.23 and 6.24. The times t_1 = 2.32 ms and t_2 = 4.56 ms may be measured on the trace shown in Figure 6.24. These times compare favourably with those calculated using equation (6.2) where t_1 = 2.292 ms and t_2 = 4.584 ms.

6.4.2 Changes in the Young's Modulus

In this study, the pile is assumed to have a uniform cross-sectional area and a uniform density throughout. The Young's modulus of the top 4.0 m pile section is 29.23×10^9 Nm^{-2} while that for the lower 4.0 m pile section is 7.31×10^9 Nm^{-2}. The displacement and velocity traces at the quarter point of this pile are shown in Figures 6.26 and 6.27. Using equation (6.1), it is found that in the lower section, the pulse will travel at half the speed of propagation in the top 4 m section. Again, using equation (6.3), the reflection coefficients at each discontinuities are found to be the same as in section 6.4.1.1 'and are shown in Figure 6.28. Figure 6.28 also offers an energy interpretation of the causes of the first 4 reflections shown in Figure 6.27.

6.4.3 Changes in the Material Density

In this case, instead of having a smaller Young's modulus in the lower half of the pile, a smaller concrete density (600.0 kgm^{-3}) is assigned to this half. The response curves for this case are shown in Figures 6.29 and 6.30 while Figure 6.31 offers an energy interpretation of the causes of the first few reflections in Figure 6.30.

6.4.4 Changes in the Poisson's Ratio

Figures 6.32 and 6.33 show the displacement and velocity traces measured at the quarter point of the pile head when the lower half of the pile has a Poisson's ratio of 0.48 which is twice that of the upper 4.0 m of the pile.

It is obvious that the Poisson's ratio has no effect on the wave propagation within a structural member. A discontinuity in the acoustic impedance in a pile introduces an interface which partially reflectes the applied pulse.

6.4.5 Effects due to Discontinuities in the Acoustic Impedance Along a Free Standing Pile

It has been shown that the reflected pulse from the interface due to a reduction in the cross-sectional area, a change to a smaller Young's modulus or a smaller density, are in phase with the applied pulse. This type of reflection is similar to a reflection from a free end (section 2.3.2.3). On the contrary, it can be expected that the reflections from discontinuities due to an increase in the cross-sectional area, a stiffer or a denser material will be similar to that from a fixed end.

6.5 The Sensitivity and Effectiveness of the Method for Non-Destructive Testing

6.5.1 Discontinuities of Finite Size

Griffiths et. al. (Ref. 6.21) suggested that in any application of seismology to small-scale problems, it should be noted that the ability of the seismic method to separate closely-spaced structures is limited to dimensions not much less than the length of the seismic wave. The seismic wavelength may be found by dividing the wave velocity by its frequency. Thus, the sonic echo method, which is one type of seismic method, may not be able to locate a defect in a pile which has a dimension smaller than the wavelength of the pulse, which is 6.98 m in the concrete pile.

In section 6.4, discontinuities which have an extent comparable with the applied signal are considered. A 4 m discontinuity is studied which is comparable with the wavelength of the applied pulse of 6.98 m. In practice, the real discontinuities encounter may have an even smaller extent. Two typical types of defective piles will be considered in this section; pile overbreak and pile necking.

6.5.1.1 The Detection of Overbreaks in Piles

Pile defects in a free standing piles may be detected by the sonic echo method. Figure 6.34 shows the 8 m free standing pile which has an overbreak at 2 m above its toe. Figures 6.35 and 6.36 show the displacement and velocity response curves of the pile measured at the quarter point of the pile head. The reflection time from the overbreak, marked by R_f in Figures 6.35 and 6.36, is approximately 3.3 ms (3.324 ms calculated from equations (6.1) and (6.2)). The overbreak is shown to be marked by a change in phase of the reflected signal indicating that an overbreak in a pile responds as a fixed end which confirmed the conclusions given in section 6.4.5.

In this study, not only the overbreak, but also the actual length of the pile may be determined by the sonic echo method. The reflection from the fixed end, marked by R in Figures 6.35 and 6.36, arrived at approximately 4.5 ms. In fact, this is a resultant of reflections and refractions from the two interfaces of the overbreak and the reflection from the fixed end.

6.5.1.2 The Detection of Neckings in Piles

Figure 6.37a illustrates the idealisation of the necking pile used in this study. Figures 6.38 and 6.39 show the displacement and velocity response curves for a pile with a neck of length 400 mm. The cross-sectional area at the necking is one quarter of the cross-sectional area of the original cross-sectional area of the pile. The finite element simulation indicates that the first reflection from the neck is approximately 3.3 ms and that there is no change in phase in the response signals indicating that a neck may be treated as a shorter, free end pile. Again, both the defect and the actual length of the pile may be detected. The reflection times from the neck and the fixed end are marked R_f and R respectively in Figures 6.38 and 6.39.

Figures 6.40 and 6.41 show the response curves of an idealised necking pile where the neck has a length of 200 mm as shown in Figure 6.37b. Also, a 2 mm crack in the 8 m pile as shown in Figure 6.37c is also simulated. The crack which extends across half the width of the pile is located 6 m below the pile head. The response curves for this study are given in Figures 6.42 and 6.43. Comparing the displacement traces in Figures 6.38, 6.40 and 6.42, it appears that a crack in a pile may be treated as a very thin neck in the pile since the nature of the reflected signals are the same. Similar effects are observed in the velocity responses. However, from equation (6.3), it is expected that the reflected signals from the necks and the crack will be the same and have a magnitude 2/3 that of the input signal as in Figure 6.24. This may be explained by the fact that the reflected pulse from the first interface is superimposed on the pulses reflected from the second interface which have opposite phases to those from the first interface. The first refracted pulse would be partially reflected and partially refracted at the second interface. This process of reflection and refraction between the first and second interfaces is continuous. With a narrow crack, the time taken for the refracted pulse to travel between the two interfaces is short. The series of reflected pulses from the second interface are superimposed on the reflected pulse from the first interface, resulting in the distortion of the reflected pulse from the first interface. With a crack, the distortion is so great that the reflected pulse from the first wave becomes insignificant and the crack cannot be detected.

It may be concluded that the ability of the sonic echo method to test the integrity of a structural member depends on the size and the extent of the defect in the structural member. Usually, reflections from the interface of the first discontinuity of significant size in a structural member may be detected. For very short necks, the signals are the resultant of reflected and refracted pulses from different interfaces. Therefore, the results may be difficult to interpret.

6.5.2 The Position of the Defect in the Pile

It is shown in section 6.5.1 that the sonic echo method may be able to locate a defect in a pile which has an extent of approximately 1/30 of the wavelength of the pulse. In this study, a 200 mm long section of pile defect, which is a concrete layer having a low Young's modulus of 7.31 Nm^{-2} is located near to the reflecting interfaces, either near to the pile head or near to the pile toe. Figure 6.44 shows the 0.4 m x 0.4 m x 8.0 m defective pile model with positions of the concrete layers with small Young's moduli shown.

Figure 6.45 shows the velocity response of the pile when there is no defect in the pile and the reflection time is approximately 4.56 ms. The velocity response of the defective pile where a layer of concrete with a small Young's Modulus is considered at 0.4 m below the pile head is given in Figure 6.46. It is obvious from Figure 6.46 that the amplitude of the detected pulse is greater than the detected pulse shown in Figure 6.45. For the same applied pulse, the difference in the detected pulse in the velocity traces may be a result of the superposition of the reflected pulse from the defective concrete layer and the applied pulse which are in phase with each other. This may also be explained by viewing the pile head as being more flexible due to the section of concrete with a small Young's Modulus. Thus the deformation of the pile head is greater for the same applied load. In this case, the reflection from the base is also detected at 4.8 ms, which is the total time required by the pulse to travel through the defective concrete layer to the base and back to the pile head. Figure 6.47 illustrates the velocity response of the free pile when the layer of weak concrete is 0.4 m above the pile toe. The reflection time from the weak concrete layer is computed to be 4.13 ms using the finite element analysis, which is as expected from the closed form solution (equations (6.1) and (6.2)). However, the reflection from the base is distorted in this case due to the superposition of the signals from the weak concrete layer and the pile base.

When there are two weak concrete layers, one near to the pile head and one near to the pile toe, the velocity responses at the pile head are as shown in Figure 6.48. This indicates that the sonic echo method could be used to show that there are two defects in a pile. It would, however, be difficult to predict their exact locations.

Here it may be concluded that the Sonic Echo Method of Testing may be used to locate the position of a single defect. Generally, the defects may be classified as the free-end or fixed-end type. The Earth Resistance Method of Testing discussed in Chapter 5 cannot be used to detect the precise location of a defect and may only be used to indicate the general integrity of the pile outwith and along the reinforced length.

6.5.3 Discontinuities without a Definite Interface

Figure 6.49a illustrates an idealisation of an overbreak pile and Figure 6.49b shows another idealisation of a necking pile. Both these idealisations have been considered to have no definite interface between the pile shaft and the defect since the change in cross-sectional area is gradual. Figures 6.50

and 6.51 are the plots of the velocity traces for a simulated Sonic Echo method of testing for these idealised pile models. The overbreak in the pile reflected a pulse which shows a change of phase from the applied pulse while a pulse reflected from a neck in a pile shows no change of phase from the applied pulse. It is also shown in Figures 6.50 and 6.51 that the reflection time from the discontinuities are similar to those obtained in Figures 6.36 and 6.39.

Therefore, the sonic echo method of non-destructive testing of a structural member is also effective in detecting defects in structural members which do not have distinct interfaces provided that the contrast in the acoustic impedance between two sections and the extent of the defect are sufficiently large.

6.6 Interpretation of Physical Model Test Results

Two concrete beam physical models (Ref. 6.5, 6.22 and 6.23) have been constructed in The Department of Civil Engineering at Edinburgh University for the investigation and development of the sonic echo method of pile testing. An approximately 6 m long concrete beam with a small increase in cross-sectional area (overbreak) was built as shown in Figure 6.52. Another 8 m long concrete beam with two overbreaks at 4 m and 6 m from one end is shown in Figure 6.53.

6.6.1 A Single Overbreak Beam Model

A typical test result (Ref. 6.22, 6.23), from the test of the beam shown in Figure 6.52 is illustrated in Figure 6.54. In this case, the overbreak is detected - by the strong return signal of opposite phase. The position of the overbreak on the trace is indicated by the first vertical cursor (shown as a dotted line).

A two-dimensional finite element idealisation was developed to simulate the same beam. The displacement and velocity responses are shown in Figures 6.55 and 6.56 respectively. In the figures, R marks the reflection from the overbreak at time 1.44 ms. As discussed in section 6.5.1.2, after the first reflection, the interpretation of the time domain signal is difficult due to the combination of signals which have been reflected and refracted on passing through different interfaces in the beam.

6.6.2 A Double Overbreak Beam Model

The positions and sizes of the two overbreaks on the 8 m beam are shown in Figure 6.53. The velocity response of the beam measured in the field is shown in Figure 6.57. A two dimensional finite element study of the same beam was undertaken and the simulated displacement and velocity traces on the same face of the beam are shown in Figures 6.58 and 6.59. It is obvious that the velocity responses in Figures 6.57 and 6.59 are similar.

The beam is supported by the two overbreaks which are in contact with the ground (Figure 6.53). Thus, the pulse propagating along the beam has minimal effect from the geometrical damping where the pulse energy is transmitted to the surrounding soil. The similarity between the field test result and the finite element simulation in this study indicates that the material damping in the concrete beam is small and may be neglected.

It is therefore suggested that the finite element idealisation may be used to represent the physical model in these studies on non-destructive testing methods. The finite element method may be used to interpret the Sonic Echo Test data where the actual shape of the structural member is unknown. In this case, finite element idealisations may be analysed and reanalysed to obtain a response similar to those obtained from the field test. Initial assumptions may be made using the field data and modifications to the simulated results may be made by adjusting the parameters in the finite element idealisation until the simulated results approach the field test results. Thus, after interpretation of the sonic echo test results using finite element analysis, a picture of the properties of the structural member may be revealed. This is essential for the prediction of the load bearing capacity of the structural member under working load. This application is most appropriate in cases where the properties of the structural member are unknown, for example when a pile is embedded in the ground.

6.6.3 Data Processing

The data obtained from a sonic echo test is in the time domain; the variation of the amplitudes of the transducer output with respect to time is recorded. However, these signals which are a result of superposition of reflected and refracted pulses from the pile boundaries and discontinuities in the pile are sometimes difficult to interpret. Reported application of the time domain data processing technique, the correlation functions, to the sonic echo test results has been shown to be promising (Refs. 6.22 and 6.23). Therefore, the time domain data processing technique will be investigated in this section in the hope of improving the results obtained from the sonic echo method of non-destructive testing.

6.6.3.1 The Use of Cross-Correlation

The cross-correlation process searches for repetitions of the source signal contained in the data set obtained from a sonic echo test. Corresponding values of the two sets of data are multiplied together and the products summed to give the value of the cross-correlation. In relation to the physical interpretation of sonic echo signals, the interpretation of the cross-correlation function is therefore to what degree the time signal obtained from a sonic echo test is similar to the applied pulse at each time shift τ. Wherever the two data sets are nearly the same, the products will usually be positive and hence the cross-correlation is large; wherever the data sets are not similar, some of the products will be positive and some negative and hence the sum will be small. If the cross-correlation function has a large negative value, it means that the two data sets would be similar if one were inverted. If a sonic echo reflection with time delay of τ_0 exists in the signal, which has not been modified by other reflected pulses, the cross-correlation function will have peak values at $\tau = \tau_0$.

The cross-correlation of two data sets x_t and y_t can be expressed as (Ref. 6.24):

$$\phi_{xy}(\tau) = \sum_k x_{(k+T)} y_k \tag{6.4}$$

where τ is the displacement of x_t relative to y_t and k is the number of data points.

6.6.3.2 The Use of Autocorrelation

The special case where a data set is being correlated with itself is called autocorrelation. In this case, equation (6.4) becomes:

$$\phi_{xy}(\tau) = \sum_k x_{(k-T)} x_k \tag{6.5}$$

The correlation has its peak value at zero time shift, that is, a data set is almost like itself before it is time shifted. If the autocorrelation should have a large value at some time shift $\Delta t \neq 0$, it indicates that the set tends to be periodic with the period Δt. Hence the autocorrelation function may be thought of as a measure of the repetitiveness of a function.

6.6.3.3 The Use of the Normalised Correlation Function

The autocorrelation function is often normalised by dividing by the energy of the trace which is shown by Telford et. al. (Ref. 6.24) to be the autocorrelation value at zero shift:

$$\phi_{xx}(\tau)_{norm} = \frac{\phi_{xx}(\tau)}{\phi_{xx}(0)} \tag{6.6}$$

The cross-correlation function, in a similar manner, is normalised by dividing by the geometric mean of the energy of the two traces:

$$\phi_{xy}(\tau)_{norm} = \frac{\phi_{xy}(\tau)}{[\phi_{xx}(0)\phi_{yy}(0)]^{0.5}} \tag{6.7}$$

Normalised correlation values must lie between ± 1. A value of $+1$ indicates perfect copy, a value of -1 indicates perfect copy if one of the traces is inverted.

6.6.4 The Application of Time Domain Techniques for the Interpretation of Model Test Results

The correlation function has been applied to the detection of echoes or reflections in the velocity time signal for concrete piles (Refs. 6.22 and 6.23). To apply the same signal processing procedure on the finite element simulated tests, a computer program was written to process the simulated test results. The interpretation of the results will be shown in the following studies in which

Δt was assumed to be 15 μs.

6.6.4.1 The Single Overbreak Beam Model

The application of autocorrelation and cross-correlation to the field data set shown in Figure 6.54 are given in Figures 6.60 and 6.61. As explained in reference 6.22, the first cursor (dotted line) in Figures 6.60 and 6.61 refers to the position of the overbreak and the second refers to the end of the beam.

The velocity signal obtained from a finite element model shown in Figure 6.56 has been autocorrelated and cross-correlated in the manner given in section 6.6.3. The autocorrelated result is shown in Figure 6.62 while the cross-correlated result is shown in Figure 6.63.

In the two dimensional finite element simulation, the overbreak is simulated using a density 4/3 (the geometrical factor between the overbreak and the beam) the density of the regular beam. This simplification has resulted in a slower wave propagation velocity within the overbreak (equation (6.1)) and hence a slightly delayed signal from the free end was expected. The Young's modulus used to model this 6 m beam is 31.10×10^9 Nm^{-2} throughout and densities 2400.0 kgm^{-3} and 3200.0 kgm^{-3} have been used to model the beam and the overbreak respectively. Recalling equation (6.1),

$$c^2 = E_p/\rho_p \tag{6.1}$$

Assuming c_1 to be the wave velocity in the straight beam and c_2 to be the wave velocity in the overbreak, it can be calculated that c_1 = 3600 ms^{-1} and c_2 = 3118 ms^{-1}. Then the time of the first reflections from the faces 1, 2 and 3, as shown in Figure 6.52, may be calculated to be 1.500 ms, 1.885 ms and 3.385 ms respectively and the time the second reflections from the faces 1 and

2 are 3.000 ms and 3.77 ms respectively (equation (6.2)).

Using a similar interpretation as given in reference 6.22, the first overbreak may be detected with 3.33% error while the free end of the beam may be detected with 3.99% error. Similar results are obtained from both the autocorrelation and cross-correlation functions.

6.6.4.2 The Double Overbreak Beam Model

The results of applying the correlation functions to the time domain velocity data obtained from the finite element idealisation of the double overbreak beam are given in Table 6.1. The table shows a comparison between the predicted reflection times for a pulse to reflect from each interface to arrive back at the face where the pulse was applied found by a closed form solution (equations (6.1), (6.2)) against the finite element simulation. The location of the faces 1, 2, 3, 4, and 5 are shown in Figure 6.53.

	Equations (6.1) & (6.2)	Autocorrelation (% error)	Cross-Correlation (%error)
Face 1	2.23 ms	2.24 ms (0.226)	2.26 ms (0.942)
Face 2	2.45 ms	-	-
Face 3	3.48 ms	3.81 ms (9.397)	3.84 ms (10.317)
Face 4	3.69 ms	-	-
Face 5	4.78 ms	4.56 ms (4.685)	4.58 ms (4.351)

Table 6.1 Comparison between the Calculated Reflection Time and the Correlation Results

In this study, it is shown that the interpretation of time domain data using correlation functions may enable one to locate the first overbreak and the end of a free beam with considerable confidence.

When interpreting the autocorrelation function shown in Figure 6.64, the first minimum and first maximum point on the curve are neglected since there will not be any reflection in the beam before the pulse is reflected from the first overbreak (see Figure 6.59). These minimum and maximum points do not appear in the cross-correlation function shown in Figure 6.65.

A physical interpretation of the application of correlation functions to the Sonic Echo Method was given in section 6.6.3.1. If an applied pulse is reflected without distortion, it may be appropriate to apply the cross-correlation function which expresses the similarity between the reflected signal and the applied signal. In contrast, the autocorrelation functions expresses the degree of similarity between the time domain data and itself. The application of the autocorrelation function may be more appropriate if the reflection pattern in the time domain is repetitive.

The autocorrelation and cross-correlation functions shown in Figures 6.60 and 6.61 are similar. This is a result of the application of some signal processing facilities such as windowing (Ref. 6.10).

6.6.4.3 Relationship between Wavelength of Pulse and the Extent of the Defect

It has been shown in section 6.5.1.2 that the ability of the sonic echo method of testing to locate a defect in a pile depends on the size of the defects. Instead of applying a pulse which has a half wavelength of 3.49 m, shorter pulses are applied to the double overbreak beam idealisation. These pulses are applied using a contact time between the hammer and the end face of the beam of 0.4 ms and 0.1 ms. A comparison of the simulated results using different pulses is tabulated in Table 6.2. Since the high frequency pulses introduced high frequency noise at the end face, cross-correlation has been used to process the velocity data to reduce the noise in the time domain data so that the interpretation of this data may be made easier.

	Closed Form Solution	FEM		
		0.8 ms pulse	0.4 ms pulse	0.1 ms pulse
Face 1 (% error)	2.235	2.112 (5.50)	2.000 (10.51)	1.920 (14.09)
Face 2 (% error)	2.350	2.784 (18.47)	2.880 (11.66)	2.400 (2.13)
Face 3 (% error)	3.381	undefine	undefine	2.960 (12.45)
Face 4 (% error)	3.496	undefine	3.632 (3.89)	3.456 (1.14)
Face 5 (%error)	4.585	4.416 (3.69)	4.304 (6.13)	4.144 (9.62)

Table 6.2 Comparison of the Reflection Time for the Double Overbreak Beam Model

6.6.4.4 Simulated Tests

Here the 8 m pile which has a 0.4 m necking at 6 m depth, shown in Figure 6.37a, is used to further illustrate why the use of the cross-correlation function is better than the autocorrelation in the interpretation of the time domain data. The velocity response of the free pile is given in Figure 6.39. A minimum has been shown in the autocorrelation coefficient function in Figure 6.66 at 1.6 ms which does not correspond to any reflection in the beam.

Comparing the cross-correlation coefficient function, given in Figure 6.67, with the autocorrelation coefficient function in Figure 6.66, it will be appreciated that the interpretation of the cross-correlation coefficient function is easier than the autocorrelation coefficient function.

6.7 Prediction of the Load Bearing Capacity of the Structural Member

The finite element analysis has been used to simulate the sonic echo method of testing on structural members. It was also shown in sections 6.6 to 6.6.4.4 that the correlation between the two dimensional finite element idealisations and the field tests on the concrete beam models are very good. Therefore, the finite element analysis may be used for the interpretation of the Sonic Echo Method of non-destructive testing. The field data such as the velocity response of the pile head or the processed time domain data, together with the finite element simulation, may provide a picture of the structural properties of the member. These properties are required to enable the engineer to assess the behaviour of the member under working load.

The approach to the prediction of the behaviour of the structural member may be undertaken by first transferring the field test data to a computer where a trace of the pile head response may be displayed. The properties of the pile and concrete may be determined from data obtained from site investigation or estimated from experience so that a suitable finite element idealisation may be prepared. This idealisation may be adjusted to model the postulated defects until a suitable fit between the simulated results and the field data is established. The final idealisation, including the postulated defects, is reanalysed to predict the behaviour of the structural member under working load or design loads.

6.8 Pile-Soil Systems

Experiments have been undertaken on free metal rods or concrete beams by a number of authors (Refs. 6.1 and 6.5) to investigate the Sonic Echo Method. The application of the non-destructive testing method on the field is mainly based on the assumptions made from these free beam model studies. Steinbach et. al. (Ref. 6.1) proposed that the principal difference between the "free hanging" and "in-the-soil" position is in the attenuation of the pulse. When a bar is surrounded by air, there is almost no transmission of energy outside the bar. When it is surrounded by moist or wet sand, some energy was radiated into the soil and the attenuation consequently increases. In this section the effects of the surrounding soil on the Sonic Echo Test results will be investigated.

The Sonic Echo Method of Non-Destructive Testing of piled foundations, may be expressed as one of wave propagation in an infinite medium. In order to simulate this real situation using the Finite Element Method, an energy absorbing boundary is introduced at the far field of the soil medium. Thus, the pile-soil interface may be maintained while the energy transmitted to the soil will be dissipated at infinity. The energy absorbing boundary is placed at 0.8 m from the vertical pile-soil interface and 2.0 m from the pile toe. A cast-in-situ pile where concrete is poured directly into the excavation has been simulated to have a perfect bond between the pile concrete and the soil. The elastic properties of the pile concrete are the same as those used in the case studies for the behaviour of a free standing pile, that is with a Young's modulus of 29.23×10^{9} Nm^{-2}, a Poisson's ratio of 0.24 and a density of 2400.00 kgm^{-3}.

Two type of energy absorbing boundaries, the superposition boundary and the unified boundary condition, are described in sections 4.4.1 and 4.4.2. The suitability of the types of boundary conditions for this study is illustrated by the following example. Figures 6.68 and 6.69 show the displacement and velocity traces for the free standing column shown in Figure 6.1b where the base of the column has a fixed support (Dirichlet boundary). When there is no fixed support at the base of the column (Neumann boundary), the displacement and velocity traces for the column are given in Figures 6.70 and 6.71. By superimposing the solutions for the fixed and free boundary conditions (equation 4.58), the resultant displacement and velocity traces are as shown in Figures 6.72 and 6.73. It is obvious from Figures 6.72 and 6.73 that there are pulse reflections from the base of the pile. This example illustrates that the superposition boundary is not suitable for the simulation of an energy absorbing boundary at the base of the pile.

Figures 6.74 and 6.75 give the displacement and velocity traces for the free standing column shown in Figure 6.1b where the unified boundary condition (section 4.4.2) is incorporated at the base of the column. These figures show that there is no reflection from the base of the column which indicates that most of the pulse energy applied at the column head has been absorbed at the energy absorbing boundary at the base of the column.

6.8.1 Elastic Properties of Soils

In the idealisation of the soil medium as a homogeneous isotropic linear elastic continuum, it is assumed that the mechanical response of every element within the soil mass may be described in terms of the elastic constants of the soil E_s and ν_s.

The material parameters characterising the isotropic elastic continuum model are the modulus of elasticity, E_s, and Poisson's ratio, ν_s. Selvadurai (Ref. 6.25) showed the typical values of Poisson's ratio for sands are 0.30 - 0.35 while those for clays are 0.40 - 0.50. Some E_s values given by Selvadurai (Ref. 6.25) are shown in Table 6.3.

Soil Type	E_s (MNm^{-2})
Very soft clay	0.30 - 3.00
Soft clay	2.00 - 4.00
Medium clay	4.50 - 9.00
Hard clay	7.00 - 20.00
Sandy clay	30.00 - 42.50
Glacial till	10.00 - 16.00
Silt	2.00 - 20.00
Silty sand	5.00 - 20.00
Loose sand	10.00 - 25.00
Dense sand	50.00 - 100.00
Dense sand and Gravel	80.00 - 200.00
Loose sand and Gravel	50.00 - 140.00
Shale	140.00 - 1400.00

Table 6.3

Also given in reference 6.25 is the empirical relationship between the unconsolidated shear strength c_u and the undrained elastic modulus E_{su} for clay soil used in the Canadian Manual on Foundation Engineering. They are:

$E_{su} = 500c_u$ for soft sensitive clays

$E_{su} = 1000c_u$ for firm to stiff clays

$E_{su} = 1500c_u$ for very stiff clays

The bulk density of some typical types of soil are given by Bell (Ref. 6.26) in which different varieties of sand have densities between 1400 - 2500 kgm^{-3}, clay between 1500 - 2150 kgm^{-3} and silt between 1820 - 2150 kgm^{-3}

The material parameters have been shown to be suitable for pile-soil interaction analysis where the elastic properties of soil employed by Poulos (Ref. 6.27), Krishnan et. al. (Ref. 6.28) and Dungar et. al. (Ref. 6.15) are within the range of values given by Selvadurai (Ref. 6.25). In addition, Krishnan et. al. (Ref. 6.28) has suggested that the Gibson soil model is the simplest possible inhomogeneous soil model which appears capable of representing many actual soil profiles with reasonable accuracy. In the Gibson soil model, the Young's modulus of normally consolidated clay is assumed to vary proportional with the effective mean pressure, and hence increases linearly with depth, thus:

$$E(z) = E_s(z/d) \tag{6.8}$$

where z is the depth below ground level, d is the diameter of a pile and E_s is the modulus at a depth of one pile diameter below the surface. Most of the examples studied here are for piles founded in soil.

Two examples considered here are piles seated on a rock mass, Eskdale Granite, which has a Poisson's ratio of 0.2, a Young's modulus of 56.6×10^6 MNm^{-2} and a density of 2650.00 kgm^{-3}.

In practice, the Young's Modulus of the soil may not be given directly.

It may be found by measuring the sound velocity of the soil (Ref. 6.29) and the density of the soil. These values may be substituted into equation (6.1) to find the value of the Young's modulus for the finite element analysis.

6.8.2 Simulated Tests on Pile-Soil Systems

The 8-node plain strain finite element has been used to idealise a more realistic application of the Sonic Echo Method to a site where pile-soil interaction is to be accounted for in the finite element analysis. Plane strain finite elements are used to simulate the restrain in the lateral direction of the finite elements. Figure 6.76 shows the finite element idealisation of one-quarter of the 'continuum'. The 0.4 m x 0.4 m x 8.0 m pile is buried in clay which has E_s = 3.00 MNm^{-2}, ν_s = 0.45 and ρ_s = 2010.00 kgm^{-3}. The hammer blow is applied along the vertical axis of the pile while the particle responses at the quarter point of the pile are measured.

Figures 6.77 and 6.78 show respectively the vertical particle displacement and velocity responses at the quarter point of the pile head as predicted by the Finite Element Analysis with Transmitting Boundaries. The velocity response shows no change of phase upon reflection of the pulse from the pile toe-soil interface. This indicates that the pile has a free end. It is also shown that the measured reflection time for the pulse to arrive at the pile head after it was first reflected from the pile toe-soil interface is longer than that for the free pile studied in section 6.3.2.1. In this study, the reflection time measured from Figure 6.78 is 4.80 ms while the reflection time measured in section 6.3.2.1 for a free pile (Ref. 6.8) is approximately 4.56 ms. Figure 6.79 shows the velocity response of the pile at the quarter point of the pile toe. It illustrates that the pulse arrived at the pile toe approximately 2.40 ms after the pulse is first applied. These figures indicate that the pulse has travelled along the pile at a constant speed of 3333.33 ms^{-1}. Obviously, the lower speed at which the pulse travelled in the pile is due to the pile-soil interaction. The effect due to different elastic parameters of the soil will be investigated in section 6.8.3.

Figures 6.80 and 6.81 show the displacement and velocity responses recorded on the ground level at the pile-soil interface. Although the reflections from the pile toe are significant, the noises between the measured pulses are so great that a reflection from a small defect in the pile may go undetected. This study indicates that the transducer for measuring the sonic echo test in a pile-soil system should be advantageously placed at the quarter point of the pile head.

6.8.2.1 A Fixed End Pile

The displacement and velocity responses of the 8.0 m pile when it is seated on a rock which has the same width as the pile, are given in Figures 6.82 and 6.83 respectively. The predicted response of the pile is similar to a fixed end pile where the reflected pulse is of opposite phase to the applied pulse. Again, it has been shown that the reflected pulse has an amplitude smaller than expected, indicating that some energy has been dissipated to the soil through the vertical pile-soil interface and some has been transmitted into the rock. The measured reflection time for the first reflected pulse is the same as when the pile is embedded in a homogeneous soil. In equation (6.3), it is shown that the amount of energy reflected from the pile toe is also dependent on the change of cross-sectional area across the interface between two media. When the level below the pile toe is covered by a layer of very wide Eskdale Granite, the pile responds almost like a perfectly fixed end pile where the reflected pulse has a change of phase from the applied pulse with most of the pulse energy reflected to the pile head. The displacement and velocity responses of this model are given in Figures 6.84 and 6.85. This shows that the Sonic Echo Method of pile testing can give information about the support condition of a pile.

6.8.2.2 Short Pulse Contact Time

An input pulse with a contact time half of that used in the previous studies in sections 6.8.2 and 6.8.2.1 is applied to the same pile-soil idealisation and the predicted displacement and velocity responses are given in Figures 6.86 and 6.87. Similar to the case of a free pile, a shorter input sonic pulse introduces noise between the recorded reflected pulses, although the noise introduced does not mix with the reflected pulses and make interpretation impossible. This also confirms that the normal range of pulse wavelengths applied in model tests in section 6.3.1 may be applied to field tests.

6.8.3 Variation of the Elastic Properties of the Soil

It has been shown in section 6.8.2 that the predicted behaviour of a pile embedded in a soil is different from that of a free standing pile. This study will investigate how different elastic parameters of the soil affect the behaviour of the pile.

6.8.3.1 Change of the Young's Modulus of the Soil

The predicted displacement and velocity responses at the pile head are given in Figures 6.88 and 6.89 for a pile which is embedded in a soil having a stiffness equal to 4 times of that used in section 6.8.2 (E_s = 12.00 MNm^{-2}, ρ_s = 2010.00 kgm^{-3}; ν_s = 0.45). The reflection time of the pulse from the pile base is the same as those shown in Figures 6.77 and 6.78. This indicates that the stiffness of the soil around the pile is not the main cause of the reduction in pulse velocity in the pile. In fact, the upward displacement of the pile head after the removal of the hammer blow has been shown to increase due to the increase in the surrounding soil stiffness from 2.50 x 10^{-7} m to 5.00 x 10^{-7} m. So approximately twice as much displacement is recovered before the first reflected pulse arrives. This is indicated in Figure 6.89 as a downward shift of the measured velocity response between the applied pulse and the first reflected pulse. In fact, this type of velocity response has been found in most field tests, which has been explained previously as being caused by electronic equipment such as integrators and filters, and the skin friction of a pile (Ref. 6.30).

Figures 6.90 and 6.91 show the displacement and velocity response curves at the quarter point of the pile head of a free standing fixed end pile where the nodes along the outer edge of the pile model have an added 2% stiffness. These show a response similar to the pile-soil system except that the reflection time in this case is the same as that of a free pile, namely 4.56 ms. This indicates that the added stiffness along the pile shaft due to the soil has caused the upward displacement of the pile head after the removal of the hammer blow. The added stiffnesses along the pile shaft, which is equivalent to a series of spring supports along the pile shaft, has made the pile rebound after the removal of the hammer blow. In addition, this may be explained as a loss of the pulse energy to the surrounding soil as the pulse travels along the pile. The loss of the pulse energy causes a lower stress and strain in the pile as the pulse travels along the pile. A lower strain in the pile corresponds to a smaller displacement in the pile, which in turn indicates a decrease in the displacement after the pulse is applied.

6.8.3.2 Change of the Density of the Soil

In this study, the soil density is increased from 2010.00 kgm^{-3}, as used in section 6.8.2, to 8040.00 kgm^{-3}. Although it is impossible to obtain such a dense soil in practice, this analysis will explain the longer time taken by the pulse to be reflected from the base of a pile embedded in soil. Figures 6.92 and 6.93 show the displacement and velocity of the pile when it is buried in such a dense soil. The measured reflection time in this case is approximately 5.44 ms. The delayed reflection is approximately 4 times that computed in section 6.8.2. The amount of upward displacement after the removal of the hammer blow is the same as in Figure 6.77, which confirms that the density of the soil does not affect the rebound of the pile. It should also be noted that the density of the soil has affected the extent of the compressed zone in the pile, which is shown in Figure 6.93 as a smaller input pulse.

Physically, a heavy structure would respond to the same exciting force with a lower frequency, that is a lower sonic velocity.

6.8.3.3 Change of the Poisson's Ratio of the Soil

Figures 6.94 and 6.95 give the predicted displacement and velocity responses when the Poisson's ratio of the soil is reduced from 0.45 to 0.225.

The response curves are almost similar to those shown in section 6.8.2 except that the rebound of the pile is less. The difference in the amount of rebound is insignificant in this case.

6.8.3.4 Overall Effects due to Surrounding Soil

It may be concluded that soil parameters will affect the sonic echo test results. The stiffness of the soil causes the pile to rebound while the density of the soil would make the pile respond to the pulse with a lower frequency. The Poisson's ratio of the soil does not affect the sonic echo test results significantly. Provided that soil properties are given, reliable interpretation of the integrity of the pile-soil system may be made.

6.8.4 Piles Embedded in Other Soil Types

6.8.4.1 Pile Embedded in Inhomogeneous Soil

Piled foundations in homogeneous clay soil have been considered above. An inhomogeneous model similar to that used by Krishnan et. al. (Ref. 6.27) will be considered. The 8.0 m pile is buried in a soil which has a Young's modulus of 0.6×10^6 Nm^{-2} at a depth of 0.4 m below the ground surface and increasing linearly with depth as given in equation (6.8).

The particle displacement and velocity responses at the quarter point of the pile head for this pile-soil model are given in Figures 6.96 and 6.97. Figure 6.96 shows that the rebound of the pile is greater than that in Figure 6.77 and is less than that in Figure 6.88.

The velocity response as shown in Figure 6.97 is intermediate between those of Figures 6.78 and 6.89 which indicates that inhomogeneous soil may be represented by homogeneous soil in the simulation without introducing serious errors.

6.8.4.2 Pile in Glacial Till

In this study, the pile is buried in Glacial Till which has a uniform Young's modulus of 16.0×10^6 Nm^{-2}, a density of 2100.0 kgm^{-3} and a Poisson's ratio of 0.3. Figures 6.98 and 6.99 shows the simulated displacement and velocity responses at the quarter point of the pile head due to an applied pulse at the pile head.

The rebound showed in Figure 6.98 has increased to 2.667 times of that given in Figure 6.77 due to the larger Young's modulus. The change in the measured reflection time is insignificant due to the small difference in the density of the soil from that given in sections 6.8.2 (Figure 6.77).

6.8.5 Detection of Faults in the Pile

The finite element idealisation with a transmitting boundary has been shown to be very useful in the study of the application of the sonic echo method to a pile-soil system. It has also been shown that the sonic echo method can be used to assess the integrity of a 'free structural member'. The ability of the sonic echo method to locate defects in a pile when it is embedded in soil will be investigated in this section. Two types of defects will be considered, a pile with a layer of concrete with a relatively smaller Young's modulus of value 7.31×10^6 Nm^{-2} and a pile with a necking at its mid-depth. It was shown in section 6.5.1.2 that the ability of the sonic echo method of testing to locate a defect in a structural member is dependent on the extent of the defect. In addition, from equation (6.3), the amount of energy reflected from a discontinuity is dependent on the physical and elastic properties between the pile concrete and the defective section. In this study, the applied pulse frequency will be similar to those used for testing a 'free standing pile'. The defective piles are considered to be embedded in clay soil.

6.8.5.1 Detection of Concrete Layer with Small Young's Modulus in the Pile

The simulated sonic echo results for a weak concrete layer at 0.4 m below the pile head and at 0.4 m above the pile toe are shown in Figures 6.100

and 6.101 respectively. The ability of the method to locate the concrete layer with a smaller Young's modulus is similar to the case for a free pile. It should be noted that in order to estimate the location of the weak concrete layer which is close to the pile toe, the pile-soil interaction should be accounted for as shown in section 6.8.4.

6.8.5.2 Detection of Necking in the Pile

The idealisation of the necking pile embedded in soil is given in Figure 6.102. The simulated test on a necking pile is given in Figure 6.103. It shows that both reflections from the necking and from the pile toe can be detected. Moreover, only the first reflections from these interfaces are distinctive while the superposition of these reflected signals has made the interpretation of the later part of the response curve difficult.

6.9 Conclusions

A two-dimensional finite element analysis has been used to simulate the sonic echo method of non-destructive testing for structural members. The application of the finite element technique to interpret the sonic echo tests results are also shown. Procedures to predict the load bearing capacity of a structural member are suggested. Due to the limitation of the two-dimensional finite element model to represent a three-dimensional field and the lack of reliable field test results, only qualitative studies on the application of the sonic echo method to the pile-soil system have been made.

The two dimensional finite element idealisation represents one quarter of a square free hanging beam which compared favourably with the field test data. In the pile-soil system simulation, the finite element idealisation represents a 0.4 m pile which is restrained in one direction by the soil and is free in another direction. The model represents one quarter of the pile-soil system where a transmitting boundary has been incorporated in the far field of the soil medium to simulate an infinite soil medium.

Regular finite element meshes have been used throughout to avoid unnecessary reflections due to the change in element stiffness resulting from the change of finite element sizes. In the free standing beam model, both 3 node and 8 node finite element idealisations give the same results if the meshes are fine enough. In the pile-soil system models, 8 node finite elements have been used to reduce the input data to be processed.

The material damping due to concrete was shown to be small and its effects are not included in the studies.

Considering a smooth pile head, it was found that a clean response at the pile head may be obtained by applying the pulse at the centre of the pile and recording the response at the quarter point by an accelerometer or velocity transducer. The finite element studies also confirmed that the pulse propagates in a free hanging beam at a speed approximately equal to the bar velocity, given by equation (6.1). The ability of the sonic echo method of testing to locate a defect in a structural member depends on the wavelength of the applied pulse, the contrast in the acoustic impedance between the defective material in the structural member and the structural member itself and the extent of the defect. The exact location of the defect may not be estimated unless the defect is at a distance of more than one quarter of the wavelength of the pulse from the applied hammer blow. The use of the correlation functions for the interpretation of the sonic echo test results is investigated. From these studies, the cross-correlation function is found to be better suited than the autocorrelation function in the interpretation of test data.

It is also shown in the examples that the interpretation of the signals obtained from a complex structure, such as the double overbreak beam, sometimes requires care in the choice of the reflection time corresponding to a defect. Therefore, it may be advisable to regard the Sonic Echo Test velocity or displacement traces as supporting information. To confirm the existence of a certain defect, Finite Element Simulation or other types of non-destructive tests, for example sonic coring, may be used.

The use of the finite element technique to interpret the sonic echo method of non-destructive testing may allow prediction of the physical and material properties of the structural member which is useful in assessing the behaviour of the structural member under working load.

The studies on the application of the sonic echo test on the pile-soil system by the finite element analysis clearly indicate the advantage of using the finite element method for the interpretation of the sonic echo test results. The effects of soil properties on the sonic echo test are shown. Although the finite element model is only two dimensional in this case, it gives qualitative results for the interaction between the pile and the soil in the sonic-echo tests, under dynamic loading. It should also be appreciated that in a real situation, the damping due to soil stiffness would be more serious since the pile is restrained on its periphery instead of one direction only as in the finite element idealisation. This in turn will reduce the sensitivity level of the sonic echo method. Therefore, in addition to those factors affecting the performance of the sonic echo method of integrity testing of a free standing pile, the soil properties around the pile will reduce the effectiveness of the sonic echo method. Again, using the finite element technique to interpret the sonic echo tests would allow prediction of the behaviour of the pile under working load by reanalysing the pile-soil idealisation to fit the simulation results to the test data.

Reference 6.

1. Steinbach, J., Vey, E., "Caisson Evaluation by Stress Wave Propagation Method", Journal of the Geotechnical Engineering Division, Proceedings of the America Society of Civil Engineers, Vol. 101, No. GT4, 361-378, April, 1975.

2. Weltman, A.J., "Integrity Testing of Piles: A Review", DoE and CIRIA Development Group Report PG4, PSA Civil Engineering Technical Guide No. 18, September, 1977.

3. Fleming, W.G.K., "Use of T.N.O. Integrity Testing System in United Kingdom", in 'Application of Stress-Wave Theory on Piles', Proceedings of the International Seminar on the Application of Stress Wave Theory on Piles, Stockholm, 331-332, 4-5 June, 1980.

4. Van Koten, H., Middendorp, P., "Interpretation of Results from Integrity Tests and Dynamic Load Testing", in 'Application of Stress-Wave Theory on Piles', Proceedings of the International Seminar on the Applicaion of Stress Wave Theory on Piles, Stockholm, 217-232, 4-5 June, 1980.

5. Fegan, I., "Testing Concrete Foundation Piles by Sonic Echo", Ph.D. Thesis, University of Edinburgh, 1981.

6. Byles, R., "Dutch Strike a Blow for Integrity Testing", New Civil Engineer, 26, 11 June, 1981.

7. Stain, R.T., "Integrity Testing", Civil Engineering, 54-73, April, 1982.

8. Cementation Piling and Foundations, "T.N.O. Testing Methods", Technical Literature.

9. Smith, I.M., "Transient Phenomena Offshore Foundation", Chapter 15 of 'Numerical Methods in Offshore Engineering, Edited by O.C. Zienkiewicz, R.W. Lewis and K.G. Stagg, John Wiley & Sons, Ltd., 1978.

10. Chan, H.F.C., "Non-Destructive Testing of Concrete Piles using Sonic Echo and Transient Shock Method", Ph.D. Thesis, University of Edinburgh, 1987.

11. Lysmer, J., Kuhlemeyer, R.L., "Finite Dynamic Model for Infinite Media", Journal of the Engineering Mecahnics Division, Proceedings of the American Society of Civil Engineers, Vol. 95, No. EM4, 855-877, August, 1969.

12. Lyemer, J., Waas, G., "Shear Waves in Plane Infinte Structures", Journal of the Engineering Mechanics Division, Proceedings of the American Society of Civil Engineers, Vol. 98, No. EM1, 85-105, February, 1972.

13. White, W., Valliappan, S., Lee, I.K., "Unified Boundary for Finite Dynamic Models", Journal of the Engineering Mechanics Division, Proceedings of the American Society of Civil Engineers, Vol. 103, No. EM5, 949-964, October, 1977.

14. Roesset, J.M., Ettouney, M.M., "Transmitting Boundary: A Comparison", International Journal for Numerical and Analytical Methods in Geomechanics, Vol. 1, 151-176, 1977.

15. Dungar, R., Eldred, P.J.L., "The Dynamic Response of Gravity Platform", Earthquake Engineering and Structural Dynamics, Vol. 6, 123-138, 1978.

16. Chow, Y.K., "Accuracy of Consistent and Lumped Viscous Dampers in Wave Propagation Problems", International Journal for Numerical Methods in Engineering, Vol. 21, 723-732, 1985.

17. Neville, A.M., "Properties of Concrete", 3rd Edition, Pitman Publishing Limited, 1981.

18. Goldsmith, W., Polivka, M., Yang, T., "Dynamic Behaviour of Concrete", Proceedings of the Society for Experimental Stress Analysis, Vol. 23, No. 1, 65-79, 1966.

19. Ashbee, R.A., Heritage, C.A.R., Jordan, R.W., "The Expanded Hysteresis Loop Method for Measuring the Damping Properties of Concrete", Magazine of Concrete Research, Vol. 28, No. 96, 148-156, September, 1976.

20. Lilley, D.M., "The Non-Destructive Testing of Model Piles Using a Resonant Vibration Technique",Ph.D. Thesis, University of Bristol, 1982.

21. Griffiths, D.H., King, R.F., "Applied Geophysics for Geologist and Engineers", Pergamon Press Ltd., Oxford, England, 1981.

22. Forde, M.C., Chan, H.F.C., Batchelor, A.J., "Acoustic and Vibration NDT Testing of Piles in Glacial Tills", Glacial Till 85, Proceedings of The International Conference on Construction in Glacial Tills and Boulder Clays, 243-256, 12-14 March, 1985.

23. Forde, M.C., Chan, H.F., Batchelor, A.J., "Interpretation of Non-Destructive Tests on Piles", Structural Fault 85, Proceedings of the Second International Conference in Structural Faults and Repair, 333-347, 30 April-2 May, 1985, London.

24. Telford, W.M., Geldart, L.P., Sheriff, R.E., Keys, D.A., "Applied Geophysics", Cambridge University Press, 1976.

25. Selvadurai, A.P.S., "Elastic Analysis of Soil Foundation Interaction", Elsevier Scientific Publishing Company, 1979.

26. Bell, F.G. (Ed.), "Foundation Engineering in Difficult Ground", Butterworth & Co. (Publisher) Ltd., 1978.

27. Poulos, H.G., "The Influence of Shaft Length on Pile Load Capacity in Clays", Technical Note, Geotechnique, Vol. 32, No. 2, 145-148, 1982.

28. Krishnan, G.G., Velez, A., "Static and Dynamic Lateral Deflexion of Piles in Non-Homogeneous Soil Stratum", Geotechnique, Vol. 33, No. 3, 307-325, 1983.

29. Abbiss, K.P., Ashby, K.D., "Determination of Ground Moduli by a Seismic Noise Technique on Land and on Sea Bed", Technical Note, Geotechnique, Vol. 33, No. 4, 445-450, 1983.

30. Reiding, F.J., Middendorp, P., Van Brederode, P.J., "A Digital Approach to Sonic Pile Testing", Proceedings of The Second International Conference on the Application of Stress-Wave on Piles, Stockholm, 88-93, 27-30, May, 1984.

Chapter 7

Finite Element Modelling of the Sonic Echo Method of Testing Masonry Structures

7.1 Introduction

The practical application of the Sonic Echo Method to Non-Destructive Testing has been illustrated by its use to locate cracks in a shear wall (Ref. 7.1). In this Chapter the use of the finite element method for simulating the application of the Sonic Echo Method to both brickwork and masonry structures is considered.

In most published two-dimensional finite element analysis of brickwork and masonry structures (Ref. 7.2, 7.3, 7.4, 7.5, 7.6), concrete equivalent material properties are assumed. That is, constant E, ρ and ν values are assumed in one or both directions. It has been shown in chapter 6 when simulating the Sonic Echo Method of Pile testing, that a discontinuity in the impedance in a pile gives rise to reflections. The velocity trace recorded at the pile head, which gives an indication of the integrity of the pile, is sometimes difficult to interpret due to the multiple reflections from the discontinuities in a pile. The study presented in this chapter considers the response of a brickwork column, which has many reflection interfaces between brick and mortar. The problem of determining a theoretical pulse velocity in a brickwork column is considered. Furthermore, the assessment of the integrity of a brickwork structural member by the Sonic Echo Method is investigated. The application of the Sonic Method to the assessment of the integrity of a large masonry bridge, is also studied. Possible procedures for testing a masonry bridge are discussed and the use of finite element analysis in the interpretation of the Sonic Method is also presented.

7.2 Propagation of a Sonic Pulse in a Layered Column

In a geophysical application of the seismic method to ground exploration, layered media is usually considered. The thickness of the layers considered are generally comparable with the wavelength of the pulse (Refs. 7.7, 7.8, 7.9). For the case of offshore oil exploration, liquid and rock layers may be considered.

It was shown in section 6.5.1.2 that a neck in a pile which has an extent of about 1/35 of the wavelength of a pulse can be located by the Sonic Echo Method. A brickwork column may have mortar layers and brick layers of about 1/300 and 1/60 of the wavelength of a typical pulse in a Sonic Echo Test. Another characteristic of a brickwork column is that it is made up of alternative layers of brick and mortar. The direct interpretation of the sonic echo test on brickwork structures using the analyses presented in Chapter 6 may not be possible.

7.2.1 The Finite Element Model

Figure 7.1 shows a typical finite element idealisation of a brickwork column of length 3.012 m. To assess the reflections due to the finite element mesh, a number of further idealisations arre considered. Particular concern is the effect of using a thin element to idealise mortar layers and a thick element for the bricks since the ratio of the thickness of the bricks to the mortar layer is 5:1. This investigation is undertaken by assuming that the mortar layers have the same properties as the bricks. A half sine function pulse which has a maximum amplitude of 5000 N and a contact time of 0.9 ms is applied to the column head. The simulated velocity response of such model is given in Figure 7.2 which shows that the pulse reflected from the fixed end arrives at the column head after 1.60 ms approximately (1.615 ms calculated using equations (6.1) and (6.2)). This indicates that the rapid change in finite element sizes does not affect the pulse velocity in the column. In addition, it does not cause serious 'noise' between the reflected signals.

Small time steps (2.0×10^{-6} s) are used for the time integration in the analysis to avoid aliasing effects, since the analysis may ignore the mortar layers during the time integration when large time steps are used. It is found that there are no significant reflections from the brick-mortar interface which indicates that the original time step (1.5×10^{-5} s) is suitable. In addition, the rate at which the signal analyser accepts data points from a field test is about 1.5×10^{-5} s. Therefore, the use of a time step of 1.5×10^{-5} s for the numeral integration would simulate the same process as in a field test.

Typical material properties for brick and mortar are used to simulate a brickwork column. The typical values of brick and mortar used by Khoo (Ref. 7.7) for finite element analysis are summarised in Table 7.1.

	Brick	Mortar
E	6.895×10^{9} Nm^{-2}	6.895×10^{8} Nm^{-2}
ν	0.1	0.1
ρ	2000 kgm^{-3}	1000 kgm^{-3}

Table 7.1

Figures 7.3 and 7.4 show the simulated velocity traces of brickwork columns which have total lengths of 0.78 m and 1.50 m respectively. From the reflection times measured from Figures 7.3 and 7.4, it is found that the brickwork columns respond as homogeneous columns and the pulse velocities in the columns are found to be 1392.86 ms^{-1} and 1284.25 ms^{-1} which are lower than those calculated from equations (6.1) and (6.2). Using equations (6.1) and (6.2) to calculate the pulse velocity in the brick and mortar layers, the calculated pulse velocities in the brickwork columns should be 1560.74 ms^{-1} and 1550.17 ms^{-1} respectively. It is obvious that the measured reflection times do not correspond to the time taken for the pulse to propagate through the different layers and reflect back from the base.

From laboratory tests on brickwork columns, it is also found that a brickwork column responds to an applied sonic pulse in a similar manner as a homogeneous column as shown in Figure 7.5 (Ref. 7.10).

7.2.2 Wave Velocity in a Multi-Layered Column

As shown in Figures 7.3 and 7.4, no clear reflections from brick-mortar interfaces are recorded. The whole column responds as a homogeneous structure. Therefore, it may be possible to find the wave velocity in a multi-layered column which consists of thin layers between relatively thick layers.

For an elastic material, the elastic modulus is defined by the following expression:

$$E = \text{stress/strain} = (P/A)/(e/L) \tag{7.1}$$

where: P is the total uniformly distributed load applied on the test specimen, A is the cross-sectional area of the specimen, e is the deformation of the specimen in the direction of the applied load and L is the original length of the specimen.

Static finite element analysis of the idealisation of a number of uniform material columns is undertaken to assess the suitability of the idealisation. One quarter of the column is simulated and the applied nodal load on the column head is 1250 N (total equivalent load applied to the column head = 5000 N). The results of these analyses are used to determine the computed values of the elastic modulus, $E_{computed}$ by substitution of the displacement into equation (7.1). The percentage error in the computed elastic modulus with respect to the input elastic modulus is also determined. The results of these analyses are given in Table 7.2.

Column Length	Input E	$E_{computed}$	% error
0.420 m	6.895×10^9 Nm^{-2}	6.901×10^9 Nm^{-2}	0.08
0.780 m	6.895×10^9 Nm^{-2}	6.901×10^9 Nm^{-2}	0.08
1.500 m	6.895×10^9 Nm^{-2}	6.898×10^9 Nm^{-2}	0.04
2.004 m	6.895×10^9 Nm^{-2}	6.896×10^9 Nm^{-2}	0.02
3.012 m	6.895×10^9 Nm^{-2}	6.896×10^9 Nm^{-2}	0.01

Table 7.2

Equation (7.1) may also be applied to the results of finite element analysis of multi-layered columns to determine E_{eq}, the values of the equivalent elastic modulus. The total vertical deformation of the column e_T is given by:

$$e_T = e_1+e_2+e_3+ \ldots\ldots\ldots\ldots+e_n$$
$$= \Sigma e_i \qquad (7.2)$$

where:

$$e_i = \frac{PL_i}{AE_i} \tag{7.3}$$

and

$$L = \Sigma\, L_i \tag{7.4}$$

where: L_i is the thickness of the ith layer in the column. Therefore, by substituting equation (7.2) into equation (7.1), and rearranging the equation, we obtain:

$$E_{eq} = \frac{P/A}{(\Sigma e_i)/L} = \frac{PL}{A\Sigma e_i} \tag{7.5}$$

Then, substituting equation (7.3) in equation (7.5), the equation becomes:

$$E_{eq} = \frac{PL}{A\Sigma((Pl_i)/(AE_i))} = \frac{L}{\Sigma(L_i/E_i)} \tag{7.6}$$

and L in equation (7.6) can be expressed as in equation (7.4) which gives:

$$E_{eq} = \frac{\Sigma L_i}{\Sigma(L_i/E_i)} \tag{7.7}$$

It has been shown in chapter 6 that the speed at which a pulse will propagate in a homogeneous column may be found from equation (6.1):

$$c^2 = E/\rho \tag{6.1}$$

The speed depends on both the elastic modulus (E) and the density (ρ) of the column. For a multi-layered column which has uniform cross-sectional area, the equivalent density of the column may be determined using:

$$\rho_{eq} = \frac{\Sigma(L_i\rho_i)}{\Sigma L_i} \tag{7.8}$$

Thus the wave velocity in such multi-layered column may be found from:

$$c_{eq}^2 = E_{eq}/\rho_{eq} \tag{7.9}$$

Hence,

$$c_{eq}^2 = \frac{(\Sigma L_i^2)}{\Sigma(L_i/E_i)\Sigma(L_i\rho_i)} \tag{7.10}$$

7.2.3 Wave Velocity in a Brickwork Column

The number of brick layers is approximately equal to the number of mortar layers in a typical brickwork column as shown in Figure 7.1. For example, if there are r layers of mortar and r+1 layers of brick in a brickwork column, then the elastic modulus of the brickwork column may be determined using:

$$E_{bw} = \frac{rL_m+(r+1)L_b}{(rL_m/E_m)+((r+1)L_b/E_b)} \tag{7.11}$$

$$E_{bw} = \frac{[rL_m+(r+1)L_b]E_mE_b}{rL_mE_b+(r+1)L_bE_m} \tag{7.12}$$

where L_m and L_b are the thickness of the mortar and brick layers respectively. If the number of brickwork courses becomes large, then this expression may be simplified to:

$$E_{bw} = \frac{(L_m+L_b)E_mE_b}{L_mE_b+L_bE_m} \tag{7.13}$$

Figure 7.6 illustrates the convergence of the E_{bw} value to that found from equation (7.7) as the total number of brick-mortar layers increases.

The density of a brickwork column which is constructed from courses of uniform thickness with bricks and mortar of the same cross sectional area becomes:

$$\rho_{bw} = \frac{rL_m\rho_m+(r+1)L_b\rho_b}{rL_m+(r+1)L_b} \tag{7.14}$$

If the number of brick-mortar courses becomes large:

$$\rho_{bw} = \frac{L_m\rho_m+L_b\rho_b}{L_m+L_b} \tag{7.15}$$

Figure 7.7 shows the convergence of the ρ_{bw} values towards the results obtained from the simplified equation (7.15).

7.3 Application of the Theory to the Study of the Sonic Echo Method of Non-Destructive Testing of a Brickwork Column

7.3.1 Case Studies

Equations (7.12) and (7.14) are used to interpret the results from a series of sonic echo tests on the finite element idealised brickwork columns of different lengths. The results are given in Table 7.3.

Column Height	E_{bw} (eqt. 7.12)	ρ_{bw} (eqt. 7.14)	c (eqt. 7.10)	c (F.E.M.)
0.780 m	2.907×10^{9} Nm^{-2}	1846.15 kgm^{-3}	1254.85 ms^{-1}	1300.00 ms^{-1} (3.6%)
1.500 m	2.842×10^{9} Nm^{-2}	1840.00 kgm^{-3}	1242.74 ms^{-1}	1275.51 ms^{-1} (2.6%)
2.004 m	2.823×10^{9} Nm^{-2}	1838.32 kgm^{-3}	1239.29 ms^{-1}	1284.62 ms^{-1} (3.7%)
3.012 m	2.806×10^{9} Nm^{-2}	1836.65 kgm^{-3}	1236.07 ms^{-1}	1255.00 ms^{-1} (1.5%)

Table 7.3

It is also found that the pulse velocity in a brickwork column along the long axis of the brick may also be predicted using equations (7.12), (6.1) and (7.14) for relatively short columns. A typical displacement trace for a 2.004 m finite element idealised brickwork column which consists of 9 brick layers and 8 mortar layers is shown in Figure 7.8. The pulse velocity calculated using the reflection time from Figure 7.8 is 1648.02 ms^{-2} compared to 1571.00 ms^{-1} calculated from equations (7.12), (6.1) and (7.14). In this case, the percentage error is approximately 5%. In addition, it is found because there are relatively less discontinuities in the same 2.004 m column, the reflections from the brick-mortar interfaces introduced some noise between consecutive reflections in Figure 7.8.

It may be shown (Ref. 7.9) that the density of brick ranges between 1300 kgm^{-3} and 2200 kgm^{-3} while the modulus of elasticity for brick ranges between 8.240×10^{9} Nm^{-2} and 2.060×10^{10} Nm^{-2}. Usually, the strength of a brick is related to its density. A series of simulated sonic echo tests on the 3.012 m brickwork column, in which one of the bricks in the column has the lowest density and elastic modulus (the faulty brick) while all other bricks have the largest density and elastic modulus, is carried out. Whether the faulty brick may be detected by the sonic echo method of non-destructive testing depends on the location of the faulty brick in the column. In practice, therefore, the sonic echo method may not be used to locate faulty bricks near the top or bottom of a brickwork column. Figure 7.9 shows the response of the brickwork column where the faulty brick is placed at the bottom of the column while Figure 7.10 shows the velocity trace of the brickwork column with a faulty brick placed at its mid-depth.

The sonic echo method of testing is also applied to four brickwork column idealisations. The idealisations are considered to be built using bricks with mean Young's modulus (Case 1), bricks with high Young's modulus (Case 2), bricks with low Young's modulus (Case 3), and alternative layers of bricks with high and low Young's modulus (Case 4). The results of the simulated tests are given in Table 7.4. Also shown in Table 7.4 is the application of the calculated sound velocity in the brickwork columnconsisting of bricks with the mean value of Young's modulus, to the interpretation of the sonic echo tests on other models. It is found that the pulse propagation velocity for the four brickwork column idealisations are within about 3% of that of the mean Young's modulus brickwork column calculated using equation (7.10). Therefore, the mean Young's modulus and density for brick and mortar may be used to calculate the wave velocity of the sonic pulse when using the sonic echo method of testing brickwork columns.

	c_{theory} (eqt. 7.10)	% diff. fr. Case 1 c^*_{theory}	$c_{idealisation}$	% deviation fr. Case 1 c^*_{theory}
Case 1	$^*2427.51\ ms^{-1}$		$2476.97\ ms^{-1}$	2.04
Case 2	$2396.79\ ms^{-1}$	1.28	$2429.03\ ms^{-1}$	0.06
Case 3	$2325.73\ ms^{-1}$	4.38	$2382.91\ ms^{-1}$	1.84
Case 4	$2288.47\ ms^{-1}$	6.08	$2353.12\ ms^{-1}$	3.06

Table 7.4

Figure 7.11 shows the simulated velocity trace of the brickwork column, in which all the bricks have the mean Young's modulus value. Figure 7.12 illustrated the simulated velocity trace of a similar column which has alternative layers of bricks with high and low Young's modulus. Although this brickwork column also responds as a homogeneous column, the extra layers of different materials have introduced some noise in the velocity trace between the input and reflected pulses. The reflected pulse is also distorted. Figure 7.13 shows the simulated velocity trace of the brickwork column where bricks with high Young's modulus are used. It is shown in Figure 7.13 that the input and reflected pulses have smaller amplitudes than those shown in Figure 7.11. This is a result of the smaller displacement at the stiffer column head in response to the same applied input pulse.

7.3.2 Limitations of the Non-Destructive Testing Method

Within the range of brick and mortar idealised, some conclusions may be drawn at this stage. In practice, the Sonic Echo Method may not be used to locate defects which are relatively small. For example, one brick with low Young's modulus in a structural member may not be detected, especially when the defect is close to one of the ends of the structural member. The extra noise between two major reflection signals may indicate the lack of consistency in the elastic properties of the bricks and mortars.

7.4 Sonic Method of Non-Destructive Testing for a Masonry Bridge

The inspection of concrete and brickwork structural member by the sonic method are shown to be relatively straightforward. The applied impulse propagates in the structural member, which may be treated as a waveguide, almost as a plane wave and reflects from a discontinuity to the excited end of the structural member where a transducer will record the reflected signal. In testing concrete piles, only the pile head is accessible. Therefore, the sonic echo method is employed.

Although the sonic method of non-destructive testing of masonry bridge will not be restricted to the echoed signal from a discontinuity, the method has been complicated by the wave system developed in the large domain due to the applied pulse and the composite nature of the masonry and the soil fill.

The non-destructive method of testing used in assessing the integrity of a masonry bridge mentioned in reference 7.11 is by the direct transmission method. In cases where both ends of a structural member may be accessed, such as a brick wall, the sonic transmission method may be employed to assess the integrity of the structural member. A pulse is applied at one end of the structural member while the time taken for the pulse to arrive at the transducer mounted on the other end of the structural member may give an indication of the integrity of the structural member. In contrast, the sonic echo method of testing may be applied to test a structural member where only one side of the structural member is accessible, such as a foundation pile. The time taken for the pulse to propagate to the reflecting end of the structural member and back to the side where the pulse is applied is used to assess the integrity of the structural member. In this section, alternative sonic testing schemes for the assessment of the integrity of a masonry bridge will be proposed. The interpretation of the sonic test results from each scheme will be shown using finite element idealisations. In the finite element idealisations, a masonry structure such as an arch, a wing wall etc. will be treated as a homogeneous isotropic body.

7.4.1 Wave Propagation in an Elastic-Half-Space

When an elastic-half-space is disturbed by a point source at the surface, the disturbance spreads out from the source in the form of a symmetrical annular-wave system (Figure 7.14). A wave is defined as a disturbance which travels through the medium (Ref. 7.12). It was also suggested by Beck (Ref. 7.13) that the properties of these waves depend critically upon the elastic constants of the medium through which they travel. Therefore, the waves are sometimes called elastic waves.

7.4.1.1 Types of Elastic Waves in the System

The derivations of the wave equations describing the elastic waves propagation in an elastic-half-space is given in many published books such as references 7.12, and 7.14 to 7.17. This section will concentrate on the discussion of the particle motions due to the elastic waves and the propagation velocities of the waves which are related to the sonic method of non-destructive testing results.

There are three principal types of waves, classified on the basis of particle motion. The first type is variously known as a dilatational, irrotational, compressional or P- wave. The particle motion associated with the dilatational wave is a push-pull motion in the same direction as the wavefront. This wave propagates at a velocity:

$$c_p = \sqrt{\{[E(1-\nu)]/[\rho(1+\nu)(1-2\nu)]\}} \tag{7.16}$$

and is the fastest travelling wave in the system.

The second type is referred to as the shear, transverse, rotational or S- wave. The particle motion associated with this kind of wave is in a direction orthogonal to the direction of the wavefront. This wave has a velocity:

$$c_s = \sqrt{[E/2\rho(1+\nu)]} \tag{7.17}$$

and is the second fastest travelling wave in the system. Unlike the dilatational waves which have only one degree of freedom along the radial direction, the shear waves have two degrees of freedom. The two degrees of freedom of the shear waves are independent, and therefore a shear wave may involve motion in only one plane. The wave motion in a horizontal plane is denoted as SH waves while the wave motion in a vertical plane is denoted as SV waves.

On the surface of an elastic-half-space, there exists the third type of waves. These waves are called surface waves because they are confined only to the neighbourhood of the surface.

The only type of surface wave of importance in the exploration seismology is the Rayleigh wave (Ref. 7.12). This wave which travels along the surface of the elastic medium involves a combination of longitudinal and transverse motion with a definite phase relation to each other. The influence of the Rayleigh wave decreases rapidly with depth. The particle motion is confined to the vertical plane which includes the direction of propagation of the wave. A particle traverses an elliptical path during the passing of the wave, the major axis of the ellipse being vertical and the minor axis being in the direction of advance of the wave. The direction of particle motion around the ellipse is called retrograde because it is opposite to the more familiar direction of motion of particles in waves on the surface of water. The velocity of Rayleigh wave depends upon the elastic constants in the vicinity of the surface and is always less than the velocity of shear waves and dilatational waves.

7.4.1.2 Discontinuity in the System

When a wave encounters a surface separating two media which have different elastic properties, part of the wave energy is reflected and the other is refracted into the other medium as shown in Figure 7.15. The reflected wave remains in the same medium as the original energy while the refracted wave propagates in the other medium with an abrupt change in the propagation direction. The amount of wave energy reflected or refracted at the interface depends on the elastic properties of the media. The reflection coefficient, R, and the refraction coefficient, T, as given by Telford et. al. (Ref. 7.12) are,

$$R = (Z_2-Z_1)/(Z_2+Z_1) \tag{7.18}$$

and

$$T = 2Z_2/(Z_2-Z_1) \tag{7.19}$$

where Z_i is the acoustic impedance and is the product of density and velocity in the ith medium (Figure 7.15). In equation (7.18), the fraction may become negative if $Z_2 < Z_1$. This means that the reflected wave is 180° out-of-phase with the incident wave.

The direction of propagation of the reflected and refracted wave may be found from the laws of reflection and refraction (Ref. 7.12):

$$p = \mathrm{Sin}\theta_i/v_i \tag{7.20}$$

where p is called the raypath parameter and has the same value for the incident, reflected and refracted waves at an interface; θ_i's are as shown in Figure 7.15 and v_i's are the wave speed in the ith medium. In Figure 7.15, if v_2 is greater that v_1, θ_2 reaches 90° when $\theta_1 = \mathrm{Sin}^{-1}(v_1/v_2)$ and θ_1 is called the critical angle. For this value of θ_1, the refracted wave is travelling along the interface. For incident angles greater than the critical angle, total reflection occurs.

It was also shown by Telford et. al (Ref. 7.12) that an incident dilatational wave may be reflected or refracted as a dilatational wave as well as a shear wave. The proportion of energy in each type of these reflected or refracted waves is also a function of the incident angle of the waves.

The laws of reflection and refraction cease to apply when a wave encounters a sharp corner where the radius of curvature is comparable to or smaller than the wavelength. In such case, the energy is diffracted rather than reflected or refracted. When a wave arrives at the sharp corner, the corner will act as a point source for the diffracted wave (Ref. 7.12) as shown in Figure 7.16 and thus the diffracted wave can extend to the geometrical shadow area.

Therefore, the wave can be detected at the geometrical shadow while the amplitude of the wave may be smaller and the transmission time may be longer than expected.

7.4.2 Finite Element Modelling of Wave Propagation in a Large Continuum

Finite element analysis has been used to study the wave propagation in a large medium. The finite element idealisation of half of the 10m x 5m homogeneous elastic continuum is given in Figure 7.17. The elastic continuum has a Young's modulus of 29.23×10^9 Nm^{-2}, a density of 2400 kgm^{-3} and a Poisson's ratio of 0.24. The dilatational wave velocity in the continuum is found to be 3788.96 ms^{-1} using equation (7.16) and the shear wave velocity is found to be 2216.15 ms^{-1} using equation (7.17).

Figures 7.18 and 7.19 show the vertical displacement and vertical velocity response along the line of symmetry indicated in Figure 7.17 when a pulse is applied. The station number in Figures 7.18 and 7.19 refers to the stations marked in Figure 7.17. Since the dilatational wave has one degree of freedom in its direction of propagation, the vertical components of the particle displacements and velocities along the axis of symmetry of the model would mainly represent the propagation of the dilatational wave. A Rayleigh wave will not occur along the axis of symmetry because there is no free surface along this boundary. There is no direct effect due to the shear wave which is propagating at a lower velocity and which caused a particle motion normal to the axis of symmetry.

In Figures 7.18 and 7.19, both the amplitudes of the displacement and velocity response decrease as the pulse arrives at the stations further away from the source. This decrease in displacement amplitude or decrease in energy density is due to geometrical damping. The geometrical damping becomes obvious when the pulses encounter an increasingly larger volume of material as they travel outward. Thus, the energy density in each wave decreases with distance from the source. The rapid drop of the displacement response after the first peak at station 0 in Figure 7.18 is also an indication of the geometrical damping. This drop in displacement is shown in the velocity response in Figure 7.19 as the negative velocity after the first peak, which has also been reported in many sonic echo pile-testing records (e.g. Ref. 7.18). Therefore, geometrical damping is also an important factor affecting the records from the sonic echo method of pile testing.

It is found that the direct transmission times for the pulse to propagate from the source to each station measured on Figures 7.18 and 7.19 are shown to be consistent with those calculated by dividing the distance from the source to the station by the propagation velocity of the pulse (equation 7.16).

Figures 7.20 and 7.21 show the horizontal components of the displacements and velocities recorded on the surface when a pulse is applied as shown in Figure 7.17. In both figures, at the time corresponding to the direct transmission of the wave from the source to the station, there are some positive minor tremors. These positive minor tremors are followed by a negative major tremor due to the arrival of the Rayleigh wave. This confirms that the direction of particle motion due to the Rayleigh wave is a retrograde ellipse.

The vertical components of the displacements and velocities recorded on the surface due to the applied pulse are given in Figures 7.22 and 7.23. It has been suggested in most publications on wave propagation in half-space (e.g. Ref. 7.12) that when the Poisson's ratio of the medium is 0.25, the Rayleigh wave has a velocity equal to 0.92 that of the shear wave. This explains why the shear wave and the Rayleigh wave near the source are indistinguishable when the two types of waves are so close together. At a distance further away from the source, the shear waves become more distinctive as the first negative minor tremor at station 7 in Figure 7.22. The measured shear wave velocity in Figures 7.22 and 7.23 is consistent with that calculated from equation (7.17). From the main tremors in Figure 7.21 and 7.23, it can be found that the particle motion due to the Rayleigh wave is a retrograde ellipse.

7.4.3 Simulated Tests on the Integrity of a Masonry Bridge using the Sonic Method

7.4.3.1 Properties of the Masonry Bridge Model

The Sonic Technique has been used to locate a void behind the wing wall of a masonry bridge (Ref. 7.11). The material properties of the bridge were not given in the reference. Therefore, this example was not chosen for the finite element studies. Another masonry arch bridge which was tested to destruction has its dimensions and material properties published in references 7.5, 7.19 and 7.20. The bridge was located on the A77 Ayr to Stranraer trunk road at Bridgemill just north of Girvan crossing the Girvan Water. The bridge, whose arch had a geometrical shape approximately parabolic, is shown in Figure 7.19 and the list of main dimensions given in Table 7.5

Span at the springings = 18.29 m

Rise = 2.85 m

Overall width = 8.30 m

Table 7.5

The arch consisted of 62 voussoirs cut to a regular shape having a depth of 0.711 m. The vault, as far as could be ascertained, had a similar thickness to the arch rib but were constructed from regular square stones.

The elastic properties used by Towler (Ref. 7.5) for the ultimate load analysis of the Bridgemill Arch Bridge is give in Table 7.6. Towler (Ref. 7.5) analysed the bahaviour of the arch rib by using the two noded, curved beam elements with three degrees of freedom at each node. In this research, where the integrity of a masonry bridge is considerd, two dimensional, eight node isoparametric plane strain finite elements are used to idealise a masonry bridge. The elements are used to represent the arch, the fill and the bridge deck.

Proprties	Arch	Infill
Young's Modulus	5.0×10^9 Nm^{-2}	5.0×10^7 Nm^{-2}
Density	2100.0 kgm^{-3}	2200.0 kgm^{-3}

Table 7.6

The Poisson's ratio for the analysis was not given by Towler (Ref. 7.5) and therefore the Poisson's ratio is assumed to be 0.1 for the masonry arch and 0.2 for the infill material.

It is also assumed that there is a bridge deck on the top of the fill that has a thickness of 0.246 m. The bridge deck is assumed to have similar properties as the arch.

It was suggested by Forde et al (Ref. 7.11) that the principal source of potential damage to masonry bridge in the United Kingdom is probably that due to water ingress through the deck and the approach road to the abutment. The water ingress results in the erosion of fines which left behind a void in the bridge and cracking in the arch or bulging of the spandrel wall, due to the cyclic expansion and contraction on cold climates where frost action is severe.

7.4.3.2 Finite Element Simulated Tests for a Masonry Bridge Model

The finite element idealisation of one half of the Bridgemill arch bridge is given in Figure 7.24 where the shaded area represents the void. The finite elements representing the void have a thickness of 0.5 m while other elements representing the fill have a thickness of 4.15 m. The objectives of the simulated tests are to locate the void between the deck and the arch and to compare the two testing schemes which will be proposed. Hammer blow, similar to the sonic echo method of pile testing, will be used as the energy source. The locations of the source and the transducers for the two testing schemes are illustrated in Figures 7.25 and 7.26. In Figure 7.25, there is only one point source for the set of transducers used to pick up the responses on the bridge deck and along the intrados. The pulse is applied to the bridge deck for easy operation on the site. This scheme may be called the 'Single Source' scheme. In Figure 7.26, a different testing scheme is proposed. The bridge to be tested will be divided into a grid and a pulse will be applied at each grid point in turn. Two transducers are placed in the vicinity of the applied pulse, one on the bridge deck where the pulse is applied while the other is located vertically beneath the applied pulse at the intrados. This scheme may be called the 'Multiple Source' scheme.

The pulses spread out from the source as dilatational, shear and Rayleigh waves. The transducers on the bridge deck detect the vertical components of the dilatational, shear and Rayleigh waves directly from the source or the reflected, refracted or diffracted waves from discontinuities in the masonry bridge. In the simulated tests, the vertical components of the direct dilatational and shear waves and the reflected, refracted or diffracted dilatational and shear waves are detected by the transducers at the intrados. When the dilatational and shear waves arrive at the intrados, they introduce a surface wave along the intrados which will also be detected by the transducers.

The fault in the bridge idealisations shown in Figure 7.25 and 7.26 is considered to be a void caused by the washing away of the fill between the deck and the arch. The finite elements used to simulate the fault have a thickness of 0.5 m which are much thinner than the other elements representing the fill having a thickness of 4.15 m.

7.4.4. Interpretation of the Simulated Test Results

Both single-source and multiple-source schemes for testing the masonry bridge idealisation are simulated. The test schemes have been applied to the masonry bridge idealisation where there are no defects in the shaded areas shown in Figures 7.25 and 7.26. In these cases, the finite elements in the shaded area have the same properties as the other elements representing the fill material. The results from these comparative studies may be used as a reference for the interpretation of the Sonic Test on a similar masonry bridge whose integrity is unknown.

The test results in each case are presented as combined time domain traces recorded at each station similar to a seismic record.

7.4.4.1 Direct Interpretation of Sonic Test Results

The results for the simulated Sonic Tests on the non-defective masonry bridge idealisation using the single-source scheme are given in Figures 7.27 to 7.30. Figures 7.27 and 7.28 show respectively the simulated displacement and velocity traces as would be recorded at the stations on the bridge deck. In the same test, the simulated displacement and velocity traces recorded at the stations along the arch intrados are shown in Figures 7.29 and 7.30.

It was noted in section 7.4.1.2 that the critical angle, θ_c, for refraction may be found using:

$$\theta_c = \mathrm{Sin}(v_1/v_2)$$

Therefore the critical angle of incidence at the interface between the fill and the arch is 5.84° for the dilatational wave and 5.37° for shear waves. Thus, using the single source scheme for testing such a masonry bridge, most of the waves arriving at the fill/arch interface are reflected because the angle of incidence is greater than 5°. In this case, only the region near the axis of symmetry and beneath the applied pulse will allow the wave to transmit across the interface.

The signals detected at the stations on the bridge deck are a resultant of the signals due to direct transmission, reflected dilatational waves and shear waves as well as the Rayleigh wave. The minor tremors shown in the traces for station 1 to 7 in Figures 7.27 and 7.28 are most probably an indication of the arrival of the dilatational waves and shear waves. The time of arrival of the pulse detected at station 0 at the arch is measured in Figure 7.29 to be

1.92 ms. This value compared favourably with the time calculated by dividing the distance travelled by the dilatational wave by its velocity calculated from equation (7.16), which gives 1.89 ms.

Comparing the displacement traces recorded on the bridge deck for the non-defective masonry bridge idealisation in Figure 7.27 and that for a defective masonry bridge idealisation in Figure 7.31, some differences between the traces may be easily identified. These differences result from the reflection and refraction of the pulses around the void between the bridge deck and the arch. Some of these differences are marked by arrows in Figure 7.31. Similarly, some difference may also be identified between the two simulated displacement traces at points along the arch for the non-defective masonry bridge idealisation in Figure 7.29 and the defective masonry bridge idealisation shown in Figure 7.33. The arrow marked in Figure 7.33 is one of the typical difference between the two traces. The identification of such features in the velocity traces seems difficult because there are no significant changes in the velocity traces as there are in the displacement traces.

The simulated displacement and velocity traces at points along the bridge deck for the multiple-source Sonic Testing on the non-defective masonry bridge model (Figure 7.24) are given in Figures 7.35 and 7.36 respectively. Figures 7.37 and 7.38 show respectively the displacement and velocity traces recorded at the stations along the arch intrados when the pulses are applied at the grid points on the deck above it. The delayed time of arrival observed in Figure 7.37 and 7.38 are the result of the increased thickness of the fill. In fact, the time of arrival in these traces cannot be calculated directly by measuring the vertical distance between the applied pulse and the transducer at the arch because the wave propagating along that path may be reflected at the fill/arch interface due to the angle of incidence being greater than the critical angle. A wave arriving at a station may go through some alternative paths. One such typical path for a wave is shown in Figure 7.39.

Figures 7.40 and 7.41 show respectively the displacement and velocity traces recorded at the stations on the bridge deck when the defective masonry bridge model shown in Figure 7.26 is tested by the multiple-source Sonic Method. The displacement and velocity traces recorded at the stations along the arch at the same time are given in Figures 7.42 and 7.43. Again, some distinctive differences between the displacement traces for the perfect bridge idealisation (Figure 7.40) and the defective bridge model (Figure 7.42) are marked by arrows in Figure 7.42.

7.4.4.2 Interpretation of the Sonic Test Results Using the Method of Elimination

It is noted in section 7.4.4.1 that the interpretation of the velocity traces directly is difficult because the extra interfaces introduced between the void and the bridge deck or the arch have not significantly distorted the velocity trace. In geophysical surveys, the method of Normal Moveout Removal has been used to find the dip of a reflecting interface underground (Ref. 7.12). A similar procedure may be helpful in the Sonic Testing of Masonry Structures to provide information about the location of the defect using velocity traces recorded on site. A finite element simulation is useful to investigate the effectiveness of such a procedure and to interpret field test data.

As an example to illustrate the method of Normal Moveout Removal for the assessment of the dip angle of a reflector underground, a two dimensional example has been shown by Telford et. al. (Ref. 7.12). The following studies on the application of the method of Normal Moveout to find the dip angle of an underground reflector is based on the examples given by Telford et. al. (Ref. 7.12). The large medium shown in Figure 7.44 has a horizontal reflector below the horizontal ground surface. Also marked in the figure are the locations of the geophones where the reflected signals may be recorded. Figure 7.45 shows an inclined reflector below the horizontal ground surface. Again, the locations of the geophones are marked and at the same relative positions from the shotpoint. 'Moveout' has been used by geophysicsts (Refs. 7.12 and 7.13) to refer to a systematic difference from trace to trace in the arrival time of a signal. In a particular case where the reflector is horizontal, the difference in arrival time between a geophone at the shotpoint and a geophone away from the shotpoint is called 'normal moveout'. Figure 7.46 shows the traces which may be obtained in a geophysical survey on the examples shown in Figures 7.44 and 7.45. Also shown in Figure 7.46 are the moveout, Δt, and normal moveout, Δt_n, which may be measured from the traces. To find the dip angle, Telford et. al. (Ref. 7.12) demonstrated that the dip moveout can be found by subtracting the arrival time for the normal moveout (Figure 7.46a) from the arrival time for the incline reflector (Figure 7.46b). The resultant traces are given in Figure 7.46c. For small dip angles, θ,

$$\theta = v\Delta t_d/\Delta x$$

where Δt_d is the dip moveout (Figure 7.46c), Δx is the distance between the geophones and v is the wave velocity in the medium above the reflector.

In fact, the calculation of the dip angle is not important in this application to the interpretation of the Sonic Test results. The purpose of this application is to highlight any defects in the masonry bridge and if possible, its location in the bridge. Thus the elimination of the reference traces, which have been obtained from the finite element analysis of the non-defective masonry bridge idealisation, from a field test result should provide some information on the integrity of the bridge. In this study, the results from the finite element analysis on the defective masonry bridge model will be used instead of the field test results.

Figure 7.47 shows the resultant displacement traces when the reference traces as shown in Figure 7.27 are eliminated from the test traces as shown in Figure 7.31. In this case, the single-source scheme is considered. It may be observed in Figure 7.47 that deviation from the reference traces indicates the presence of defects in the bridge tested. Figure 7.48 shows the resultant velocity traces after the elimination of the reference traces as shown in Figure 7.48 from the test traces in Figure 7.32. In both Figures 7.47 and 7.48, the difference between the test traces and the reference traces are mainly concentrated near the source. This indicates that there is a defect near to the source. If the location of the defect is far away from the source, it may be undetected because the time range considered in the test simulation is too short for the deviations further away from the source to be seen. Similarly, the resultant displacement and velocity traces for signals recorded along the arch are given in Figures 7.49 and 7.50. These traces also show a defect near the source by the large deviations in the resultant traces between the source and station 3.

Using the multiple-source scheme, the resultant displacement and velocity traces from the stations on the bridge deck are shown in Figure 7.51 and 7.52 respectively. The displacement traces shown in Figure 7.51 indicate clearly that there is a defect in the bridge model between stations 1 and 3.

This defect is also revealed in the velocity trace (Figure 7.52) since the traces between stations 1 and 3 are most affected. The disturbances on the traces beyond station 5 are much smaller. The resultant displacement and velocity traces for the stations along the arch are given in Figures 7.53 and 7.54. These figures again show that the suspected defect lies between stations 1 and 3.

The depth of the defect from the bridge deck may also be found in this case from the calculated reflection time from Figure 7.52. The reflection time measured at station 2 in Figure 7.52 is 2.03 ms. Knowing the depth of the bridge deck, the defect is found to be located 0.38 m below the source while the actual depth of the defect in the finite element idealisation is measured to be 0.374 m below the deck.

The use of this method of elimination for the interpretation of the Sonic Method of Testing masonry bridge using Finite Element Technique has been shown to allow the assessment of the integrity of a masonry bridge and the location of the defect if one exists. In practical situations, the reference traces may be obtained from the finite element analysis of the bridge which is to be tested while the test traces may be obtained from the site. The resultant traces may reveal the integrity of the bridge and the location of the defect. The bridge idealisation may be analysed for working or ultimate loads using finite element method. In this way, the load bearing capacity of the bridge may be predicted before the engineer decides on any remedial work that may be required. The determination of the load bearing capacity using a non-linear Finite Element Analysis has been considered by others (Ref. 7.5 and 7.21).

7.5 Conclusions

A two dimensional Finite Element Study of Sonic Pulse propagation in a multi-layered column has been undertaken. An irregular finite element mesh which has rapid changes in the element aspect ratio has been shown not to affect the pulse propagation in the column.

It is found that the propagation of a sonic pulse in a multi-layered column may be treated as in a homogeneous column by transforming the individual material elastic properties to the equivalent elastic properties representing the whole column. The transformation equations are given in equations (7.10), (7.11), (7.14) and (7.15). The equations are most suitable for columns which have a large number of interfaces. It may be concluded that brickwork should be treated as an anisotropic material in finite element analysis.

It is obvious that the sonic echo method of integrity testing may be applied to brickwork structures in a way similar to its application to concrete structures, provided that the extent of the defect is significant. Mean elastic properties of bricks may be used in the interpretation of the sonic echo tests on brickwork structural members. From the interpretation of these test results, it may be possible to predict the relative stiffness of the brickwork column by observing the magnitude of the applied pulse or the reflected pulses.

The wave system developed in a large continuum due to a disturbance on the surface is studied. The types of signal that can be detected at a node or station in the finite element idealisation are shown. The Bridgemill Arch Bridge, a masonry bridge, is idealised using two-dimensional 8-node isoparametric finite elements. The finite elements representing the masonry arch and the fill are assumed to have isotropic elastic properties. The same idealisation is used to model the non-defective bridge and the defective bridge. Two possible Sonic schemes, the single-source scheme and the multiple-source scheme, for testing a bridge are suggested. The interpretation of the test results using direct interpretation and the Method of Elimination are shown. It is shown that the multiple-source scheme can provide more reliable information about the integrity of the bridge. It is also shown that the results from the multiple-source scheme are easier to interpret by the Method of Elimination.

The idealisation represents one half of the bridge. The defective bridge is simulated by introducing a void between the bridge deck and the arch. The examples considered have illustrated how the finite element technique may be used to interpret the results from the site tests on a masonry bridge using the Sonic Method.

References 7.

1. Komeyli-Birjandi, F., Forde, M.C., Whittington, H.W., "Sonic Investigation of Shear Failed Reinforced Brick Masonry", Masonry International, No. 3, 33-40, November, 1984.

2. Benedetti, D., Benzoni, G.M., "A Numerical Model for Seismic Analysis of Masonry Building: Experimental Correlation", Earthquake Engineering and Structural Dynamics, Vol. 12, 817-831, 1984.

3. Samarasinghe, W., Page, A.W., Hendry, A.W., "A Finite Element Model for the In-Plane Behaviour of Brickwork", Proceedings of the Institution of Civil Engineers, Part 2, Vol. 73, 171-178, March, 1982.

4. Sawko, F., Rouf, M.A., "A Proposed Numerical Model for Structural Masonry", Masonry International, No. 5, 22-27, July, 1985.

5. Towler, K.D.S., "The Non-Linear Finite Element Analysis of Bridgemill Masonry Arch Bridge", Masonry International, No. 5, 38-48, July, 1985.

6. Towler, K.D.S., "Applications of Non-Linear Finite Element Codes to Masonry Archs", Proceedings of the Second International Conference on Civil and Structural Engineering Computing, Vol. 2, 197-202, Civil-Comp Press, Edinburgh, 1985.

7. Khoo, C.L., "A Failure Criterion for Brickwork and Axial Compression", Ph.D. Thesis, University of Edinburgh, February, 1972.

8. Steinbach, J., Vey, E., "Caisson Evaluation by Stress Wave Propagation Method", Journal of the Geotechnical Engineering Division, Proceedings of the American Society of Civil Engineers, GT4, 361-378, April, 1975.

9. Sahlin, S., "Structural Masonry", Prentice-Hall, Inc., Englewood Cliffs, New Jersey, 1971.

10. Sibbald, A., Forde, M.C., "Dynamic Soil Structure Interaction of Masonry Sewers", Foundations and Tunnels - 87, Proceedings International Conference on Foundations and Tunnels, Engineering Technics Press, Vol. 2, 255-266, March, 1987.

11. Forde, M.C., Komeyli-Birjandi, F., Batchelor, A.J., "Fault Detection in Stone Masonry Bridges by Non-Destructive Testing", Structural Faults 85, The Second International Conference on Structural Faults and Repair, 373-379, Engineering Technics Press, Edinburgh, 1985.

12. Telford, W.M., Geldart, L.P., Sheriff, R.E., Keys, D.A., "Applied Geophysics", Cambridge University Press, 1976.

13. Beck, A.E., "Physical Principles of Exploration Methods", The MacMillan Press Ltd., 1981.

14. Heiland, C.A., "Geophysical Exploration", Prentice-Hall Inc., 1940.

15. Ewing, W.M., Jardetzky, W.S., Press, F., "Elastic Waves in Layered Media", McGraw-Hill Book Company, Inc., 1957.

16. Richart, F.E., Hall, J.R., Woods, R.D., "Vibrations of Soils and Foundations", Prentice-Hall, Inc., 1970.

17. Timoshenko, S.P., Goodier, J.N., "Theory of Elasticity", Third Edition, International Student Edition, McGraw-Hill Inc., 1970.

18. Cementation Piling and Foundation, "TNO Testing Methods", Technical Literature, October, 1983.

19. Hendry, A.W., Royles, R., "Acoustic Emission Observations on a Stone Masonry Bridge Loaded to Failure", Structural Faults 85, The Second International Conference on Structural Faults and Repair, 285-291, Engineering Technics Press, Edinburgh 1985.

20. Crisfield, M.A., "Finite Element and Mechanism Methods for the Analysis of Masonry and Brickwork Arches", TRRL Research report 19, Department of Transport, 1985.

21. Crisfield, M.A., "Computer Methods for the Analysis of Masonry Arches", Civil-Comp 85, Proceedings of The Second International Conference on Civil and Structural Engineering Computing, Civil-Comp Press, Vol. 2, 213-219, 1985.

Chapter 8

Studies on Vibration Methods of Non-Destructive Testing

8.1 Introduction

In chapters 6 and 7, the finite element analysis method has been applied to the study of the operation and interpretation of the sonic echo method of testing concrete structural member and masonry structures. The study of the application of the vibration tests will be undertaken in this chapter using the finite element method.

In a sonic echo test, a pulse is applied to a structural member or a structure by a hammer blow. The integrity of the structural member or the structure may be assessed by observing the characteristics and the magnitude of the transmitted or reflected pulses. The interpretation of the test results has concentrated on the time domain data. With vibration tests, whether a steady state vibration test or a shock test (Refs. 8.1, 8.2, 8.3, 8.4), a time varying force is applied. A continuous sinusoidal force is applied in the steady state vibration test while a pulse similar to the sonic echo test is applied in the shock test. The interpretation of the vibration test results are, however, considered using the frequency domain data. The time varying forces are applied to the pile head and the pile head responses are recorded using an accelerometer or a transducer. The pile head responses recorded in the time domain are then transformed to its frequency components by using a micro-computer or a signal processor. Some physical properties of the pile may be inferred from a plot of the mechanical admittance against the applied frequencies. The mechanical admittance is defined as the ratio of the velocity response divided by the applied force in the frequency domain which is the reciprocal of the mechanical impedance.

Since a time varying force is applied in the vibration tests, the finite element analysis, which has been applied to simulate the sonic echo tests, may be applied to the study of the vibration tests. Some modifications to the computer program are required to allow for the application of a continuous sinusoidal force. The recording of the pile head responses in the time domain is the same as those in the sonic echo tests.

In order to clarify the interpretation of the results from the vibration tests, the behaviour of ideal piles must be considered first. The application of the steady state vibration test and the shock test on an ideal pile are considered. The simulated results for the steady state vibration test and the shock test will then be compared. The method of signal processing to transform the time domain data into the frequency domain for the interpretation of the shock test will be presented. The interpretation of the shock method of testing a structural member will be demonstrated by examples on testing free standing columns. The ability of the vibration tests to highlight the integrity of a pile-soil system will also be discussed.

8.2 Signal Processing

The presentation of the steady state vibration test results in the frequency domain is straightforward. The frequency and the amplitude of the applied vibration force are known while the maximum velocity responses may be measured on the pile head using a transducer. Therefore, the plot of the mechanical admittance of the pile against the applied vibration frequency on the pile head may be obtained directly by using a x-y recorder (Ref. 8.3) to plot the corresponding calculated values. Mechanical admittance is defined as the ratio of the velocity spectrum divided by the force spectrum, $|V/F|$, (Refs. 8.3, 8.4). The mechanical admittance may be considered as the transfer function of the pile-soil system from which the velocity response, V, may be derived from a known input function F.

The pulse applied to the pile head in a shock test may be considered as consisting of a wide range of frequencies. The pile under test may respond to the frequencies and maximum responses may occur at the resonant frequencies. Both the applied pulse signal and the velocity response signal are measured in the time domain and must be transformed into the frequency domain for interpretation. This transformation is usually undertaken using the Fourier transform.

8.2.1 Fourier Transform

Fourier discovered that the frequency content of a periodic time signal may be expressed as a combination of weighted sine and cosine functions with harmonically related frequencies (Ref. 8.5). This infinite sum of functions is called the Fourier Series which mathematically, may be expressed as (Ref. 8.6):

$$x(t) = \frac{a_0}{2} \sum_{n=1}^{\infty} \left(a_n \cos\left(\frac{2\pi nt}{T}\right) + b_n \sin\left(\frac{2\pi nt}{T}\right)\right) \tag{8.1}$$

where T is the periodic time function x(t). The amplitude of the sine and cosine waves in the series, which are the values of the coefficients a_0, a_n and b_n, may be found using equations derived by Fourier. The equations are widely published in most physics texts on Vibrations and Waves. The coefficients in equation (8.1) are given by Gough et. al. (Ref. 8.7) as:

$$a_0 = \frac{2}{T} \int_{-T/2}^{T/2} x(t)dt \tag{8.2}$$

$$a_n = \frac{2}{T} \int_{-T/2}^{T/2} x(t)\cos\left(\frac{2\pi nt}{T}\right)dt \tag{8.3}$$

$$b_n = \frac{2}{T}\int_{-T/2}^{T/2} x(t)\sin\left(\frac{2\pi nt}{T}\right)dt \qquad (8.4)$$

Knowing these coefficients enables the magnitude and phase at each frequency in the function x(t) to be calculated.

The resultant evaluation of the Fourier series is known as the Fourier transform. The representation of a time function by the Fourier series, however, is restricted to signals which are periodic. This restriction may be circumvented by allowing the period to approach infinity. Equation (8.5) defines the Fourier transform of a time function to its frequency components, the Forward Fourier transform (Ref. 8.6):

$$S_x(f) = \int_{-\infty}^{\infty} x(t)e^{-i2\pi ft}dt \qquad (8.5)$$

The expression $e^{i2\pi ft} = \cos(2\pi ft) - \sin(2\pi ft)$ is called the kernel of the Fourier transform. $S_x(f)$ is known as the Fourier transform of x(t) and contains the amplitude and phase information for all the frequencies which make up x(t) even though x(t) is not periodic.

8.2.2 Discrete Fourier Transform

It is obvious that equation (8.5) will take a continuous function in the time domain and transform it into a continuous function in the frequency domain. In order to calculate the Fourier transform of a time function using a computer, the continuous time function must be converted to a set of discrete data. Usually, the data points are chosen at equal intervals, Δt. After the discretisation in the time domain, equation (8.5) becomes:

$$S_x'(f) = \Delta t \sum_{n=-\infty}^{+\infty} x(n\Delta t)e^{-i2\pi fn\Delta t} \tag{8.6}$$

The choice of the time interval, Δt, should be such that there are at least two samples per period of the highest frequency component present in the signal (Refs. 8.8, 8.9). If the time interval chosen is too big, some of the higher frequency components are shifted down in frequency, distorting the frequency representation. This effect is called the Aliasing effect.

Equation (8.6) indicates that an infinite number of samples should be considered. However, a finite number of samples accumulated over a finite time must be chosen for an approximated computation. The truncation in the time domain may result in "rippling" in the frequency domain. Due to the truncation, equation (8.6) is modified to:

$$S_x''(f) = \Delta t \sum_{n=0}^{N-1} x(n\Delta t)e^{-i2\pi fn\Delta t} \tag{8.7}$$

Finally, the Fourier transform pair given in equation (8.7) has to be modified to discrete Fourier transform pairs. That is, the Fourier transform is sampled at discrete frequencies:

$$S_x'''(m\Delta f) = \Delta t \sum_{n=0}^{N-1} x(n\Delta t)e^{-i2\pi(m\Delta f)(n\Delta t)} \tag{8.8}$$

for m = 0, ... , N−1

Due to the discretisation in the frequency domain, it is equivalent to an infinite repetition of the function in the time domain with a period T_r. From the relations given in equation (8.8), it may be observed that only N/2 complex quantities in the frequency domain may be obtained for N points in the time domain data. This is because two values, the real and the imaginary parts, are required to describe each time data.

8.3 Simulation of the Vibration Tests

The interpretation of the vibration tests is based on the resultant shape of the graph which showed the mechanical admittance $|V_0/F_0|$ against the applied frequencies. V_0 is the maximum velocity recorded by the transducer placed on the pile head and F_0 is the amplitude of the applied force. In the steady state vibration test, the mechanical admittance may be found directly by dividing the measured velocity by the amplitude of the applied force. Simulation of the steady state vibration test, thus, required the application of an sinusoidal varying force on the pile head and measuring the response on the pile head. Figure 8.1 shows a typical finite element idealisation of one quarter of a 8 m long and 400 mm x 400 mm free standing pile. The cyclic force is applied at the centre of the pile head while the velocity responses are measured at the quarter point on the pile head.

8.3.1 Steady State Vibration Test on a Fixed End Pile

Figure 8.2 showed a typical cyclic applied force which has a frequency of 100 Hz. Figures 8.3 and 8.4 showed two typical predicted velocity response curves of the pile head. The applied frequency is 10 Hz for the velocity response shown in Figure 8.3 while the applied frequency is 100 Hz for the velocity response shown in Figure 8.4. It may be observed that the velocity response in Figures 8.3 and 8.4 is the resultant of the combined frequencies of the applied frequency on the pile head and the first resonant frequency of the free standing fixed end pile. The first resonant frequency for the 8 m fixed end pile (Figure 8.5) may be found by using equation (8.9):

$$f = c/(4L) \tag{8.9}$$

where f is the first resonant frequency, c is the longitudinal propagation velocity in the pile and L is the length of the fixed end pile (8 m). Figure 8.5 shows the mode shape for the first resonant mode of the 8.0 m fixed end pile. The longitudinal propagation wave velocity may be found by using the relationship defined in section 2.3.2.1:

$$c = E/\rho \tag{8.10}$$

which is found to be 3490 ms^{-1} for a concrete having a Young's modulus equal to 29.23 x 10^9 Nm^{-2} and bulk density equal to 2400.00 kgm^{-3}. Hence the first resonant frequency is 109.06 Hz. Beats may be observed clearly when the applied frequency is near to the resonant frequency in Figure 8.4. Figure 8.6 shows a plot of the function y1:

$$y1 = \sin(2\pi fx+\tfrac{1}{2}\pi) + \sin(2\pi f_1x-\tfrac{1}{2}\pi) \tag{8.11}$$

where f is the first resonant frequency and f_1 is the applied frequency 10 Hz. And Figure 8.7 shows the function y2:

$$y2 = \sin(2\pi fx+\tfrac{1}{2}\pi) + \sin(2\pi f_2x-\tfrac{1}{2}\pi) \tag{8.12}$$

where f_2 is 100 Hz.

Comparison of Figure 8.3 with Figure 8.6 and Figure 8.4 with Figure 8.7 confirms that the response of the pile is a combination of the applied frequency and the resonant frequency of the pile.

Finite element analysis has been undertaken to test the 8 m idealised pile (Figure 8.1) over an applied frequency range of 10 Hz to 800 Hz and the measured maximum velocity responses in each case are found using a computer program. The idealised free standing pile is considered to have fixed support at its base. The applied frequencies, the corresponding maximum velocity responses and the corresponding mechanical admittances are given in Appendix E. The mechanical admittance of the idealised pile corresponding to each applied frequency is given in Figure 8.8. The peaks shown in Figure 8.8 correspond to the first three resonant frequencies of the idealised 8 m fixed end pile.

8.3.2 Steady State Vibration Test on a Free End Pile

The 8 m idealised pile shown in Figure 8.1 is now considered as 'floating' in the space with no fixed support. A simulation of a steady state vibration test on this idealised pile is undertaken over an applied frequency range of 10 Hz to 800 Hz. The applied frequencies at the pile head, the corresponding maximum velocity responses at the pile head and the corresponding calculated mechanical admittances are listed in Appendix E. A graph showing the mechanical admittance of the idealised pile plotted against the corresponding applied frequencies is given in Figure 8.9. Again, the peaks shown in Figure 8.9 correspond to the first three resonant frequencies found for the 8 m idealised free end pile.

8.3.3 Shock Tests on Fixed End and Free End Piles

The shock test described by Higgs (Ref. 8.4) is a rapid method of measuring the mechanical admittance of the pile by the simultaneous measurement of pile head velocity in relation to the applied force. In the shock test, a pulse is applied by tapping a load cell, which is placed on the pile head, by a light hammer. The response of the pile to the applied pulse is measured by a transducer placed on the pile head similar to the sonic echo tests. The applied pulse may be considered to consist of a wide range of frequency pulses. The pile responds to the frequencies and most significantly to those which have the same frequencies as its resonant frequencies. Both the applied pulse and the velocity response are thus measured in the time domain. Therefore, it is necessary to process the signals so that they are transformed to their frequency components. This may be undertaken by using the Fourier transform.

8.3.3.1 Choice of a Time Step for the Simulation

It was pointed out in section 8.2.2 that the time interval, Δt, used in sampling the time domain data should allow two sampling points for the highest frequency components being considered. In addition, the time interval should also be chosen so that the applied pulse may be described correctly. In the interpretation of the mechanical admittance against the applied frequency plot in a vibration pile testing, the gradient of the graph at low frequency is required to indicate the stiffness of the pile-soil system. Therefore, the rate of sampling the frequency data, Δf (equation (8.8)), must also be considered. Using Shannon's sampling theorem (Ref. 8.6):

$$F_{max} < \frac{1}{2\Delta t} \tag{8.13}$$

where F_{max} is the maximum frequency considered. From section 8.2.2:

$$F_{max} = \frac{N}{2} \Delta f \tag{8.14}$$

Combining the equations (8.13) and (8.14):

$$\frac{N}{2}\Delta f < \frac{1}{2\Delta t} \tag{8.15}$$

Therefore, the total number of data points in the time domain, N, must be:

$$N > \frac{1}{\Delta f \Delta t} \tag{8.16}$$

Consider an input pulse having a 1.0 ms contact time and allowing five sampling points for the pulse. Δt is then 0.2 ms. The target frequency resolution, Δf, is 2.5 Hz. Therefore, the total number of data points required in the time domain should not be less than 2000.

8.3.3.2 Tests on the Idealised Pile Model

Simulated shock tests on the idealised pile model (Figure 8.1) have been undertaken. The velocity response of the pile head when the base of the pile is fixed is illustrated in Figure 8.10. Figure 8.11 shows the input pulse in the time domain. The applied pulse is a half sine function and is the same as that used in the sonic echo tests. Frequency analysis on the velocity response and the input pulse are carried out using the Fourier transform. The resultant frequency domain data for the velocity signals and the input signal is given in Figures 8.12 and 8.13 respectively. It is obvious in Figure 8.12 that the idealised pile responds to its resonant frequencies which are observed as peaks in the graph. Dividing the velocity spectrum by the force spectrum in the frequency domain, we may obtain the mechanical admittance for the pile. The graph showing the mechanical admittance of the free standing pile against the applied frequencies is given in Figure 8.14. The results from this simulated shock test (Figure 8.14) agree well with that obtained from the simulated steady state vibration tests (Figure 8.8).

The 8 m idealised pile (Figure 8.1) is also tested by the shock method when it is 'floating' in space without any fixed support. The same 1.0 ms contact time half sine function input pulse was applied. The time domain velocity response at the pile head is given in Figure 8.15. The velocity response and the mechanical admittance in the frequency domain are shown in Figures 8.16 and 8.17 respectively.

It may be concluded here that the finite element simulations have verified that the shock test is a rapid method for measurement of the mechanical admittance of a pile. The method may be used as an alternative to the steady state vibration test as the shock test is much simpler in its operation on site while similar information about the integrity of the pile may be obtained. The shock test will be studied further to reveal the ability of the vibration method to indicate the integrity of a pile soil system.

8.3.3.3 Interpretation of the Shock Tests on the Idealised Free Standing Piles

The frequencies at which resonance occur in Figures 8.8, 8.9, 8.14, and 8.17 are approximately equally spaced at intervals of frequency:

$$df = c/(2L) \tag{8.17}$$

where c is the velocity of pulse propagation along the pile and L is the length of the pile. When the pile has a fixed end, that is, an infinitely rigid base, the lowest frequency of resonance has a value of c/4L (Figures 8.8 and 8.14). When the pile has a free end, that is an infinitely compressible base, the lowest resonance occurs at a very low frequency (Figures 8.9 and 8.17). These results agree with those published by Davis et. al. (Ref. 8.3).

It was also mentioned (Ref. 8.3) that when the pile is supported on an elastic base with normal compressibility, the lowest frequency of resonance lies in an intermediate position between that of the fixed end and the free end pile. To simulate this compressible base for the idealised pile shown in Figure 8.1, the nodal stiffness at the base of the idealised pile is increased to represent a spring at its base. In this study, the stiffness of the spring has been considered to be 1% that of the original nodal stiffness. A simulated shock test on this idealised pile has been undertaken and the resultant mechanical admittance of the pile is plotted against the applied frequencies as shown in Figure 8.18. The result again agree with the proposed theory (Ref. 8.3).

8.3.4 Modifications to the Finite Element Analysis

Although the simulation of the frequency response of a free standing column using the finite element analysis has been shown to be promising in section 8.3.3.3, a closer look at the resonant frequencies may reveal that the higher modes of resonant frequencies are lower than those expected from the closed form solution. A comparison of the resonant frequencies calculated using the closed form solution (equations (8.9) and (8.16)) for a fixed end column and those obtained from the finite element analysis (Figure 8.12) is given in Table 8.1:

Closed Form Solution	Finite Element Analysis
109.07	110.00
327.19	322.50
545.31	525.00
763.44	712.50
981.56	880.00
1199.69	1027.50

Table 8.1 Time Step = 0.2 ms

Frequency resolution = 2.5 Hz

Finite element analyses are undertaken to simulate the response of the 8.0 m column using a coarse finite element mesh (10 elements) and a fine finite element mesh (80 elements). It is found that there is no improvement in the resonant frequencies. In these interpretations, the time step for the time integration is 0.2 ms. Another numerical test is carried out using a smaller time step of 0.05 ms for the time integration in the finite element analysis. It is found that there is a substantial improvement in the computed resonant frequencies. The 0.4m x 0.4m x 8.0m fixed end pile which is idealised by 20 8-node finite elements is analysed using a time step of 0.05 ms for the time integration in the finite element analysis. The resultant frequency response is shown in Figure 8.19 and a comparison of the values of the first six resonant frequencies is given in Table 8.2:

Closed Form Solution	Finite Element Analysis
109.07	110.00
327.19	325.00
545.31	545.00
763.44	760.00
981.56	975.00
1199.69	1190.00

Table 8.2 Time Step = 0.05 ms

Frequency resolution = 5.0 Hz

The error in the prediction of the resonant frequencies using the finite element analysis shown in Table 8.1 is mainly caused by the inaccurate prediction of the pile response in the time domain by using a large time step for the time integration. The error is unlikely to be caused by the application of the discrete Fourier transform because the resonant frequencies found from the steady state and the transient state vibration tests are similar. Therefore the time step used for the time integration in the finite element analysis must be kept sufficiently small to ensure the accuracy of the finite element simulation. Since the time step used for the analysis has been reduced, the total number of time intervals must be increased to preserve a reasonable frequency resolution. For the analysis shown in Figure 8.19, 4000 time points are needed. It is obvious by studying Table 8.2 that the deviation between the closed form solution and the finite element analysis has increase at higher modes of resonant frequencies. Therefore, the frequency range considered in the following studies will be below 1000 Hz.

8.4 Case Studies on an Idealised Free Standing Column

Before studies on the application of the shock test to a pile-soil system are carried out, it is worthwhile to simulate the shock tests on a free standing column to understand the test results due to an anomaly along the free standing column. The 0.4m x 0.4m x 8.0m idealised finite element model shown in Figure 8.1 is again used for this study. The idealised column is considered to have a fixed support at its base. The material properties for the finite elements are given in Table 8.3:

Young's Modulus	=	29.23×10^{9} Nm^{2}
Poisson's Ratio	=	0.24
Bulk Density	=	2400.00 Kgm^{-3}
Bar Velocity	=	3490.00 ms^{-1}

Table 8.3

Accounting for the symmetry of the idealised column, each finite element is considered to have a thickness of 0.2 m. Four cases have been studied. They are the simulation of the shock tests on a non-defective column, a column with a neck, a column with an overbreak and a column with a section of weak concrete. The weak concrete section is assumed to have a low Young's modulus. For a column with a neck, finite elements between the depth of 4.8 m and 5.6 m from the pile head are considered to have a thickness of 0.1 m to simulate the neck. This reduces the cross sectional area of the column to half of its original cross sectional area. The same elements are assigned a thickness of 0.4 m to simulated an overbreak at that level. Thus, the overbreak has a cross sectional area twice the original cross sectional area. The weak concrete section is considered to have a smaller Young's modulus

(8.00×10^9 Nm^{-2}) and a smaller bulk density (2000.00 kgm^{-3}). The resultant bar velocity for this section is 2000.00 ms^{-1}.

The mechanical admittance of the 8.0 m perfect column plotted against the applied frequencies obtained from a simulated shock test on the idealised perfect column is given in Figure 8.20. This mechanical admittance trace is obtained by dividing the velocity spectrum shown in Figure 8.19 by an appropriate force spectrum. Therefore, it may be inferred from Table 8.2 that the resonant frequencies are separated at approximately equal intervals of 215.00 Hz. The first five computed resonant frequencies are 110.00 Hz, 325.00 Hz, 545.00 Hz, 760.00 Hz and 965.00 Hz.

8.4.1 Test on a Column with a Neck

Figure 8.21 shows the graph of the mechanical admittance of the necking pile plotted against the applied frequencies. It may be observed from this graph that the resonant frequencies are found to appear at unequal intervals. The computed first resonant frequency, which is 105.00 Hz, is slightly lower than that for the perfect column, which is found to be 110.00 Hz. The second resonant frequency is higher than that found for the perfect column by 20.00 Hz while the third resonant frequency is found to be lower than that for the the perfect column by 30.00 Hz. Apparently, these changes in the frequency response are due to the introduction of the neck along the column.

8.4.2 Test on a Column with an Overbreak

The mechanical admittance of the overbreak column plotted against the applied frequencies is given in Figure 8.22. While the computed first and fourth resonant frequencies for the overbreak column are the same as that found for the perfect column, the second and third resonant frequencies are found to be different from those for the perfect column. The second resonant frequency is found to be 25.00 Hz lower and the third resonant frequency is 15.00 Hz higher than the corresponding resonant frequencies for the perfect column. Therefore the neck and the overbreak in the column shift the resonance frequencies about those for the perfect column in opposite directions.

8.4.3 Test on a Column with a Section of Weak Concrete

Figure 8.23 illustrates the mechanical admittance of the defective column (having a section of weak concrete) against the applied frequencies. The first resonant frequency is found to be much lower than that for the perfect column. In fact, the frequency intervals between the first four resonant modes are similar to those for the necking column. The shifting of the frequency peaks from those of the perfect column is similar to that of a necking column.

8.4.4 Interpretation of Test Results on the Idealised Free Standing Columns

The first five resonant frequencies shown respectively in Figures 8.20, 8.21, 8.22, and 8.23 for the perfect column, the necking column, the overbreak column and the column with a section of weak concrete (weak column in Table 8.4) are given in Table 8.4.

Frequency Mode	1	2	3	4	5
Perfect Column	110.00	325.00	545.00	760.00	975.00
Necking Column	105.00	345.00	515.00	750.00	1015.00
Overbreak Column	110.00	300.00	560.00	760.00	940.00
Weak Column	95.00	330.00	470.00	715.00	945.00

Table 8.4

Figure 8.24 shows a simulation of a steady state vibration test on a defective pile which is embedded in soil by Davis et. al. (Ref. 8.3) using an electrical analogue. Davis et. al. (Ref. 8.3) interpreted the result by considering the primary maxima as the response due to the defective pile section while the secondary maxima are used to estimate the total length of the pile.

In the frequency response traces shown in Figures 8.20 to 8.23, the traces do not seem to consist of primary and secondary maxima as shown by Davis et. al. (Ref. 8.3). The reason may be due to the fact that there is no damping by the surrounding soil, resulting in very sharp peaks at resonant frequencies. The defective pile model studied by Davis et. al. (Ref. 8.3) consists of two sections, the defective concrete section and the sound concrete section. These two section may be considered as two vibrating systems which contribute to the primary and secondary maxima shown in Figure 8.24. Whereas the finite element idealised defective columns shown in Table 8.4 may be considered to consist of three sections. The frequency response curve for the finite element simulated tests thus consists of three sets of vibration. Concentrating on the first four resonant frequencies obtained for the perfect column, the necking column and the overbreak column, it can be seen that there is a match between the first and the fourth resonant frequencies. Taking the average of the frequency intervals between the first and fourth resonant frequencies, it is found that the average resonant frequency interval is 215.00 Hz for the necking column. This is the expected frequency interval for the whole length of the column. For the overbreak column, the average resonant frequency interval between the first and fourth resonant frequencies is found to be 216.67 Hz.

For the column with a section of weak concrete, there does not appear to be any match between its resonant frequencies and those obtained for the perfect column. To interpret the results for the column with a section of weak concrete, if its resonant frequencies were to be shifted 15.00 Hz to the right hand side, a reasonably good match between the first and the fifth resonant frequencies is found for this column and the perfect column. Applying the same interpretation as those for the necking column and the overbreak column, it is found that the mean frequency interval between the first and the fifth resonant frequencies is 200.00 Hz.

Another two sets of tests on the defective columns have been simulated to study the frequency response (mechanical admittance plotted against applied frequencies) of the defective columns due to changes in the physical dimensions or the material properties of the defective section. The cases studied in sections 8.4.1, 8.4.2 and 8.4.3 will be treated as type Case 1 for each defect type for comparison with the result of the following case studies. The cross sectional area of the neck of the necking column has been reduced to 37.5% (Case 2) and to 25.0% (Case 3) of the cross sectional area of the column shaft. The size of the overbreak has been increased to 3 times (Case 2) and to 4 times (Case 3) that of the cross sectional area of the column shaft. The longitudinal wave propagation velocity in the defective concrete section is reduced to 1500.0 ms^{-1} (Case 2) and 1000.0 ms^{-1} (Case 3) by reducing the Young's modulus to 4.5×10^9 Nm^{-2} and 2.0×10^9 Nm^{-2} respectively. The frequency response for these studies are interpreted in the same way as mentioned above by considering the average interval between resonant frequencies. The first five resonant frequencies for each case are given in Table 8.5:

Necking Column

	1	2	3	4	5
Case 1 (50.0%)	105.00 Hz	345.00 Hz	515.00 Hz	750.00 Hz	1005.00 Hz
Case 2 (37.5%)	100.00 Hz	350.00 Hz	500.00 Hz	745.00 Hz	1030.00 Hz
Case 3 (25.0%)	95.00 Hz	355.00 Hz	470.00 Hz	740.00 Hz	1045.00 Hz

Overbreak Column

	1	2	3	4	5
Case 1 (200.0%)	110.00 Hz	300.00 Hz	560.00 Hz	760.00 Hz	940.00 Hz
Case 2 (300.0%)	110.00 Hz	280.00 Hz	560.00 Hz	755.00 Hz	925.00 Hz
Case 3 (400.0%)	105.00 Hz	265.00 Hz	560.00 Hz	750.00 Hz	915.00 Hz

Weak Column

	1	2	3	4	5
Case 1 (2000.0 m/s)	95.00 Hz	330.00 Hz	470.00 Hz	715.00 Hz	945.00 Hz
Case 2 (1500.0 m/s)	85.00 Hz	330.00 Hz	430.00 Hz	695.00 Hz	885.00 Hz
Case 3 (1000.0 m/s)	65.00 Hz	325.00 Hz	390.00 Hz	630.00 Hz	765.00 Hz

Table 8.5

From the results shown in Table 8.5, the average resonant frequency intervals between the first four resonant frequencies for the necking column and the overbreak column are found to be 215.00 Hz. This may be considered as the response for the whole length of the column, which is the same as the resonant frequency intervals for the perfect column.

It may be concluded here that a neck or an overbreak in a free standing column will result in a different frequency response from that of a perfect column. The way a corresponding resonant frequency has shifted away from that for a perfect column resonant frequency due to the necking column is opposite to the shift due to the overbreak column. It should be noted that at some resonant frequencies, the corresponding resonant frequencies for the three columns, the perfect column, the necking column and the overbreak column, are similar. By averaging the resonant frequency intervals between the overlapped resonant frequencies, the overall length of the column may be found by using equation (8.17) where df is the average separation between the resonant frequencies. The interpretation, however, does not apply to the column with a section of weak concrete. There is only one resonant frequency in the resultant frequency response, namely the second resonant frequency, which is close to the corresponding resonant frequency for the perfect column. Thus, the other limit required to consider the average resonant frequency interval is not clear.

It is also shown in Table 8.5 that the first resonant frequency decreases when the cross sectional area in the neck of the column is reduced. The first resonant frequency is also decreased when the cross sectional area of the overbreak is increased and when the longitudinal wave propagation velocity in the weak concrete section is decreased. The decrease in the first resonant frequency is insignificant when the area of the overbreak is increased. On the contrary, the first resonant frequency decreases significantly when the Young's modulus in the weak concrete section is reduced.

Davis et. al. (Ref. 8.3) proposed that at low exciting frequency, a straight line response may be obtained at the start of the mechanical admittance curve. The inverse of the slope of this straight line measures the apparent stiffness of the head of the pile. It was shown that a pile, which has a compressible base, has a greater gradient than a pile which has a rigid base.

From the free standing column case studies, a similar effect has been observed. The mechanical admittance curve for the free standing columns at low frequencies (0 - 50 Hz) are shown in Figure 8.25a. It is difficult to compare the initial slope of these lines because they start from different levels. Therefore, the lines have been shifted to a common origin (Figure 8.25b) so that their initial slopes may be compared easily. In Figures 8.25a and 8.25b, the lines have been annotated P8F, N8F, O8F, and W8F. Annotation P8F corresponds to the results obtained from the simulated test on the perfect column and N8F represents the results obtained from the simulated test on the necking column. Similarly, O8F and W8F annotated the results obtained from simulated tests on the overbreak column and the column with a section of weak concrete respectively.

In the case studies on the free standing columns, the columns are considered to have fixed supports. Therefore, the initial gradients shown in Figure 8.25b are not indication of the fixity of the pile base. In fact, they may be considered as indications of the flexibility of the column. Obviously, in Figure 8.25b, the necking column and the column with a section of weak concrete are more flexible than the perfect column while the overbreak column is found to be the stiffest.

8.5 Shock Test on a Pile-Soil System

In section 8.4.4, it has been shown that the shock test on a free standing column can give indications of the approximate length of the column as well as the relative stiffness of the column. Davis et. al. (Ref. 8.3) simulated the steady state vibration of a pile-soil system using an electric analogue. The pile considered has a section of 1.0 m deep of weak concrete near the pile head. The pile-soil system together with the simulated results are given in

Figure 8.24. The response of the pile-soil system when tested by the shock method will be studied using the finite element approach. The material properties of the pile-soil system given in Figure 8.24 are summarised in Table 8.6.

	Sound Concrete	Weak Concrete	Soil	Base
E (Nm^{-2})	3.84×10^{10}	1.48×10^{10}	2.13×10^{8}	4.80×10^{10}
ρ (kgm^{-3})	2400.00	2200.00	1824.00	1824.00
c_p (ms^{-1})	4000.00	2600.00	341.94	5129.10
c_s (ms^{-1})	2339.59	1286.77	200.00	3000.00
G (Nm^{-2})	1.31×10^{10}	3.64×10^{9}	7.30×10^{7}	1.64×10^{10}

Table 8.6

where c_p is the propagation velocity of the compression wave and c_s is the propagation velocity of the shear wave.

Since the Poisson's ratios for the pile-soil system are not given and it has been shown in section 6.8.3.3 for the sonic echo tests that the Poisson's ratio of the materials has insignificant effect on the dynamic response of the pile-soil system, the Poisson's ratio for the concrete and the soil are assumed to be 0.24 for the finite element analysis in this chapter.

8.5.1 Effects due to the Surrounding Soil

In order to interpret the finite element simulation of the shock test on the pile-soil system shown in Figure 8.24, some controlled simulation tests are carried out to study the effects that the base and the surrounding soil have on the frequency response of the pile. Figure 8.26 shows a finite element idealisation of one quarter of a 1.0m x 1.0m x 10.0m non-defective free standing pile supported on an elastic base. The mechanical admittance of the pile plotted against the applied frequencies is given in Figure 8.27. This graph shows that the free standing pile has a free end and the length of the pile can be found by measuring the intervals between the resonant frequencies. The average interval between the first five resonant frequencies is found to be 188.75 Hz, which corresponds to a length of 10.60 m. The overestimation of the pile length is due to the small difference in the impedance between the pile concrete and the base. Thus, the free standing pile and the elastic base responds as a single system.

Figure 8.28 shows the finite element idealisation of a pile-soil system. The idealisation represents a strip of the pile-soil system where the pile has a width of 0.5 m, the base has a depth of 0.5 m and the surrounding soil has a width of 1.0 m. The far side of the soil and base elements are considered to have energy absorbing boundaries to simulate the geometrical damping effects while the interface between the pile and the soil may be maintained. Due to a limitation on the maximum CPU time allowed by the computer, the restrictions on finite element sizes, and the size of the time step required for the time integration, the finite element idealisation shown in Figure 8.28 has been selected as a compromise between these factors.

The pile, which has no defect, is first considered to be embedded in a soil which has a smaller Young's modulus than that used by Davis et. al. (Ref. 8.3). The base also has a smaller Young's modulus than those shown in Figure 8.25. The Young's moduli used in this study are 7.30×10^{7} Nm^{-2} and 1.64×10^{10} Nm^{-2} for the surrounding soil and the base respectively. The frequency response curve for this study is illustrated in Figure 8.29. At low frequencies, the pile-soil system responds as one system and gives rise to small resonant frequency intervals between the second and the fourth resonant frequencies. After the fourth resonant frequency, it can be seen that the resonant frequency intervals between the resonant frequencies are between 170.00 Hz and 190.00 Hz. These higher frequencies should correspond to the response of the pile. The expected separation between the resonant frequencies is 200.00 Hz for a 10.0 m concrete pile where the longitudinal wave velocity of the pile concrete is 4000.0 ms^{-1}. The computed frequencies using the finite element may be a result of the inertia effect of the surrounding soil. As mentioned in section 6.8.3.4, the inertia of the surrounding soil affects the reflection time of the sonic pulse which corresponds to a lower frequency response. In addition, the small difference between the impedances of the pile concrete and the base has also been shown to affect the frequency response.

8.5.2 Test on a Faulty Pile

The top 1.0 m of the pile shown in Figure 8.28 is assumed to be defective concrete in this study. The elastic properties for this defective pile concrete is given in Table 8.6 as the elastic properties for the week concrete. The frequency response curve for a simulated test on this pile-soil system is given in Figure 8.30. Comparison of the frequency response curves shown in Figures 8.29 and 8.30 illustrates that the defective concrete section in the pile affects the general shape of the frequency response curve. Since the first five resonant frequencies between the two traces are similar, it may be concluded that the defective concrete section at the top of the pile mainly affects the higher frequency response.

Obviously, the frequency response from the finite element simulation (Figure 8.30) is quite different from those shown in Figure 8.24. The reason for this discrepancy may be due to the different assumptions made in the two approaches. In the electric analogue, it is assumed that only the lumped electrical components representing the defective pile vibrate while the surrounding soil is considered to provide damping to the vibration. On the contrary, in the finite element analysis, the defective pile as well as the soil surrounding it are set into vibration due to the applied pulse. Therefore, the effect of the soil on the pile vibration is more significant. Another discrepancy between the two models is that in the finite element analysis, the three dimensional system has been approximately by the two dimensional finite elements, whereas the electric analogue is a one dimensional simulation.

To demonstrate the effects of the surrounding soil on the frequency response of the pile-soil system, the elastic properties of the surrounding soil have been changed. Figure 8.31 shows the frequency response for the pile-soil system given in Figure 8.28 where the Young's modulus of the soil is reduced to 7.30×10^7 Nm^{-2}. Figure 8.31 shows that the less stiff soil surrounding the pile affects the resonant frequencies at below 1000.0 Hz. It is also demonstrated in Figures 8.30 and 8.31 that the stiffness of the soil has a damping effect on the amplitude of the resonant frequencies.

Figure 8.32 illustrates the frequency response for the pile-soil system where the material properties of the system are the same as in the previous study except that the Poisson's ratio for the soil has been increased from 0.24 to 0.4 to simulate a saturated clay soil. The computed frequency response for this pile-soil system is given in Figure 8.31 as the frequency response curve. This result shows that the Poisson's ratio of the soil has no significant effect on the frequency response of a pile-soil system.

8.6 Conclusions

The Finite Element Method has been applied to simulate the steady state vibration test and the shock method for testing the integrity of a structural member. The Discrete Fourier Transform has been used to transform the time domain data into frequency domain data for the interpretation of the shock test results. A suitable time step has been chosen for the case studies to avoid aliasing effects in the frequency range of interest. The time step used for the finite element analysis and the limit on the maximum CPU time allowed by the computer has prevented the consideration of a bigger domain. These factors also limit the total number of time integration in the finite element analysis which in turn limits the frequency resolution in the frequency domain.

It has been demonstrated that the shock method is a quick method to obtain the mechanical admittance of a pile provided that a suitable signal processor is available. The interpretation of the shock test results has been shown using case studies involving idealised free standing columns. A sensible interpretation of the results obtained from the application of the shock test to necking and overbreak columns is possible. The results obtained from tests on defective columns which have a section of weak concrete along its length has been found to be difficult to interpret.

The simulated shock test on the pile soil given in Figure 8.24 iss found to be different from those given in reference 8.3. The differences may be due to the different assumptions used for the finite element analysis and the electric analogue model. The soil has only a damping effect on the vibration of the pile in the electric analogue. In an finite element analysis, both the pile and the soil respond to the pulse and may vibrate as one system. It is shown that the Poisson's ratio has no significant effect on the frequency response of a pile-soil system.

References 8.

1. Paquet, J., "Étude Vibratoire des Pieux en Béton Réponse Harmonique et Impulsionelle Application au Controle", Annls. Inst. Tech. Batim., 21st year, No. 245, 789-803, May, 1968.

2. Briard, M., "Controle des Pieux par la Méthode des Vibrations", Annls. Inst. tech. Batim., 23rd year, No. 270, 105-107, June, 1970,.

3. Davis, A.G., Dunn, C.S., "From Theory to Field Experience with the Non-Destructive Vibration Testing of Piles", Proceedings of the Institution of Civil Engineers, Part 2, December, 571-593, 1974.

4. Higgs, J.S., "Integrity Testing of Concrete Piles by Shock Method", Concrete, The Journal of the Concrete Society, Vol. 13, 31-33, October, 1979.

5. Broch, J.T., "Mechanical Vibration and Shock Measurements", Brüel & Kjaer, October, 1980.

6. HP 85 User Manual, "Theory of Fourier Transform"

7. Gough, W., Richards, J.P.G., Williams, R.P., "Vibrations and Waves", Ellis Horwood Ltd., 1983.

8. Ono, K., "Foundamentals of Acoustic Emission", University of California, 18-19, 1979.

9. Brigham, E.O., "The Fast Fourier Transform", Prentice-Hall, Inc., 1974.

Chapter 9

General Conclusions and Future Developments

9.1 General Conclusions

A comprehensive tool, the Finite Element Technique, has been applied to the investigation of Non-Destructive Testing Methods for civil engineering structures and structural members. Using the finite element approach, some of the shortcomings of the Earth Resistance Method of Testing have been revealed. The studies are undertaken using two dimensional and three dimensional finite element analyses. Some suggestions to overcome the limitation of the testing method have been proposed. The application of the three dimensional finite element analysis to interpret field test results has also been shown to be appropriate.

The application of the Sonic Echo Method to the testing of structural members has been investigated using the finite element technique. The ability of the testing method to locate defects in a free beam and in a pile-soil system has been studied. The effects on the displacement and velocity traces of a sonic echo test due to the surrounding soil has been investigated. Additional signal processing techniques are also simulated to investigate the appropriateness of applying such signal processing techniques to the interpretation of the sonic echo test results.

The response of a multi-layered free standing column to an applied pulse has been investigated. Provided that the layers are thin, the response of the multi-layered column is approximately the same as that of a homogeneous column. It is also found that the propagation velocity of a sonic pulse in the multi-layered column may be computed from the material properties of its composite materials. This indicates that the dynamic behaviour of a brickwork or a masonry structure may be analysed using the finite element technique by considering the brickwork or masonry as a homogeneous body. A procedure for the assessment of the integrity of a masonry bridge has been developed based on the sonic echo method of testing using finite element models. The method of interpretation of the simulated test results has also been discussed.

The Steady State Vibration Test and the Shock Method of Testing have been investigated using the finite element technique. Since the shock test can be used to find the Mechanical Admittance of a pile more quickly than the steady state vibration test, the shock method has been used for the case studies on vibration tests. The application of the finite element method to simulate the shock test is more suitable than its application to simulate the steady state vibration tests where the analysis required the solution of multiple loading cases. This is because the finite element system has to be analysed for each applied frequency in the steady state vibration test, while the finite element system is analysed only once in the shock test. The simulation of the shock test is similar to the simulation of the sonic echo test using the finite element method except that the time steps used for the time integration in the finite element analysis must be so chosen to ensure that the frequency resolution of the mechanical admittance in the frequency domain is high enough. The transformation of time domain data into frequency domain data has been undertaken using the Discrete Fourier Transform. Case studies on the application of the shock tests to a free standing column and a pile-soil system have been undertaken. The interpretation of the test results in the frequency domain has been discussed.

The finite element method has been shown to be a suitable tool for the investigation of non-destructive testing methods. The tool may be used in the development of a testing method as well as for the interpretation of test results.

The application of the finite element technique to simulate the static field problem such as the earth resistance method of testing is straightforward and prevailing computer resources have allowed both two dimensional and three dimensional simulation of the testing method. The simulation of the sonic echo method and the vibration methods of testing in the time domain required a large amount of computing time for the time integration in the finite element analysis. This has restricted the size of the domain considered. To simulate the geometric damping effects in such pile-soil system, an energy absorbing boundary is introduced to simulate the infinite soil mass. For the two dimensional simulation of the sonic echo method and the vibration methods of testing, plane stress elements are used to simulate free standard structural members. For the analysis of a pile-soil system or a masonry bridge, plane strain elements are used. Plane strain and plane stress elements are used in these studies because a change in the loading position of the pile soil system may be incorporated efficiently.

The earth resistance method of testing may be used to assess the integrity of a pile-soil system. Only the integrity of the pile-soil system in the region between the reinforcing cage in the pile and the return current electrode may be assessed. The correct interpretation of the test results on the pile-soil system depends on the availability of information on the properties of the pile concrete and the surrounding soil. Without this information, the test results may be misleading. The testing method is suitable for testing foundation piles which are embedded in homogeneous soil and piles that are reinforced for their whole length. Another favourate condition for carrying out the earth resistance test is when the resistivity of the surrounding soil is much lower than the resistivity of the pile concrete. For a necking pile embedded in a soil with lower resistivity than the pile concrete, the testing method may be able to locate the defect if the necking void is filled with a material which has a lower resistivity than the pile concrete. Defects at a greater depth inside the pile may not be detected despite the fact that the reinforcing cage may be extended beyond the defective section.

The ability of the sonic echo method of testing to locate a defect in a foundation pile is not restricted by the length of the reinforced section of the pile. The effects due to the surrounding soil will not distort the resultant displacement or velocity traces to such an extent as to cause mis-interpretation of the test results. The testing method may give indications on the approximate position and the nature of a defect in a foundation pile. The sonic echo method may not be able to locate defects which have an extent much smaller than the wavelength of the sonic pulse, such as a crack in a pile. Test results from piles which have more than one defect that are close together may be difficult to interpret due to the superposition of the reflected and refracted pulses at different reflecting interfaces between the defects. The location of the first reflecting interface in the pile is likely to be identified by using the sonic echo test. Perhaps the ease of locating the first reflecting interface is also dependent on the impedance of the two sides of the interface, which dictates the amount of pulse energy reflected, and therefore, the extent of the defect in the pile. The depth of a pile to which a sonic pulse may access limits the ability of the testing method to locate defects in a pile. This limitation is dependent on the damping properties in the pile-soil system, which include the material damping and the geometrical damping. The testing method based on the propagation of a sonic pulse seems promising in locating defects in foundation piles as well as in a masonry bridge.

The investigation of the vibration methods of testing using the finite element technique can be extended considerably. Having verified that the shock test is an alternative to the steady state vibration test in finding the mechanical admittance of a pile, most of the case studies have been undertaken by simulating the application of the shock test to assess the integrity of a free standing column or a pile-soil system. Although it may be possible to excite a pile-soil system to high frequencies to reveal the integrity of the pile-soil system using analogue model studies, it is not practical in the field test to excite the pile to such high frequencies as the frequency range of the applied pulse is limited. In addition, the sampling rate of the velocity responses in the time domain also restricts the frequency range considered. From the case studies, the vibration tests do not allow easier identification of the the location of a defect in a pile. Although the mechanical admittance of the pile at low frequencies may give an indication of the stiffness of the pile-soil system, the location of the defect is difficult to assess. Since the operation of the sonic echo test and the vibration test are similar, the test results obtained from a field test should be analysed in both time and frequency domain to find the location of the defect. If a defect is detected using the time domain analysis, the frequency domain analysis, which gives indication of the ability of the pile to carry load (Ref. 9.1), may be used to predict the stiffness of the pile under working load. The physical dimension of the pile may possibly be inferred from the frequency domain interpretation of the test data. These interpretations of the frequency domain data should be further investigated in future development of this research.

The reliability of these non-destructive testing methods for the assessment of the integrity of a structure or a structural member depends on the assumptions made on their material properties. The possibility of these errors must be considered during the interpretation.

The non-destructive testing methods have been investigated under idealised conditions using the finite element analysis. These analyses do not guarantee that a similar situation may be possible on the site since appropriate equipment of suitable sensitivity must be available. The results from such an analysis may help in the selection of equipment used in acquiring on-site data by estimating the probable range of data values. The reliability of the non-destructive testing methods in locating defects in a civil engineering structure or a structural member depends on knowing the material properties of the structure or the structural member being tested. These methods of non-destructive testing may be used to assess the integrity of a structure or a structural member while the load bearing capacity of the structure or the structural member may not be assessed.

The finite element technique can also be used to interpret field test results by comparing the field test results with the simulated test results. This may enable the engineer to predict the behaviour of the structural member or the structure under working load condition. The engineer may use the finite element idealisation which gives the same response as the field test result for re-analysis to predict the behaviour of the structure or the structural member under working load. The finite element simulations of the two dimensional analysis of the earth resistance method may also be used to provide guidelines for the interpretation of field test results.

9.2 Future Developments

A wide range of techniques have been considered in this thesis but studies on the vibration methods of testing could be considered in further detail. It may be possible to use the finite element analysis to investigate the relationship between the load deflection behaviour of a pile under load test and the mechanical admittance of the pile-soil system at low frequencies. The relationship between the mechanical admittance and the physical dimension of a pile may also be investigated.

A system may be developed to interpret the non-destructive test results by using the finite element approach. An expert system may be developed to interpret the non-destructive test results and use is made of the finite element simulation to confirm the interpretation by providing the system with site data and non-destructive test data, the system may analyse the test data by observing abnormal responses in the test data by comparison with simulated test results under ideal site conditions. Then the system may search through a list of possible causes of such abnormal responses and confirm its interpretation by using finite element simulations. The list of possible causes of the abnormal test results may be drawn from a series of finite element analyses and field test experiences.

It is found that the sonic pulse propagates at a lower velocity in a brickwork column. This indicates that a brickwork structure may be used as a cushion to reduce the damaging effects on a structure due to a shock wave which may be the result of an explosion nearby. Research into the use of brickwork or masonry structures to resist dynamic loadings using the finite element analysis may be possible. The research may be used to investigate an optimum form of layered structure which may damp the shock wave effectively. In addition, the research may also be used to design a kind of shock barrier to protect a structure from damage by shock waves which may be caused by an explosion nearby.

References 9.

1. Davis, A.G., Dunn, C.S., "From Theory to Field Experience with the Non-Destructive Vibration of Piles", Proceedings of the Institution of Civil Engineers, Part 2, 571-593, December, 1974.

Appendix A. Derivation of the Admittance Relationships for a 20-node Isoparametric Finite Element

A.1 Introduction

To use a small number of elements to represent a relatively complex form which is liable to occur in the real problem, finite elements which may be mapped into distorted forms are used. The shape functions of such finite elements are usually defined by the use of a natural coordinate system, for instance, ε, η, ζ coordinates (Figure A.1). The element properties of each of the elements in the global coordinate system, x, y and z, may be obtained by suitable transformation from the natural coordinates to the global coordinates. In the simulation of the continuum for the assessment of the integrity of a pile-soil system using the Earth-Resistance Method, the 20-node isoparametric finite element (Figure A.1) was used. The derivation of the Admittance Relationships for such a finite element follow.

A.2 Shape Functions for 20-node Isoparametric Brick Element

The general forms of shape functions for a 20-node isoparametric brick element are given in many standard finite element texts (Ref. A.1, A.2, A.3). The shape functions for the 20-node isoparametric finite element shown in Figure A.1 are given in equations (A.1) in terms of natural coordinates, ε, η and ζ:

$$
\begin{aligned}
N_1 &= \tfrac{1}{8}(1+\varepsilon)(1+\eta)(1+\zeta)(\varepsilon+\eta+\zeta-2)\\
N_2 &= \tfrac{1}{8}(1-\varepsilon)(1+\eta)(1+\zeta)(-\varepsilon+\eta+\zeta-2)\\
N_3 &= \tfrac{1}{8}(1-\varepsilon)(1-\eta)(1+\zeta)(-\varepsilon-\eta+\zeta-2)\\
N_4 &= \tfrac{1}{8}(1+\varepsilon)(1-\eta)(1+\zeta)(\varepsilon-\eta+\zeta-2)\\
N_5 &= \tfrac{1}{8}(1+\varepsilon)(1+\eta)(1-\zeta)(\varepsilon+\eta-\zeta-2)\\
N_6 &= \tfrac{1}{8}(1-\varepsilon)(1+\eta)(1-\zeta)(-\varepsilon+\eta-\zeta-2)\\
N_7 &= \tfrac{1}{8}(1-\varepsilon)(1-\eta)(1-\zeta)(-\varepsilon-\eta-\zeta-2)\\
N_8 &= \tfrac{1}{8}(1+\varepsilon)(1-\eta)(1-\zeta)(\varepsilon-\eta-\zeta-2)\\
N_9 &= \tfrac{1}{4}(1-\varepsilon^2)(1+\eta)(1+\zeta)\\
N_{10} &= \tfrac{1}{4}(1-\varepsilon)(1-\eta^2)(1+\zeta)\\
N_{11} &= \tfrac{1}{4}(1-\varepsilon^2)(1-\eta)(1+\zeta)\\
N_{12} &= \tfrac{1}{4}(1+\varepsilon)(1-\eta^2)(1+\zeta)\\
N_{13} &= \tfrac{1}{4}(1-\varepsilon^2)(1+\eta)(1-\zeta)\\
N_{14} &= \tfrac{1}{4}(1-\varepsilon)(1-\eta^2)(1-\zeta)\\
N_{15} &= \tfrac{1}{4}(1-\varepsilon^2)(1-\eta)(1-\zeta)\\
N_{16} &= \tfrac{1}{4}(1+\varepsilon)(1-\eta^2)(1-\zeta)\\
N_{17} &= \tfrac{1}{4}(1+\varepsilon)(1+\eta)(1-\zeta^2)\\
N_{18} &= \tfrac{1}{4}(1-\varepsilon)(1+\eta)(1-\zeta^2)\\
N_{19} &= \tfrac{1}{4}(1-\varepsilon)(1-\eta)(1-\zeta^2)\\
N_{20} &= \tfrac{1}{4}(1+\varepsilon)(1-\eta)(1-\zeta^2)
\end{aligned}
\tag{A.1}
$$

A.3 Admittance Relationship for the 20-node Finite Element

It was shown in section 4.2.3.1 that the [B] matrix depends on the derivatives of the shape functions with respect to global coordinates. However, the shape functions, which are expressed in terms of natural coordinates, cannot be directly used to obtain the derivatives with respect to the global coordinates. Therefore, another set of coordinate transformations are required to relate the natural coordinate system to the global coordinate system. If the set of natural coordinate system, ε, η, ζ, and the global coordinate system, x, y, z, shown in Figure A.1 are related. The derivatives of the shape functions with respect to the natural coordinate system may be found using the chain rule of differentiation as follows:

$$\begin{aligned}
\frac{\partial N_i}{\partial \varepsilon} &= \frac{\partial N_i}{\partial x}\frac{\partial x}{\partial \varepsilon} + \frac{\partial N_i}{\partial y}\frac{\partial y}{\partial \varepsilon} + \frac{\partial N_i}{\partial z}\frac{\partial z}{\partial \varepsilon} \\
\frac{\partial N_i}{\partial \eta} &= \frac{\partial N_i}{\partial x}\frac{\partial x}{\partial \eta} + \frac{\partial N_i}{\partial y}\frac{\partial y}{\partial \eta} + \frac{\partial N_i}{\partial z}\frac{\partial z}{\partial \eta} \\
\frac{\partial N_i}{\partial \zeta} &= \frac{\partial N_i}{\partial x}\frac{\partial x}{\partial \zeta} + \frac{\partial N_i}{\partial y}\frac{\partial y}{\partial \zeta} + \frac{\partial N_i}{\partial z}\frac{\partial z}{\partial \zeta}
\end{aligned} \tag{A.2}$$

which may be expressed in matrix form as:

$$\begin{Bmatrix} \dfrac{\partial N_i}{\partial \varepsilon} \\ \dfrac{\partial N_i}{\partial \eta} \\ \dfrac{\partial N_i}{\partial \zeta} \end{Bmatrix} = \begin{bmatrix} \dfrac{\partial x}{\partial \varepsilon} & \dfrac{\partial y}{\partial \varepsilon} & \dfrac{\partial z}{\partial \varepsilon} \\ \dfrac{\partial x}{\partial \eta} & \dfrac{\partial y}{\partial \eta} & \dfrac{\partial z}{\partial \eta} \\ \dfrac{\partial x}{\partial \zeta} & \dfrac{\partial y}{\partial \zeta} & \dfrac{\partial z}{\partial \zeta} \end{bmatrix} \begin{Bmatrix} \dfrac{\partial N_i}{\partial x} \\ \dfrac{\partial N_i}{\partial y} \\ \dfrac{\partial N_i}{\partial z} \end{Bmatrix} \tag{A.3}$$

$$= [J] \begin{Bmatrix} \dfrac{\partial N_i}{\partial x} \\ \dfrac{\partial N_i}{\partial y} \\ \dfrac{\partial N_i}{\partial z} \end{Bmatrix} \tag{A.4}$$

where [J] is called the Jacobian matrix. The left hand side of equation (A.3) can be evaluated as the functions N_i are dependents of the local coordinates ε, η and ζ. For isoparametric elements, the same interpolation functions are used for the interpolation of the element coordinates and unknown variables (ϕ) in the element. That is the same shape functions which are defined in the natural coordinate system are used for the interpolation of the element coordinates and the unknown variable (ϕ) in the element. Therefore:

$$x = \sum_{i=1}^{20} N_i x_i$$
$$y = \sum_{i=1}^{20} N_i y_i \qquad (A.5)$$
$$z = \sum_{i=1}^{20} N_i z_i$$

Thus the Jacobian matrix may be found explicitly in terms of the local coordinates:

$$[J] = \begin{bmatrix} \sum \frac{\partial N_i}{\partial \varepsilon} x_i & \sum \frac{\partial N_i}{\partial \varepsilon} y_i & \sum \frac{\partial N_i}{\partial \varepsilon} z_i \\ \sum \frac{\partial N_i}{\partial \eta} x_i & \sum \frac{\partial N_i}{\partial \eta} y_i & \sum \frac{\partial N_i}{\partial \eta} z_i \\ \sum \frac{\partial N_i}{\partial \zeta} x_i & \sum \frac{\partial N_i}{\partial \zeta} y_i & \sum \frac{\partial N_i}{\partial \zeta} z_i \end{bmatrix} \qquad (A.6)$$

The derivatives of the shape functions with respect to the global coordinate system may be found by inverting the Jacobian matrix, thus:

$$\begin{Bmatrix} \frac{\partial N_i}{\partial x} \\ \frac{\partial N_i}{\partial y} \\ \frac{\partial N_i}{\partial z} \end{Bmatrix} = [J]^{-1} \begin{Bmatrix} \frac{\partial N_i}{\partial \varepsilon} \\ \frac{\partial N_i}{\partial \eta} \\ \frac{\partial N_i}{\partial \zeta} \end{Bmatrix} \qquad (A.7)$$

Therefore, the electric field potential-potential relations for a 20-node finite element are:

$$\{E^e\} = \begin{Bmatrix} E_x \\ E_y \\ E_z \end{Bmatrix} = [J]^{-1} \begin{bmatrix} \frac{\partial N_1}{\partial \varepsilon} & \frac{\partial N_2}{\partial \varepsilon} & \cdots\cdots & \frac{\partial N_{20}}{\partial \varepsilon} \\ \frac{\partial N_1}{\partial \eta} & \frac{\partial N_2}{\partial \eta} & \cdots\cdots & \frac{\partial N_{20}}{\partial \eta} \\ \frac{\partial N_1}{\partial \zeta} & \frac{\partial N_2}{\partial \zeta} & \cdots\cdots & \frac{\partial N_{20}}{\partial \zeta} \end{bmatrix} \begin{Bmatrix} \phi_1 \\ \phi_2 \\ \vdots \\ \vdots \\ \phi_{20} \end{Bmatrix} \tag{A.8}$$

or

$$\{E^e\} = [J]^{-1}[B_L]\{\phi^e\} \tag{A.9}$$

where $[B_L]$ is the matrix containing the derivatives of the shape function with respect to the natural coordinate system. The admittance relationship becomes:

$$[S^e] = \int_{\Omega^e} [B_L]^T[J]^{-T}[s][J]^{-1}[B_L]\{\phi^e\}d\Omega^e \tag{A.10}$$

In equation (A.10), the volume integration has been considered over the global coordinate system. It is, therefore, necessary to change the volume integral to be expressed in terms of natural coordinates and to change the limits of integration. Zienkiewicz (Ref. A.1) showed that the element volume integration in equation (A.10) may be expressed as:

$$[S^e] = \int_{-1}^{1}\int_{-1}^{1}\int_{-1}^{1} [B_L]^T[J]^{-T}[s][J]^{-1}[B_L]\det[J]\ d\varepsilon d\eta d\zeta \tag{A.11}$$

where det[J] is the determinant of the Jacobian matrix. Integrating equation (A.11) algebraically is difficult and the integration is usually carried out numerically using a Gauss Quadrature process. Assuming that:

$$G(\varepsilon,\ \eta,\ \zeta) = [B_L]^T[J]^{-T}[s][J]^{-1}[B_L] \tag{A.12}$$

the integral in equation (A.11) may be expressed as:

$$In = \int_{-1}^{1}\int_{-1}^{1}\int_{-1}^{1} G(\varepsilon,\ \eta,\ \zeta)\ d\varepsilon d\eta d\zeta \tag{A.13}$$

which may be obtained numerically by first evaluating the inner integral while keeping $d\eta$ and $d\zeta$ constant. Thus:

$$\int_{-1}^{1} G(\varepsilon,\ \eta,\ \zeta)\ d\varepsilon = \sum_{i=1}^{n} H_i G(\varepsilon_i,\ \eta,\ \zeta)$$

$$= G'(\eta,\ \zeta) \tag{A.14}$$

where n is the number of Gauss points used in the numerical integration in the ε direction. Similarly, for constant $d\zeta$:

$$\int_{-1}^{1} G'(\eta,\ \zeta)\ d\eta = \sum_{j=1}^{n} H_j G'(\eta_j,\ \zeta)$$

$$= G''(\zeta) \tag{A.15}$$

and finally,

$$\int_{1}^{1} G''(\zeta)\ d\zeta = \sum_{k=1}^{n} H_k G''(\zeta_k) \tag{A.16}$$

On expansion, the integral is:

$$\int_{-1}^{1}\int_{-1}^{1}\int_{-1}^{1} G(\varepsilon,\ \eta,\ \zeta)\ d\varepsilon d\eta d\zeta = \sum_{k=1}^{n}\ \sum_{j=1}^{n}\ \sum_{i=1}^{n} H_kH_jH_iG(\varepsilon_i,\ \eta_j,\ \zeta_k) \tag{A.17}$$

where n is the number of integration points in each direction. It has been assumed that the number of integration points in each direction are the same. The admittance matrix may therefore be found numerically:

$$[S^e] = \sum_{k=1}^{n}\ \sum_{j=1}^{n}\ \sum_{i=1}^{n} H_kH_jH_i[B_L]^T[J]^{-T}[s][J]^{-1}[B_L]\ \det[J] \tag{A.18}$$

A.4 Conclusions

The shape functions for the 20-node isoparametric finite element as shown in Figure A.1 were given. The admittance relationships for such an element were derived. The number of Gauss points required in each direction of the element for exact integration depends on the sizes of the finite elements used for idealisation. It has been suggested that two (Ref. A.1) or three (Ref. A.3) Gauss points in each direction would be sufficient to obtain accurate results from the numerical integration.

References A

1. Zienkiewicz, O.C., "The Finite Element Method in Engineering Science", McGraw-Hill Publishing Company Limited, 1971.

2. Bathe, K., Wilson, E.L., "Numerical Methods in Finite Element Analysis", Prentice-Hall, Inc., 1976.

3. Segerlind, L.J., "Applied Finite Element Analysis", John Wiley & Sons, Inc., 1976.

Appendix B Derivation of the Stiffness Relationships for the 8-node Isoparametric Element

B.1 Introduction

The 8-node isoparametric finite element was used to idealise a pile or a pile-soil system when the sonic echo method of testing was used to assess the integrity of such systems was simulated. This type of finite element was also used to idealise a masonry bridge where a simulation of the sonic method of testing the integrity of the bridge was undertaken. The derivation of the stiffness relationships for the 8-node isoparametric plane element as shown in Figure B.1 are similar to the derivation of the admittance relationships for the 20-node isoparametric brick element. The 8-node finite element as shown in Figure B.1 has two degrees of freedom at each node. The shape functions of the element may therefore be expressed in terms of natural coordinate system, ε and η shown in Figure B.1, and may be transformed to the global coordinate system, x and y shown in Figure B.1, to obtain the idealised element properties in the finite element idealisation.

B.2 Shape Functions for the 8-node Isoparametric Plane Element

The shape functions for the 8-node plane element as shown in Figure B.1 are given by Segerlind (Ref. B.1) and expressed in natural coordinates they are:

$$
\begin{aligned}
N_1 &= -\tfrac{1}{4}(1-\varepsilon)(1-\eta)(\varepsilon+\eta+1)\\
N_2 &= \tfrac{1}{2}(1-\varepsilon^2)(1-\eta)\\
N_3 &= \tfrac{1}{4}(1+\varepsilon)(1-\eta)(\varepsilon-\eta-1)\\
N_4 &= \tfrac{1}{2}(1-\eta^2)(1+\varepsilon)\\
N_5 &= \tfrac{1}{4}(1+\varepsilon)(1+\eta)(\varepsilon+\eta-1)\\
N_6 &= \tfrac{1}{2}(1-\varepsilon^2)(1+\eta)\\
N_7 &= -\tfrac{1}{4}(1-\varepsilon)(1+\eta)(\varepsilon-\eta+1)\\
N_8 &= \tfrac{1}{2}(1-\eta^2)(1-\varepsilon)
\end{aligned}
\tag{B.1}
$$

B.3 Stiffness Relationship for the 8-node Isoparametric Plane Element

The stiffness relationships for static plane strain or plane stress analysis as given in equation (4.32) are:

$$[K^e]\{\delta^e\} = \{P^e\} \tag{4.32}$$

where $[K^e]$ is the elemental stiffness matrix:

$$[K^e] = \int_{\Omega^e} [B]^T[D][B]\, d\Omega^e \tag{B.2}$$

in which [B] matrix is the strain-displacement matrix. This matrix defines the strain-displacement relationship in the element. The [D] matrix, which contains elastic constants, defines the stress-strain relationship in the finite element.

The shape functions for the 8-node finite element (Figure B.1) are given in equation (B.1) as functions of the natural coordinates, ε and η. However, the [B] matrix as given in equation (4.26) contains the derivatives of the shape functions with respect to the global coordinate system, x and y.

Therefore, transformation matrix is required to transform the derivatives from the natural coordinate system to the global coordinate system. Again, the chain rule of differentiation is used:

$$\begin{aligned} \frac{\partial N_i}{\partial \varepsilon} &= \frac{\partial N_i}{\partial x}\frac{\partial x}{\partial \varepsilon} + \frac{\partial N_i}{\partial y}\frac{\partial y}{\partial \varepsilon} \\ \frac{\partial N_i}{\partial \eta} &= \frac{\partial N_i}{\partial x}\frac{\partial x}{\partial \eta} + \frac{\partial N_i}{\partial y}\frac{\partial y}{\partial \eta} \end{aligned} \tag{B.3}$$

and expressed in matrix form:

$$\begin{Bmatrix} \dfrac{\partial N_i}{\partial \varepsilon} \\ \dfrac{\partial N_i}{\partial \eta} \end{Bmatrix} = \begin{bmatrix} \dfrac{\partial x}{\partial \varepsilon} & \dfrac{\partial y}{\partial \varepsilon} \\ \dfrac{\partial x}{\partial \eta} & \dfrac{\partial y}{\partial \eta} \end{bmatrix} \begin{Bmatrix} \dfrac{\partial N_i}{\partial x} \\ \dfrac{\partial N_i}{\partial y} \end{Bmatrix} \tag{B.4}$$

$$\begin{Bmatrix} \dfrac{\partial N_i}{\partial \varepsilon} \\ \dfrac{\partial N_i}{\partial \eta} \end{Bmatrix} = [J] \begin{Bmatrix} \dfrac{\partial N_i}{\partial x} \\ \dfrac{\partial N_i}{\partial y} \end{Bmatrix} \tag{B.5}$$

where [J] is the Jacobian matrix for the 8-node finite element. Since both the left hand side of equation (B.5) and the Jacobian matrix can be evaluated, the derivatives of the shape functions with respect to the global coordinate system may be found by inverting the Jacobian matrix:

$$\begin{Bmatrix} \dfrac{\partial N_i}{\partial x} \\ \dfrac{\partial N_i}{\partial y} \end{Bmatrix} = [J]^{-1} \begin{Bmatrix} \dfrac{\partial N_i}{\partial \varepsilon} \\ \dfrac{\partial N_i}{\partial \eta} \end{Bmatrix} \tag{B.6}$$

The [B] matrix for the 8-node finite element will be:

$$[B] = \begin{bmatrix} \frac{\partial N_1}{\partial x} & 0 & \frac{\partial N_2}{\partial x} & 0 & \cdots\cdots & \frac{\partial N_8}{\partial x} & 0 \\ 0 & \frac{\partial N_1}{\partial y} & 0 & \frac{\partial N_2}{\partial y} & \cdots\cdots & 0 & \frac{\partial N_8}{\partial y} \\ \frac{\partial N_1}{\partial y} & \frac{\partial N_1}{\partial x} & \frac{\partial N_2}{\partial y} & \frac{\partial N_2}{\partial x} & \cdots\cdots & \frac{\partial N_8}{\partial y} & \frac{\partial N_8}{\partial x} \end{bmatrix} \tag{B.7}$$

Thus, the coefficients in the [B] matrix in equation (B.7) may be obtained from the appropriate components in equation (B.6).

The [D] matrix to be used in this case is the same as in equations (4.29) and (4.30) for plane stress and plane strain conditions respectively.

The volume of the finite element, $d\Omega^e$, in equation (B.2) may be transformed to an integral with respect to the natural coordinate system thus:

$$\int_{\Omega^e} d\Omega^e = t * \int_{-1}^{1}\int_{-1}^{1} \det[J]\, d\varepsilon d\eta \tag{B.8}$$

where t is the thickness of the finite element. The integral with respect to the natural coordinate system may be found numerically using the Gauss Quadrature process. The integral on the right hand side of equation (B.8) may be expressed using the Gaussian Quadrature formula as:

$$t * \int_{-1}^{1}\int_{-1}^{1} G(\varepsilon, \eta)\det[J]\, d\varepsilon d\eta = t * \sum_{j=1}^{n}\sum_{i=1}^{n} H_j H_i G(\varepsilon_i, \eta_j)\det[J] \tag{B.9}$$

where $G(\varepsilon, \eta)$ is $[B]^T[D][B]$ and n is the number of Gauss points in each direction. Assumption has been made such that the number of Gauss points in each direction of the natural coordinate system are the same. Therefore, the elemental stiffness matrix is:

$$[K^e] = t * \sum_{j=1}^{n} \sum_{i=1}^{n} H_j H_i [B]^T [D][B] \det[J] \tag{B.10}$$

B.4 Conclusions

The shape functions for the 8-node finite element shown in Figure B.1 are given. A brief description of the derivation of the stiffness relationship for such a finite element is given. The elemental stiffness matrix for the 8-node finite element may be obtained using numerical integration. Again, the number of Gauss points required in each direction in order to obtain an accurate integration depends on the size of the finite elements. This type of finite element has been used for the two dimensional simulation of the sonic echo method and vibration methods of integrity testing of civil engineering structures in Chapters 6 and 8. The same type of finite element has also been used in Chapter 7 to idealise a masonry bridge. The idealisation is used to study the application of the sonic method of testing on the masonry bridge to assess the integrity of the bridge.

References B

1. Segerlind, L.J., "Applied Finite Element Analysis", John Wiley & Sons Inc., 1976.

Appendix C Flow Charts for the Main Analysis Programs

The flow charts shown in this Appendix were used in the development of the two main analysis programs. The flow chart shown in Figure C.1 was used for the Analysis of the Electricity Flow Problem. The flow chart shown in Figure C.2 was used for the Dynamic Analysis of a Pile-Soil System using Explicit Time Integration.

The Frontal Solution Method (Refs. C.1, C.2, C.3, C.4) was used in both analyses. Advantage has been taken of the symmetry of the Admittance and Stiffness Matrices so that only the upper half of the matrices were stored in the disc file. Newmark's Method of Time Integration (Refs. C.5, C.6, C.7) was used for the time integration in the Dynamic Analysis of a Pile-Soil System. The Energy Absorbing Boundary condition for the simulation of an infinite boundary in the pile-soil system had been incorporated at the stage when the Damping matrix is formed. Since the Applied Load in the dynamic analysis may vary with time, the boundary condition data was input at each time step. Assuming that the support to the pile-soil system under consideration was the same throughout the analysis, the Effective Stiffness Matrix was solved once at the first time step to reduce the total computing time. The reduced effective stiffness matrix was used to modify the effective load vector at each time step. The same reduced effective stiffness matrix was also used for backsubstitution at each time step to compute the nodal displacements at time $t+\Delta t$.

References C.

1. Zienkiewicz, O.C., "The Finite Element Method in Engineering Science", McGraw-Hill Publishing Company Limited, 1971.

2. Hinton, E., Owen, D.R.J., "Finite Element Programming", Academic Press Inc., (London), Ltd., 1977.

3. Cheung, Y.K., Yeo, M.F., "A Practical Introduction to Finite Element Analysis", Pitman Publishing Limited, 1979.

4. Irons, B., Ahmad, S., "Techniques of Finite Element", Ellis Horwood Limited, 1980.

5. Bathe, K., Wilson, E.L., "Numerical Methods in Finite Element Analysis", Prentice-Hall Inc., 1976.

6. Smith, I.M., "Programming The Finite Element Method", John-Wiley and Sons Ltd., 1982.

7. Newmark, N.M., "A Method of Computational for Structural Dynamics", Journal of the Engineering Mechanics Division, Proceedings of the American Society of Civil Engineers, Vol. 85, No. EM3, 67-94, July, 1959.

Appendix D

Two Dimensional Finite Element Modelling of Mineshaft Detection Techniques using the Resistivity Method

D.1 Introduction

The electrical method which has been used for integrity testing for reinforced concrete piles may also be applied to detect abandoned mineshafts in an old coalmine workings (Ref. D.1, D.2). This Appendix illustrates how the finite element method may be used to simulate the electrical resistivity testing method for mineshaft detection in areas of abandoned mineworkings. Both Tripole and Quadripole configurations for mineshaft detection are described. A two dimensional model is developed which enables the distribution of equipotentials on horizontal or vertical sections through the mineshaft and surrounding ground to be plotted and studied. Comparison of the equipotential distributions for the ground model with and without the mineshaft are given. The response curves for these examples are also given to aid the interpretation of the measurements made during the resistivity testing. The use of the resistivity method for locating spoil heaps is also considered.

Resistivity prospecting methods, in which current is applied by conduction to the ground through electrodes, depend for their operation on the fact that any subsurface variation in conductivity alter the form of the current flow within the earth and thus affects the distribution of electric potential. The degree to which the potential at the surface is affected depends on the size, shape, location and electrical resistivity of the subsurface masses. It is therefore possible to obtain information about the subsurface distribution of these bodies from potential measurements made at the surface.

D.2 Resistivity Prospecting

The basic principle of resistivity measurement is that a controlled current is passed between two electrodes driven into the ground at some distance apart, while the potential difference between two or more electrodes placed at some other points in the area under investigation is measured. The applied current is usually a low frequency alternating current. This will avoid the errors in the readings due to the electrochemical electromotive force (polarization) being produced between the metal electrodes and the ground. In addition, low frequency alternating currents will not be affected by natural earth currents which produce a slowly varying potential difference across the electrodes.

D.2.1 Electrode Configurations

Griffiths et. al. (Ref. D.3) suggested that it would be more useful if the current flow can be concentrated within the depth from the surface which it is proposed to investigate. This may be done by limiting the separation of the current electrodes.

It was suggested by Kunetz (Ref. D.4) that the most frequently used quadripoles are; the Wenner configuration (Figure D.1), in which the electrodes are equally spaced and the Schlumberger configuration (FigureD.2), in which the distance between the potential electrodes is small when compared with the distance between the current electrodes. If one of the current electrodes is removed to infinity, a tripole configuration is obtained as shown in Figure D.3. Usually, the current electrode is removed an appreciable distance so that any asymmetry introduced by discontinuities in the earth's resistivity may be neglected. In addition, the tripoles offer a considerable advantage in rough terrain in that only three electrodes and correspondingly less cable are required to be moved to execute resistivity exploration. In this Appendix, the Wenner configuration and a tripole configuration will be considered.

D.2.2 Response Curve

The definition for a response curve mentioned in section 5.3.1 is also applicable in this study. Interpretation of a response curve is made by a comparison with ideal theoretical curves. For the Wenner configuration, the physical property to be considered is the apparent resistance of the soil between adjacent points but with the tripole configuration, however, the measured voltage reduction between adjacent stations is considered.

D.2.3 Applications

A mineshaft is the link between surface and subsurface excavation. Therefore a steeply dipping interface between the mineshaft and the surrounding soil would normally be expected with a consequent marked difference in resistivity. If the shaft is filled with water or mud it represents a zone of relatively higher conductivity. Conversely, if it is filled with air, a zone of extremely high resistivity should be found owing to the existence of the air which can be considered as an insulator.

To use electrical trenching where the electrodes are kept at constant separation throughout the exploration, both the current and potential electrodes are moved as an entirety across the surface in a predetermined direction as shown in Figure D.4. For each electrode position, the apparent resistivity between the potential electrodes may be measured. Any abnormal response in the area may therefore be spotted.

The tripole resistivity system shown in Figure D.5 operates by applying a low frequency current to the ground and measuring the resulting surface potentials. In homogeneous ground the applied current diverges radially away from the point source electrode, and the measured surface potential gradient diminishes inversely with the square of distance away from the source. In the presence of a subsurface void, the current is forced to flow around the high resistivity zone, distorting the surface potential distribution and thereby revealing any anomaly. Old spoil heaps may be located and their approximate thickness determined by comparison of resistivity field measurements with a suitable finite element simulation.

D.3 Case Studies

The finite element idealisations used in these studies are shown in Figures D.4 and D.5 for each case. In addition, typical arrangements for the position of the electrode during testing are shown. The finite element shown in Figure D.4 represents a plan view of the site when the electrical trenching method is being used. The same mesh will be used to represent the vertical section of the problem studied in the tripole prospecting as shown in Figure D.5. The conductivity of the clay soil was assumed to be 520.55 x 10^{-3} mho/m in case studies considered in this paper. In both cases it has been assumed that the shaft is filled with air of zero conductivity. The results for the two dimensional simulations are represented by a computer plot of the percentage equipotential in either the horizontal or vertical section. The current flow lines were omitted for the sake of clarity. Additionally, a plot of the response curve for each case is given.

The apparent resistance of soil between potential electrodes is measured for each electrode position when using the electrical trenching method. Since the survey lines may be represented by the straight lines in the x and y coordinate directions in the finite element mesh, the problem may thus be simulated two dimensionally by considering a uniformly distributed applied electric current flow from one edge to the opposite edge of the mesh. Figures D.7 and D.9

give the equipotential contours for homogeneous ground when electric current is applied in two directions. Figures D.8 and D.10 give respectively the apparent resistance curves along A-B and C-D. Figures D.11 to D.14 show the corresponding equipotential distributions and apparent resistance curves for the same applied current when a mineshaft exists in the middle of the field. When a void is present in the survey area, the current is forced to flow around the high resistance zone, therefore the surface potential distribution is moved nearer to the void. However, for a given applied current the local surface potential is increased, indicating a higher than normal apparent resistance.

Placing one of the current electrodes to infinity (or some significant distance away) gives the tripole configuration discussed earlier. A change in the position of the current electrodes results in a change of the relative position between the current electrode and subsurface construction. In this study, the current electrode has been fixed at the middle of the survey line while the void to be examined has been placed at different positions in the section to reveal its disturbance to the potential measurements. In this case the cavity could for example be a tunnel. The effects of other subsurface construction on resistivity measurements could also be examined if required.

Figure D.15 illustrates that, in homogeneous ground, the observed potential has a generally smooth spatial characteristic. Figure D.16 shows the equivalent response curve on the ground surface which is included in later figures for comparison and is referred to as the perfect ground model. The equipotentials in Figure D.15 are almost circular indicating that the idealisation is sufficient. If the relative distance from the electrode to any one boundary is reduced then the equipotentials would have been distorted.

Figures D.17 to D.26 show that an air-filled cavity will cause the equipotential lines to move nearer to the void and result in a higher than normal perturbation in the surface potential in the locality of the cavity. Figures D.17 to D.20 illustrate that the nearer the tunnel is located to the ground surface, the more significant the effect on the response curve. Figures D.21 to D.24 show that the bigger the cavity , the larger the area over which the voltage and equipotential is affected. Finally, Figures D.23 to D.26 show that the nearer the cavity is located to the current electrode, the more significant the effect on the response curve resulting in easier measurement in the field.

For comparison the equipotential contours for a similar tunnel to that shown in Figure D.23 but filled with material of high conductivity 5.237 mho/m is shown in Figure D.27. The soil was assumed to be of lower conductivity, that is to say 520.55 x 10^{-3} mho/m. The response curve for this situation together with the response curve for the tunnel is shown in Figure D.23 and the homogeneous ground model shown in Figure D.15 are shown in Figure D.28.

Figures D.29 and D.30 show the percentage equipotential distribution in a vertical section where a spoil heap of conductivity 380.00 x 10^{-6} mho/m lies on top of a clay soil. These figures should be compared with the distribution for a homogeneous ground shown in Figure D.15. The equipotential contours for the spoil heap studies are closely spaced and flattened within the upper layer indicating that the lines of electric current flow are distorted downwards. The response curve for these studies, shown in Figure D.31, illustrates that a shallow, higher resistance upper coal layer gives a sharp peak in the response curve whereas a homogeneous, lower resistance clay soil gives a comparatively flatter response curve. Figure D.32 shows the equipotential distribution for an area that includes an infill of spoil material. The equipotentials are shown to have moved nearer to the higher resistance spoil material on the left hand side.

Figure D.33 gives the corresponding response curve where the spoil heap may be detected by a higher voltage drop between adjacent stations.

These studies indicate that the finite element method provides a valuable simulation technique for interpretation of resistivity methods of site investigation in areas of abandoned mineworkings.

D.4 Conclusions

The two dimensional finite element method discussed in this paper has been shown to enable the simulation of the electric field distribution around a mineshaft during resistivity exploration. Since the simulation is only two dimensional, the results cannot be used for accurate comparative purposes with field tests. The response curve for each model, however, gives qualitative indications of the effects of ground anomalies. Interpretation of a response curve should be made by a comparison with ideal theoretical curves. The examples presented in this paper show that it is possible to estimate the range of operation and sensitivity of the resistivity methods. For example, the depth to diameter ratio of the tunnel which will affect the significance of the results.

In the simulation studies, flat ground surfaces have been considered. In practice, the presence of a relief on the earth's surface also disturbs the electric field. Kunetz (Ref. D.4) showed that the current density is increased at the bottom of valleys and decreased near the top of a hill or mountain. Thus, the equipotential surfaces will be more dense in the valley bottom and less dense near the top of hills and mountains. Further work should be undertaken to account for this topology influence when the finite element method is used to interpret field results.

The idealisation used in this study actually represents an infinitely long rectangular well placed at the centre of the field where a uniformly distributed current is applied between a film at opposite edges for electrical trenching. The tripole configuration may be interpreted as an infinitely long tunnel in the ground when the electric current is applied through a long conductor at the middle of the ground surface. Three dimensional simulation is required to interpret the true physical characteristics of the problem.

The finite element method is also shown to be a valuable aid to interpretation of site investigations for the determination of the location and depth of spoil heaps.

References D.

1. Tomlinson, M.J., "Foundation Design and Construction", Pitman Publishing, 1980.

2. Topping, B.H.V., Whittington, H.W., Wong, F.L., "Two Dimensional Finite Element Modelling of Mineshaft Detection Techniques Using The Resistivity Method", Mineworkings 84, Proceedings of the International Conference on Construction in Areas of Abandoned Mineworkings, Engineering Technics Press, 1984.

3. Griffiths, D.H., King, R.F., "Applied Geophysics for Geologists and Engineers", Pergamon Press, Oxford, 1981.

4. Kunetz, G., "Principles of Direct Current Resistivity Prospecting", Geopublication Associates, Gebruder Borntraeger, Berlin, 1966.

Appendix E

E.1 Results for a Simulated Steady State Vibration Test on a Fixed End Pile

Frequency	$\lvert V_0 \rvert$	$\lvert V_0/F_0 \rvert$
10.00000	4.07571e-03	1.63028e-06
20.00000	8.28975e-03	3.31590e-06
29.76191	1.26518e-02	5.06074e-06
39.68254	1.81031e-02	7.24124e-06
50.00000	2.49473e-02	9.97894e-06
59.52381	3.27962e-02	1.31184e-05
69.44444	4.44861e-02	1.77944e-05
78.12500	5.92670e-02	2.37068e-05
89.28571	9.84045e-02	3.93618e-05
100.00000	2.25482e-01	9.01926e-05
108.69565	1.28657e+00	5.14626e-04
119.04762	2.10172e-01	8.40686e-05
125,00000	1.33357e-01	5.33428e-05
138.88889	7.36370e-02	2.94548e-05
147.05882	5.91110e-02	2.36444e-05
156.25000	4.81201e-02	1.92480e-05
166.66667	3.94849e-02	1.57939e-05
178.57143	3.30838e-02	1.32335e-05
192.30769	2.81790e-02	1.12716e-05
208.33333	2.31620e-02	9.26480e-06
227.27273	2.37721e-02	9.50886e-06
250.00000	3.07719e-02	1.23087e-05
263.15789	3.63594e-02	1.45437e-05
277.77778	4.90536e-02	1.89651e-05
294.11765	6.72065e-02	2.68826e-05
312.50000	1.99040e-01	7.96158e-05
326.79739	1.25343e+00	5.01372e-04
333.33333	2.94302e-01	1.17720e-04
357.14286	6.64095e-02	2.65638e-05
384.61538	4.65727e-02	1.86290e-05
416.66667	2.81111e-02	1.12444e-05
454,54545	3.16706e-02	1.26682e-05
500.00000	7.85730e-02	3.14292e-05

545.55374	7.31915e-01	2.92766e-04
555.55556	1.42205e-01	5.68820e-05
625.00000	2.66168e-02	1.06467e-05
714.28571	6.46265e-02	2.58506e-05

E.2 Results for a Simulated Steady State Vibration Test on a Free End Pile

Frequency	$\lvert V_0 \rvert$	$\lvert V_0/F_0 \rvert$
10.00000	2.06911e-01	8.27642e-05
20.00000	1.03139e-01	4.12554e-05
29.76191	6.84215e-02	2.73686e-05
39.68254	5.15175e-02	2.06070e-05
50.00000	4.05515e-02	1.62206e-05
59.52381	3.35156e-02	1.34062e-05
69.44444	2.77664e-02	1.11065e-05
78.12500	2.49987e-02	9.99950e-06
89.28571	2.21019e-02	8.84076e-06
100.00000	1.89083e-02	7.56332e-06
108.69565	1.78871e-02	7.15486e-06
119.04762	2.03178e-02	8.12714e-06
125.00000	2.16294e-02	8.65178e-06
138.88889	2.63565e-02	1.05426e-05
147.05882	2.89712e-02	1.15885e-05
156.25000	3.40306e-02	1.36122e-05
166.66667	4.20521e-02	1.68208e-05
178.57143	5.64270e-02	2.25708e-05
192.30769	8.70535e-02	3.48214e-05
208.33333	2.45868e-01	9.83472e-05
218.15009	1.14788e+00	4.59150e-04
227.27273	2.03142e-01	8.12568e-05
250.00000	6.91505e-02	2.76602e-05
277.77778	4.02395e-02	1.60958e-05
312.50000	2.57408e-02	1.02963e-05
333.33333	2.71094e-02	1.08437e-05
357.14286	3.56181e-02	1.42472e-05
390.62500	5.68555e-02	2.27422e-05
416.66667	2.19067e-01	8.76268e-05
436.30017	2.05820e-01	8.23280e-05
450.45045	1.26003e-01	5.04010e-05
500.00000	3.34710e-02	1.33884e-05
531.91489	2.61860e-02	1.04744e-05

561.79775	3.56602e-02	1.42641e-05
591.71598	5.69160e-02	2.27664e-05
625.00000	4.06117e-01	1.62446e-04
649.35065	1.28081e-01	5.12324e-05
654.45026	7.01770e-02	2.80708e-05
680.27211	5.24580e-02	2.09832e-05
709.21986	3.42096e-02	1.36838e-05
740.74074	2.82179e-02	1.12871e-05
833.33333	5.97360e-02	2.38944e-05

List of Published Works

1. B.H.V. Topping, H.W. Whittington, F.L. Wong, "A Two-Dimensional Finite Element Simulation of Earth Resistivity Testing of Reinforced Concrete Pile-Soil System", NDT-83, Proceedings of the International Conference on Non-Destructive Testing, Engineering Technics Press, 100-112, 1983.

2. B.H.V. Topping, H.W. Whittington, F.L. Wong, "Two-Dimensional Finite Element Modelling of Mineshaft Detection Techniques using the Resistivity Method", Mineworkings 84, Proceedings of the International Conference on Construction in Areas of Abandoned Mineworkings, Engineering Technics Press, 221-244, 1984.

3. B.H.V. Topping, H.W. Whittington, F.L. Wong, "The Use of a Two-Dimensional Finite Element Simulation for the Interpretation of the Electrical Resistivity Method in Non-Destructive Testing of Reinforced Concrete Piles", UKSC 84, Proceedings of the United Kingdom Simulation Council Conference on Computer Simulation, Butterworths, 403-419, 1984.

4. F.L. Wong, B.H.V. Topping, "Three Dimensional Finite Element Simulation of the Resistivity Technique for Non-Destructive Testing of Reinforced Concrete Piles", Structural Faults 85, Proceedings of the Second International Conference on Structural Faults and Repair, Engineering Technics Press, 311-321, 1985.